GigaHertz Symposium 2010

Sjöland, Henrik

2010

LUND UNIVERSITY

GigaHertz Symposium 2010

9-10 March 2010
Lund University
Sweden

www.gigahertz.nu

Editor: **Henrik Sjöland**
Department of Electrical and Information Technology
Lund University
Box 118
SE-221 00 Lund
Sweden

http://www.commtech.lth.se

www.hswc.lth.se

http://www.eit.lth.se/sos

www.ieee.org

SNRV
SVENSKA NATIONALKOMMITTÉN
FÖR RADIOVETENSKAP

www.radiovetenskap.kva.se

Sponsors of GigaHertz Symposium 2010

Platinum Sponsors:

Communication Technology Lund
http://www.commtech.lth.se

High Speed Wireless Communication Center
www.hswc.lth.se

Rohde & Schwarz
www.rohde-schwarz.com

Silver Sponsors:

AWR, www.awrcorp.com

MicroComp Nordic AB, www.mcnab.se

Exhibitors at GigaHertz Symposium 2010

Ageto MTT, www.agetomtt.se

Agilent, www.agilent.com

Amska, www.amska.se

Anritsu, www.anritsu.se

AWR, www.awrcorp.com

MicroComp Nordic AB, www.mcnab.se

National Instruments, www.ni.com

Rohde & Schwarz, www.rohde-schwarz.com

Welcome to GigaHertz Symposium 2010

The GigaHertz Symposium is a biennal conference in the field of GigaHertz technology. It is a meeting place for researchers in the field from industry, academia, and research institutes. The conference alternates between Swedish Universities. This is the 10th GigaHertz Symposium, and it is arranged by Lund University. It is a special honor for us to host the 10th anniversary of the Symposium!

The conference venue is at the very heart of Lund University, at Palaestra, the King's house, and the main university building. These are all classical university buildings with a long academic history. The conference dinner will take place at Akademiska Föreningen. It is located very close to the other buildings and belongs to the student union. This is a place for activities such as spex and balls. In May there will be a Karneval in Lund, and the main site is around these buildings. It occurs once every four years, and if you have never seen it, I recommend you to return in May to get a first-hand experience!

The scope of the Symposium is broad, ranging from devices to systems, and from single GHz frequencies up to several THz. During two days more than 80 papers will be presented, among them invited papers from leading researchers in different areas. There will be both parallel sessions and plenary sessions. In addition to this there is an exhibition with 8 companies. Looking at the well-filled program and all the excellent abstracts in this book makes me very happy!

I would like to thank everyone who has contributed to this event; the invited speakers, the contributors who have chosen to present their work at the symposium, the program committee, the session chairmen, and of course all the conference delegates. I would also like to thank the people at Kongresscentrum, especially Magnus Nygren and Eva Wendel, and the people at the department of Electrical and Information Technology, especially Pia Bruhn, for all their practical assistance. Finally I would like to thank the sponsors and exhibitors for supporting the Symposium!

I hope you will enjoy GigaHertz Symposium 2010!

Henrik Sjöland
General Chairman
GigaHertz Symposium 2010

Program Tuesday March 9

09.00 – 10.00 Registration, Palaestra lobby

10.00 – 12.00 Session 1, Palaestra auditorium,
chairman: Henrik Sjöland, Lund University

10.00 Welcome

10.10 Invited: III-V-Nanowire FET for Low-Power RF-Applications: Approaches and Results
Franz-J. Tegude, University of Duisburg-Essen

10.50 Invited: Trends and Future Challenges in Antenna Design for Smart Phones
Richard Breiter, Nokia

11.30 Development and Application of an Active Microwave System for Medical Imaging
Vitaliy Zhurbenko, Technical University of Denmark

11.45 Towards an integrated transceiver: GaN MMIC processing and design at Chalmers
Christer Andersson, Chalmers

12.00 – 13.15 Lunch and Exhibition, Palaestra lobby and exhibition room
Platinum Sponsor: **Rohde & Schwarz**

13.15 – 15.15 4 parallel sessions

Session 2: System and system issues, Palaestra lower
chairman: Per Sjöstrand, Saab

Session 3: MMICs and RFICs, Palaestra upper
chairman: Jan Grahn, Chalmers

Session 4: Passive Components and RF MEMS Circuits, Kings House (Kungshuset)
chairman: Spartak Gevorgian, Chalmers

Session 5: Digital and Mixed Signal, Main University Building
chairman: Sven Mattisson, Ericsson

15.15 – 15.45 Coffee and Exhibition, Palaestra lobby and exhibition room
Silver Sponsor: **AWR**

15.45 – 17.10 Session 6, Palaestra auditorium
chairman: Gerhard Kristensson, chairman of SNRV, Lund University

15.45 Invited: Carrier Aggregation - Another RF Design Challenge
Lars Sundström, Ericsson

16.25 Ultra-Wideband Low-loss All-Silicon MEMS Phase Shifters for High-Performance Electronic Beam-Steering Applications
N. Somjit, KTH

16.40 A PLL based 12GHz LO Generator with Digital Phase Control in 90 nm CMOS
A. Axholt, Lund University

16.55 Highly Efficient Dynamic Load Modulation Transmitter
C. Fager, Chalmers

19.00 Dinner, Akademiska Föreningen, Lilla Salen

Program Wednesday March 10

08.30 – 09.40 Session 7, Palaestra auditorium,
chairman: Lars-Erik Wernersson, Lund University

08.30 Invited: THz in Space Science, Biology and Medicine
Peter Siegel, Caltech

09.10 Invited: Millimeter wave design in bulk and SOI CMOS
Baudouin Martineau, ST

09.40 – 10.10 Coffee and Exhibition, Palaestra lobby and exhibition room
Silver Sponsor: **MicroComp Nordic AB**

10.10 – 12.10 4 parallel sessions

Session 8: Active Components, Palaestra lower
chairman: Gunnar Malm, KTH

Session 9: Antennas, EMC and Measurement Technology, Palaestra upper
chairman: Anders Rydberg, Uppsala University

Session 10: THz Technology, Kings House (Kungshuset)
chairman: Staffan Rudner, FOI

Session 11: Modules and Packaging, Main University Building
chairman: Hans-Olof Vickes, Saab Microwave Systems

12.10 – 13.20 Lunch and Exhibition, Palaestra lobby and exhibition room
Platinum Sponsor: **Rohde & Schwarz**

13.20 – 15.05 Session 12, Palaestra auditorium
chairman: Pietro Andreani, Lund University

13.20 Invited: Indium antimonide based high-speed transistors for low power dissipation applications
Tim Ashely, QinetiQ

13.50 Invited: RF Integration Trends in Mobile Phones
Martin Isberg, ST-Ericsson

14.20 Vertical InAs Nanowire Wrap Gate Transistors for Integration on a Si Platform
Lars-Erik Wernersson, Lund University

14.35 60, 70, and 80 GHz front-end modules for multi-Gbps wireless communication
Sten Gunnarsson, Sivers IMA

14.50 Integrated receivers for 220 GHz SAR-applications
Herbert Zirath, Chalmers

15.05 – 15.15 Closing, Palaestra auditorium
Henrik Sjöland, Lund University
NN

Parallel Session Papers, Tuesday March 9, 13.15-15.15

Session 2: System and system issues, Palaestra lower

chairman: Per Sjöstrand, Saab

13.15 Experimental System and Simulations of a Vertical SAR, P-O. Frölind, A. Gustafsson, L. Pettersson, P. Andersson, and J. Svedin, FOI

13.30 System Design for Solid State S-Band Marine Radar, A. Nelander, B. Carlegrim, and R. Jonsson, FOI

13.45 UWB Ranging Hardware Platform, A. De Angelis[1], J-O Nilsson[2], I. Skog[2], P. Händel[2], [1]University of Perugia, Italy, [2]KTH

14.00 Model-Based Adaptation of RF Power Amplifiers, T. Eriksson, A. Soltani and C. Fager, Chalmers

14.15 M-Sequence UWB Radar for Industrial Applications, D. Andersson#, K. Wallin#, O. Javashvili* and C. Beckman*, #Radarbolaget, *University of Gävle

14.30 Wireless Body Area Networks (WBANs) and Efficient, Energy Conservative Designs, M. Jobs and A. Rydberg, Uppsala University

14.45 Techniques for Communication Robustness in Train Environment, A. Rydberg[1], A. Westman[1], M. Grudén[1], J. Platbardis[2], and P. Hallbjörner[3], [1]Uppsala University, [2]TNT Elektronik AB, [3]SP Technical Research Institute of Sweden

Session 3: MMICs and RFICs, Palaestra upper

chairman: Jan Grahn, Chalmers

13.15 65nm CMOS SOI Circuit Design for a 100Gb/s Optical SCM Transceiver, M. Salter[1], D. Platt[1], L. Pettersson[1], Lars Aspemyr[2], and M. Bao[2], [1]Acreo, [2]Ericsson

13.30 Broadband Mixer, LNA and Power Combiner in 65nm SOI CMOS, M. Salter, D. Platt, and L. Pettersson, Acreo

13.45 E-band MMIC chipset for multi-Gb/s wireless links, M. Ferndahl[1], M. Gavell[1], and H. Zirath[1,2], [1]Gotmic AB, [2]Chalmers

14.00 SiGe Bipolar Limiting Amplifier with a Bit Rate of 50 Gbit/s for Optoelectronic Receivers, S. Klinger, M. Schmidt, M. Grözing, and M. Berroth, Universität Stuttgart

14.15 Double Balanced Sub-Harmonic SiGe Mixer for the 79 GHz Automotive Band, B. Panzner#, L. Pettersson*, M. Salter*, D. Jakonis* and M. Ferndahl‡, #Otto-Von-Guericke-Universität, *Acreo, ‡Chalmers

14.30 Wideband GaN MMIC Development, J. Holmqvist, N. Billström, Saab AB

14.45 Low-phase noise InGaP HBT VCO design, D. Kuylenstierna, H. Zirath, R. Kozhuaharov, B. Hansson, I. Angelov, Chalmers

Session 4: Passive Components and RF MEMS Circuits, Kings House (Kungshuset)
chairman: Spartak Gevorgian, Chalmers

13.15 24 GHz and 35 GHz RF MEMS Phase Shifters Fabricated in a Standard GaAs MMIC Process Technology, R. Malmqvist et. al., FOI

13.27 Millimeter-Wave Switch based on Air-Gap-MEMS Switched Capacitors, A. Enayati[1,2], X. Rottenberg[1], P. Ekkels[1], W. De Raedt[1] and G. A. E. Vandenbosch[2],[1]IMEC, [2]K. U. Leuven

13.39 Using Homogenisation Methods to Calculate the Effective Permittivity when Testing Microwave Properties of Carbon NanoTubes Grown in Alumina Membrane, M. Höijer et. al., FOI

13.51 Broadband Planar Balun, T. Windahl and J. Grabs, Saab AB

14.03 Compact broadband directional coupler, J. Grabs and T. Windahl, Saab AB

14.15 Q-factor Comparisons between new GAP Waveguide Technology and Standard Rectangular Waveguide, E. Pucci et. al., Chalmers

14.27 Millimeter-Wave RF MEMS Reconfigurable High-Impedance Surfaces for Radar Applications, M. Sterner[1], D. Chicherin[2], A.V. Räisänen[2], G. Stemme[1], J. Oberhammer[1], [1]KTH, [2]Aalto University

14.39 RF MEMS Matching Networks for Frequency Tunable SiGe LNA, R. Malmqvist, FOI

14.51 $Ba_xSr_{1-x}TiO_3$ Based Solidly Mounted Tunable FBARs, A. Vorobiev and S. Gevorgian, Chalmers

15.03 Growth and RF Characterization of Multiferroic $BiFeO_3$ Films, A. Vorobiev and S. Gevorgian, Chalmers

Session 5: Digital and Mixed Signal, Main University Building
chairman: Sven Mattisson, Ericsson

13.15 A Novel FPGA-based 2.5Gbps D-QPSK Modem for High Capacity Microwave Radios, Z. He†, J. Chen‡, Y. Li‡, and H. Zirath†‡,†Chalmers, ‡Ericsson

13.30 Parabolic Synthesis Methodology, E. Hertz and P. Nilsson, Lund University

13.45 A/D Conversion for Software Defined Radio, F.Qazi, T.Sundström, S.Ahmad, J.Wikner, C.Svensson, J.Dąbrowski, Linköping University

14.00 Power Consumption in Digital Filter Architectures in 65 nm CMOS Technology, Y. Sherazi, J. Rodrigues, and P. Nilsson, Lund University

14.15 On MB OFDM-UWB Channel Estimation, J. Löfgren and P. Nilsson, Lund University

14.30 Digital Cross-Correlators: Two Approaches, E. Ryman et. al., Omnisys and Chalmers

14.45 High-Resolution Digital Backend for Superconducting Microresonators, J. Riesbeck, Omnisys

Parallel Session Papers, Wednesday March 10, 10.10-12.10

Session 8: Active Components, Palaestra lower

chairman: Gunnar Malm, KTH

10.10 An electrically tuned probe for noncontacting microwave measurements, K. Yhland[1], J. Stenarson[1] and K. Andersson[2],[1]SP Technical Research Institute of Sweden, [2]Chalmers

10.25 60 GHz Wavelet Generator for Impulse Radio Applications, M. Egard, M. Ärlelid, E. Lind, and L-E Wernersson, Lund University

10.40 Oscillator for 60 GHz Super Regenerative Receiver, M. Ärlelid, M. Egard, E. Lind, and L.-E. Wernersson, Lund University

10.55 A large-signal GaAs InGaP HBT model optimized for design of low phase-noise VCOs, S. Lai, I. Angelov, D. Kuylenstierna, R. Kozhuharov, and Herbert Zirath, Chalmers

11.10 Low-Frequency Noise in Vertical InAs Nanowire FETs with Lg=35nm, K-M Persson, E. Lind, A. Dey, C. Thelander, H. Sjöland, and L-E Wernersson, Lund University

11.25 Characterization of graphene-based field-effect transistors, S. Bevilacqua et. al., Chalmers

11.40 Cryogenic behaviour of InAs/AlSb HEMTs for low-noise amplifiers, G. Moschetti et. al., Chalmers

11.55 Linear and non-linear frequency modulation up to 3.2 GHz in nanocontact spin torque oscillators, P. K. Muduli et. al., KTH

Session 9: Antennas, EMC and Measurement Technology, Palaestra upper

chairman: Anders Rydberg, Uppsala University

10.10 Microwave breakdown in space borne RF equipment, J. Rasch et. al., Chalmers

10.25 Concept of Gap Waveguide and Measured Results for First Demonstrator, A. U. Zaman et. al, Chalmers

10.40 Comparison of Diversity Gains of Wideband Antennas Measured in Anechoic and Reverberation Chambers, X. Chen, N. Jamaly, J. Carlsson, J. Yang, P.-S. Kildal, and A. Hussain, Chalmers

10.55 Design of Cryogenic 2-14 GHz Eleven Feed for Reflector Antennas for Future Radio Telescopes, J. Yang et. al., Chalmers

11.10 Vulnerability of Radio Technologies Used in Wireless Industry Automation, J. Chilo[1] and P. Stenumgaard[1,2], [1]University of Gävle, [2]FOI

11.25 Multipath Environment Simulator for evaluation of Terminals, N. Jamaly, J. Carlsson and P.-S. Kildal, Chalmers

11.40 Low-profile directive antenna using metamaterial slab for RFID tags, X. Hu[1,2], A. Rydberg[2], [1]Zhejiang University, China, [2]Uppsala University

11.55 Characterization of Active Beamforming Phased-Array Feeds for the Next Generation Radio Telescopes: Numerical Modeling and Experimental Verification, M. Ivashina, Netherlands Institute for Radio Astronomy (ASTRON)

Session 10: THz Technology, Kings House (Kungshuset)
chairman: Staffan Rudner, FOI

10.10 340 GHz GaAs monolithic membrane supported Schottky diode circuits, H. Zhao et. al. Chalmers

10.22 Investigation of harmonic generation in suspended graphene, O. Habibpour, S. Cherednichenko, J. Vukusic , and J. Stake, Chalmers

10.34 RF sensor for face recognition behind masking, J. Svedin et. al., FOI

10.46 A 210 GHz radar system for 3D stand-off detection, J. Svedin et. al., FOI

10.58 Assessment of Various Epitaxial Lift-off Methods for Heterostructure Barrier Varactor, M. Dastjerdi , A. Sanz-Velasco, J. Vukusic, and J. Stake, Chalmers

11.10 Development of a 0.6 THz HBV frequency tripler, J. Liljedahl, T. Bryllert, J. Vukusic and J. Stake, Chalmers

11.22 A Compact 340 GHz Heterodyne Imaging System, R. Dahlbäck et. al., Chalmers

11.34 Investigation of passivation methods for HBV diodes, A. Malko, J. Liljedahl, J. Stake, J. Vukusic and T. Bryllert, Chalmers

11.46 Multipixel terahertz receivers, S.Cherednichenko, V.Drakinskiy, and W.Wei, Chalmers

11.58 Near Field Terahertz Imaging for Biological Tissue Measurements , J. Hjerdt, M. Grudén, A. Rydberg, T. Ekegren and J. Bergqvist, Uppsala University

Session 11: Modules and Packaging, Main University Building
chairman: Hans-Olof Vickes, Saab Microwave Systems

10.10 Microwave Filters Suitable for Pick-and-Place Mounting, S. Kristiansson and H.-O. Vickes, Saab

10.22 Packaging of Microstrip Circuits using GAP Waveguide Approach, E. Rajo-Iglesias et. al., Chalmers and Universidad Carlos III de Madrid

10.34 Single and Dual Fundamental Wideband Surface Mount VCO's covering 2-25 GHz, R. Christoffersen[1], S. Gunnarsson[1,2], A. Brandt[1], C. Stoij[1], and D. Kuylenstierna[2], [1]Sivers IMA, [2]Chalmers

10.46 Embedded Circulators and Isolators with LTCC Compatible Ferrite Tapes, T. Jensen and V. Krozer, DTU

10.58 60GHz Si integrated cavity oscillator, D. Dancila[1,2], X. Rottenberg [1], H.A.C. Tilmans[1], W. De Raedt [1] and I. Huynen[2], [1]IMEC/SSET, [2]UCL/EMIC

11.10 Ultra low-noise HEMT amplifiers at cryogenic temperatures, J. Grahn et. al., Chalmers

11.22 Cryogenic 2-14GHz low noise receiver for radio astronomy based on Eleven feed, M. Pantaleev et. al., Onsala Space Observatory, Chalmers

11.34 A 24 GHz SOP VCO with 20 % tuning range, M. Törmänen and H. Sjöland, Lund University

11.46 Six-Port Multi-Gigabit Receiver, J. Östh[1], A. Serban[1], Owais[1], M. Karlsson[1], S. Gong[1], J. Haartsen[2] and Peter Karlsson[2], [1]Linköping University,[2]Sony Ericsson

11.58 Six-Port Direct Carrier Modulator at 7.5 GHz, A. Serban[1], J. Östh[1], Owais[1], M. Karlsson[1], S. Gong[1], J. Haartsen[2] and Peter Karlsson[2], [1]Linköping University,[2]Sony Ericsson

Program Committee GigaHertz Symposium 2010

Prof. Henrik Sjöland (General Chairman)	Lund University and Ericsson Research
Prof. Spartak Gevorgian	Chalmers and Ericsson Research
Prof. Jan Grahn	Chalmers
Dr. Mats Gustafsson	Lund University
Dr. Tom K. Johansen	Denmark Technical University
Dr. Niclas Keskitalo	Ericsson and University of Gävle
Prof. Viktor Krozer	Denmark Technical University
Dr. Thomas Lewin	Ericsson Research
Dr. Gunnar Malm	Royal Institute of Technology (KTH)
Prof. Sven Mattisson	Ericsson Research and Lund University
Prof. Staffan Rudner	Swedish Defence Research Agency (FOI)
Prof. Anders Rydberg	Uppsala University
Dr. Per Sjöstrand	Saab
Prof. Lars-Erik Wernersson	Lund University
Prof. Hans-Olof Vickes	Saab Microwave Systems
Dr. Klas Yhland	SP Technical Research Institute of Sweden

Invited Speakers at GigaHertz Symposium 2010

Prof. Tim Ashely, QinetiQ
Indium antimonide based high-speed transistors for low power dissipation applications

Mr. Richard Breiter, Nokia
Trends and Future Challenges in Antenna Design for Smart Phones

Mr. Martin Isberg, ST-Ericsson
RF Integration Trends in Mobile Phones

Dr. Baudouin Martineau, ST
Millimeter wave design in bulk and SOI CMOS

Prof. Peter Siegel, Caltech
THz in Space Science, Biology and Medicine

Prof. Lars Sundström, Ericsson Research
Carrier Aggregation - Another RF Design Challenge

Prof. Franz-J. Tegude, University of Duisburg-Essen
III-V-Nanowire FET for Low-Power RF-Applications: Approaches and Results

Table of Contents

Session 1

10.00-12.00 Tuesday 9 March 2010

GigaHertz 2010, Lund, 9/10 March 2010

Invited Paper

III-V-Nanowire FET for Low-Power RF-Applications: Approaches and Results

Franz-J. Tegude, Univ. Duisburg-Essen
Solid State Electronics Department

Nanowire fieldeffect transistors (NW-FET) are a straight forward continuation of downscaling in microelectronics. Further, because of their excellent transport properties, III-V-semiconductor materials have demonstrated record high frequency potential. This contribution addresses homo- and heterostructure InAs-n-channel MISFET prepared by a bottom-up approach, employing the vapor-liquid-solid (VLS) epitaxial growth mode and using different gate dielectrics. Single and multi NW arrangements are processed yielding gate lengths in the sub-micrometer range. Due to the nanometer scale two aspects become core problems with respect to FET device performance and characterisation: parasitics, and mismatch to nearly exclusively used 50 Ohm rf measurement environment. Transit frequencies of about 10 GHz and f_{max} values in excess of 20 GHz are presented, together with deembedding techniques, to yield intrinsic and parasitic device parameters. In addition, rf characteristics are used for transport data evaluation, because standard methods like Hall characterisation are not immediately applicable to nanowire geometry. Modelling and technological approaches for the fabrication of simple fundamental circuits, including also highly functional tunnelling structures, will be addressed.

Trends and Future Challenges in Antenna Design for Smart Phones

Richard Breiter, Nokia Devices R&D, Symbian Antenna Solutions, richard.breiter@nokia.com

The talk will focus on the challenges and opportunities in the coming 5 years in the area of antennas for mobile devices and the antenna innovations needed to solve the technical challenges and to improve the consumer experience of the devices with its associated services and applications. The trend is that mobile devices have to support an increasing amount of wireless systems and frequency bands. During 2009 we have seen mobile devices with various cellular systems (GSM, WCDMA, CDMA, etc.) and frequency bands (4 GSM bands, 5 WCDMA bands, etc.). On the non-cellular system side, we have seen mobile devices with GPS, BT, WLAN, NFC, FM Tx, internal FM Rx, DVB-H, etc. The trend will for sure continue - with LTE being one of the next key systems - and at the same time we will also see a greater need to have all/many of these wireless systems and frequency bands in the very same device. If we add a new antenna each time we add a new system or frequency band, a mobile device will soon be over-crowed with antennas taking up too much space and a metal cover device will end up looking like a Swiss cheese. This leads to a need for smart holistic solutions and innovations to enable 20+ frequency bands and 15+ wireless systems in 2015 devices.

One thing is to enable the functionality of these systems and to support all the frequency bands, another thing is to ensure the right performance levels enabling excellent consumer experience for the different services and applications in small beautiful mobile devices. With new services and applications, excellent radiated performance is not just needed in voice mode but also in e.g. internet browsing-, navigation-, gaming- and paring/sharing mode. As the cellular data traffic is growing and there is a need for being connected everywhere, radiated cellular performance will continue to play an important role for both consumers (in terms of e.g. dropped calls and data speed) and not at least for operators (in terms of e.g. network coverage and capacity).

Smart solutions will not only rely on traditional antenna radiator innovations; antenna design in 2015 will to a much larger extend include system, HW and SW elements. Emerging technologies, such as low loss tunable capacitors, will play an important role in enabling new and smarter antenna solutions.

The ultimate antenna solution could consist of an intelligent system and a few reconfigurable antennas each being able to work with every system in any frequency band. Given the use cases (being the systems in use, the data needs, how the user interacts with the devices, etc.) the system will adaptively and seamlessly configure all the antennas for overall best performance. To enable all this and due to the challenges ahead of us, competences, research and innovations are needed within the area of antenna technologies for mobile devices – not only from companies like Nokia, but also from universities, research institutes and suppliers.

Development and Application of an Active Microwave System for Medical Imaging

Vitaliy Zhurbenko, Tonny Rubæk, and Viktor Krozer

Technical University of Denmark, Ørsteds Plads Building 348, 2800 Kgs. Lyngby, Denmark. vz@elektro.dtu.dk

Over the last few decades, there has been a significant increase in demands for the diagnostic instruments for medical screening, and breast cancer detection in particular. Statistics published by the Cancer Research UK organisation indicates that the breast-cancer incidence rates have increased by more than fifty percent over the last twenty-five years. Worldwide, more than a million woman are diagnosed with breast cancer every year, making it the most common cancer and the second leading cause of cancer-deaths among women today. The early detection of this type of cancer greatly improves the chances of successful treatment and survival.

Contemporary breast-cancer screening and diagnosis techniques consist primarily of mammography, ultrasonography, and magnetic resonance imaging. Despite their proven efficiency, these techniques are compromised by high recall rates and a low positive predictive value due to their limited sensitivity, especially in the case of young women with dense breasts. Many technical, biological and pathophysiological issues associated with breast cancer detection still remain unsolved, and the high incidence of breast cancer continues to represent an important challenge for the mentioned conventional modalities. This acute problem has motivated the research community to improve the existing breast screening tools and to develop alternative or complimentary diagnostic systems to the widely used X ray mammography. The goal of the efforts is to build a low health-risk, fast, sensitive, and noninvasive diagnostic device, capable of detecting breast tumors with minimum discomfort for the patient irrespective of their age and breast density.

Research over the last years has revealed that microwave imaging can be an accurate method for breast cancer detection. In addition, microwave imaging is a nonionizing and noninvasive modality and does not require breast compression. Among the various alternative breast imaging modalities being pursued to improve breast cancer detection, microwave imaging is attractive due to the high dielectric property contrast between the cancerous and normal tissue.

In this work, the research and development of a microwave imaging system designed to reconstruct the dielectric properties of the female breast is presented. A brief review of the ongoing research in the field of microwave imaging of biological tissues is given, with major focus on the breast tumor detection application. Within the various microwave imaging techniques under development, the active frequency domain method is found to be one of the most promising and is chosen as a basis for the development of the imaging instrument. The active frequency domain method allows for a wide dynamic range, which is important for image quality. It is based on the measurement of the complex transmission coefficient in several directions through the imaging domain which contains the biological object to be imaged (the breast). This data is then used to reconstruct an image, which consists of a spatial distribution of the complex permittivity in the imaging domain. Using this image, the cancer tissue can be detected due to its dielectric property contrast compared to normal tissue. The image-reconstruction algorithm used in the microwave imaging system is based on nonlinear inverse scattering. The forward problem is solved using the method of moments. The minimization is performed using an iterative Newton-type algorithm.

The instrument employs a multichannel high sensitive superheterodyne architecture, enabling parallel coherent measurements. In this way, mechanical scanning, which is commonly used in measurements of an electromagnetic field distribution, is avoided. The system is capable of acquiring three-dimensional images and provides comparatively short acquisition time which is important for patient comfort.

The performance of the system is investigated by an analysis of the accuracy of the amplitude and phase measurements as well as by image reconstruction experiments.

Towards an integrated transceiver: GaN MMIC processing and design at Chalmers

Christer Andersson, Kristoffer Andersson, Martin Fagerlind, Anna Malmros, Niclas Ejebjörk, Mattias Thorsell, Niklas Rorsman

Microwave Electronics Laboratory, Chalmers University of Technology
SE-412 96 Göteborg

GaN based HEMTS, based on the AlGaN /GaN heterostructures, offer new possibilities in the design of transmit and receive modules (transceivers). GaN microwave semiconductor technology has characteristics which are suitable for applications where both high breakdown electric fields and low losses are of importance.

At the Microwave Electronics Laboratory at Chalmers University of Technology we have activities in the wide bandgap microwave area which includes:

- Application specific optimization of GaN HEMTs (material, device design, processes)
- Modelling (TCAD and electrical)
- Characterization of WBG devices (s-parameters, LSNA, load-pull)
- Circuit design
- MMIC processing

Examples of on-going sub-projects are:

1. SiC varactor

SiC Schottky diode varactors for high RF power load modulation is developed. This application requires high capacitance tuning range at high RF power levels, high breakdown voltage, high Q-factors. The first varactors varactors were inserted in anti-series into a pulse-width modulated class-E amplifier output matching network

The amplifier exhibited 3W peak output power at 2GHz with 60% constant drain efficiency over a 6dB dynamic range.

2. Ta ohmic contacts on GaN

A new type of ohmic contact metallization is developed. The contacts are based on Tantal. The advantage with this metallization is lower anneal temperature, better thermal stability, and better morphology (edge definition)

3. AlGaN/GaN Passivations

The passivation is very important for the performance of GaN-based HEMTs. LPCVD silicon nitride is currenly being developed at Chalmers with good results.

4. GaN-based integrated circuits(MMICs)

One of the major efforts at Chalmers is the design and fabrication of MMICs. The picture below shows an integrated transceiver (LNA+switch+power amplifier).

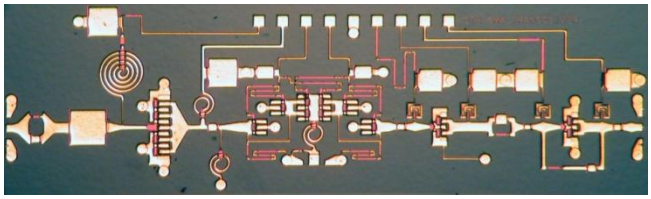

A micrograph of a a integrated transceiver.

Acknowledgement: This research has been carried out in the Microwave Wide Bandgap Technology project financed by Swedish Governmental Agency of Innovation Systems (VINNOVA), Swedish Energy Agency (STEM) Chalmers University of Technology, Ericsson AB, Furuno Electric Co., Ltd., Infineon AG, Norse Semiconductor Laboratories AB, Norstel AB, NXP Semiconductors BV, and Saab AB.

Session 2

13.15-15.15 Tuesday 9 March 2010

Experimental System and Simulations of a Vertical SAR

Per-Olov Frölind, Andreas Gustafsson, Lars Pettersson, Patrick Andersson, and Jan Svedin
Swedish Defence Research Agency, FOI, P. O. Box 1165, SE-581 11 Linköping, Sweden
per-olov.frolind@foi.se

There is an interest for exploiting radar imaging for surveillance and mapping of urban and topographic terrain. A vision of down-looking small systems is in mind, see Fig.1. The radar is pointed in a vertical direction to enable to look into narrow canyons found in urban or topographic terrain [1]. For obtaining the imaging resolution we exploit the radar range registration for height information, antenna size in the cross-flight direction and synthetic aperture in the flight direction. Thus, we obtain a 3D image of horizontal coordinates (x-y) and height coordinates(z).

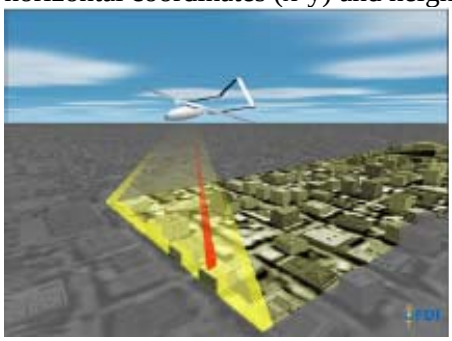

Fig.1. Vision of 3D radar imaging of an urban environment.

One of the challenges is to achieve cross-flight resolution and coverage, defined by the antenna size and beam directivity. A conventional antenna array solution will include several antenna elements and be very large and complex. A suggestion is to design an antenna array with reduced antenna elements by thinning the receiver elements traded by the number of transmitter elements, see Fig.2. [1]

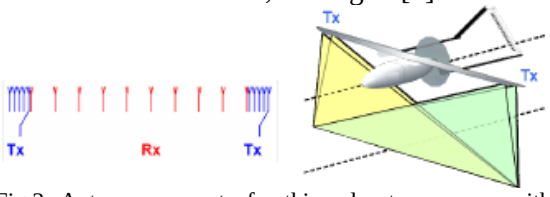

Fig.2. Antenna concept of a thinned antenna array with a set of transmitters (Tx) and receiver antenna elements (Rx) mounted along the wings.

An experimental setup has been put in place for development and evaluation of antenna array configurations. The setup is constructed with a xy-table to obtain two perpendicular axes for movable antenna positions. The accuracy of the positioning is in order of 50 micrometer, and the travelling range is 2 by 1 meter. The transmitter always follows the antenna receiver array movement in the x-, flight, direction, see Fig.3. The system includes a FMCW transceiver from SIVERSIMA operating at 23-26 GHz and horn antennas which are manufactured in-house at FOI.

Fig.3. The experimental setup xy-table, with x and y travelling ranges of 2 and 1 meter, respectively.

Measurements have been performed in order to calibrate and parameterise the experimental system using well defined calibration targets, such as corner-reflectors. In the future the system will be used for testing different antenna configurations and asses the corresponding image quality in terms of resolution and side lobe levels.

In parallel simulations have been performed for different antenna configurations which will be confirmed in measurements using the experimental setup. An example of simulation result of a point target 3D impulse response is shown in Fig.4.

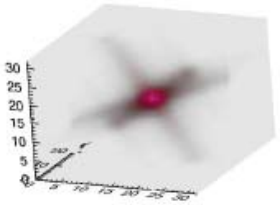

Fig.4. A 3D simulation result of a point reflector.

Thus, an experimental setup have been design and built for conducting illustrative 3D radar measurements results. A signal processing scheme is developed for generating 3D high resolution images based on the registered radar data. We foresee a parallel development of the simulation scenarios and the real measurements where appropriate.

References:

[1] FOI-D--0337 *"System concepts for 3D-radar"*, March 2009

System Design for Solid State S-Band Marine Radar

Anders Nelander, Börje Carlegrim, Rolf Jonsson
Swedish Defence Research Agency (FOI)
Linköping, Sweden
anders.nelander@foi.se

Marine radars have usually been designed with magnetron transmitters, rotating waveguide array antennas, non-coherent receivers in transceiver units and separate processing and display units. Marine radar is heavily regulated for safety reasons. Apart from regulations, low cost and high reliability are important factors for shipping customers. Present marine radars typically need to replace the magnetron transmitter every year. However, new developments in solid state components and new requirements from spectrum regulations have increased the need for new designs and implementations.

This paper describes the cooperative development work of FOI and Consilium Marine & Safety to design new marine radar systems that have improved performance and conform to the new regulations. This work is performed within the FOCUS Centre of Excellence to explore new possibilities in sensor technology and sensor related research at FOI.

The new design should use semiconductor based power amplifiers to allow better reliability and lower life cycle cost. The small target detection performance should be increased by coherent Doppler processing and diversity techniques. The out of band emissions from the transmitter should be decreased to conform to the requirements for communications and other adjacent band spectrum users. The short range coverage should be as small as possible to enhance near target ranging. The sea clutter should be suppressed by Doppler filtering. Pulse compression should be used to enhance range resolution.

The proposed waveform in the figure below is a multiple pulse length waveform with NLFM pulse compression to get the desired range resolutions and range coverage. This waveform requires a 200 W peak power transmitter. A special requirement is the minimum short range coverage of 40 m which means that the shortest pulses must be less than about 200 ns pulse length. The proposed waveform starts with four short 0.2 µs pulses in the first time frame of 150 µs. The next two time frames contain two medium length 12 µs pulses. The next time frame contains one long 120 µs pulse and the final four time frames contain the long pulse receive interval. This gives a pulse burst repetition interval of 1200 µs.

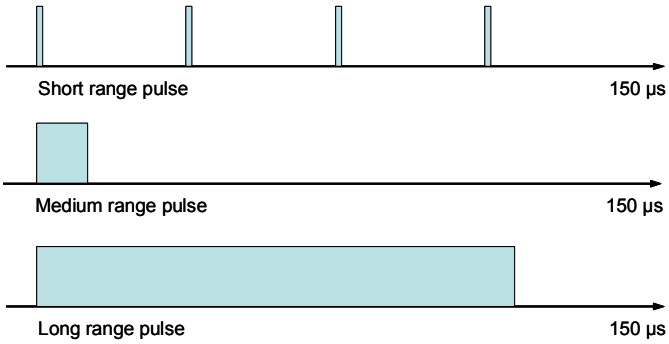

For the design of a semiconductor based RF power amplifier, several types of materials and components are available. Our choice is a Si based bipolar solution with four stages. The experimental breadboard power amplifier is shown in the figure below. The RF power amplifier is built form commercial transistor modules with additional matching networks. The class C operation means that the output power is very sensitive to the input power level and the leakage signal from the up conversion between pulses is quite small. The complete power amplifier has a power consumption of 85 W and an average output power of 24 W at 12% duty cycle, leaving about 60 W to be dissipated as heat. The peak output power is 200 W. The pulse rise time seems to be influenced by two different processes. First, there is a relatively rapid rise to 70% of the maximum output power in less than 100 ns. After the initial increase, the output power continues to increase so that the 10-90% rise time becomes 2.5 µs, and this is most likely a thermal process. The fall time is about 5 ns and it is more critical for transmit receive switching. The rise time and the fall time affects the transmit signal spectrum as well as other transient effects and spurious signals between pulses.

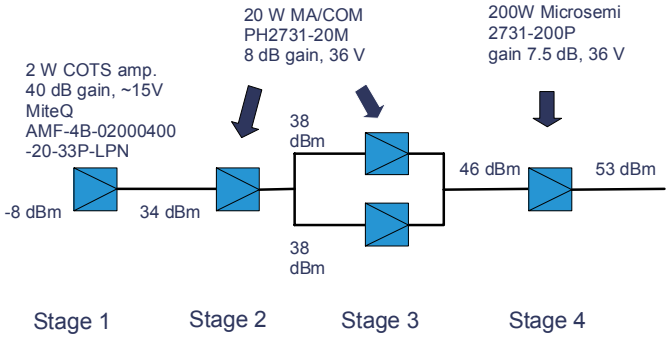

UWB Ranging Hardware Platform

Alessio De Angelis[1◇], *John-Olof Nilsson*[2], *Isaac Skog*[2], *Peter Händel*[2]
[1]Department of Electronic and Information Engineering, University of Perugia, Italy
[2]Signal Processing Lab, ACCESS Linnaeus Center, Royal Institute of Technology, Stockholm, Sweden
[◇]deangelis@diei.unipg.it

Introduction

This paper describes a research activity focused on the development of an indoor positioning and navigation platform using Ultra Wide Band (UWB) signals. Extended descriptions of the system and experimental results have been presented in [1] and [2]. The fine time resolution of the UWB pulses, allowing for centimeter-order ranging accuracy and multipath mitigation, represents the main motivation for their use in indoor positioning applications.

System architecture

The realized system measures the Round-Trip Time of UWB pulses propagating between a master unit and several active responders, indicated as slaves. For the prototype implementation, a baseband pulse generator based on a Step Recovery Diode (SRD) has been built [3], the schematic is shown in Fig. 1.

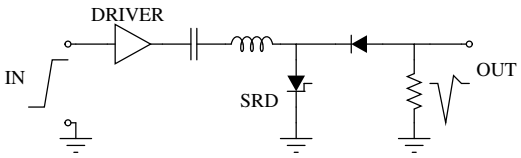

Figure 1: SRD pulse generator diagram.

This circuit provides a 9 V pulse with a rise time of about 680 ns and 300 ps fall time. The pulse 10-dB bandwidth is about 500 MHz. Furthermore, pulse detection is performed by means of a non-coherent energy detector approach. Finally, the employed Time-to-Digital Converter (TDC) commercial integrated circuit measures the Round-Trip-Time with a rms accuracy of 50 ps. Fig. 2(a) shows the block diagram of the master device, while a photo of the realized prototype is shown in Fig. 2(b).

Experimental results

If the slaves are placed in known positions, the master is capable of self-localization. The results of a static position measurement experiment are shown in Fig. 3.

The platform has been employed for the development of a sensor-fusion approach, to integrate UWB positioning with Inertial Navigation, see [1] and [2].

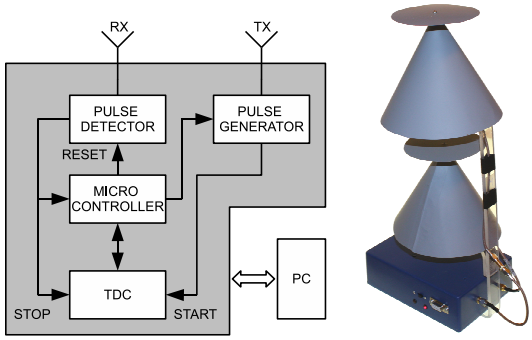

Figure 2: (a) block diagram of the master device, (b) picture of the realized prototype.

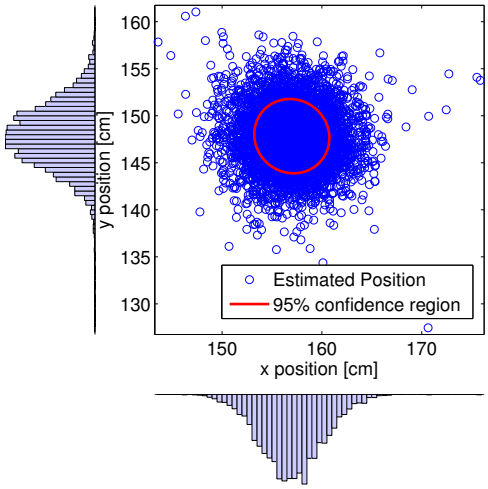

Figure 3: Static positioning experimental results.

References

[1] A. De Angelis, J. O. Nilsson, I. Skog, P. Händel, and P. Carbone. Indoor positioning by ultra wideband radio aided inertial navigation. In *XIX IMEKO World Congress*, Lisbon, Portugal, Sept. 6-11 2009.

[2] J. O. Nilsson, A. De Angelis, I. Skog, P. Carbone, and P. Händel. Signal processing issues in indoor positioning by ultra wideband radio aided inertial navigation. In *17th EUSIPCO*, Glasgow, Scotland, Aug. 24 -28 2009.

[3] A. De Angelis, M. Dionigi, R. Giglietti and P. Carbone. Experimental Low-Cost Short Pulse Generators, *IEEE I2MTC 2008*, Victoria, BC, Canada, May 12-15, 2008.

Model-Based Adaptation of RF Power Amplifiers

Thomas Eriksson[1], Ali Soltani[1] and Christian Fager[2]
[1]Department of Signals and Systems [2]Department of Microtechnology and Nanoscience
Chalmers University of Technology, Göteborg, Sweden
{ thomase, christian.fager, asoltani }@chalmers.se

Abstract: Digital predistortion is a common method to compensate for nonlinear and memory effects in power amplifier. Since amplifier characteristics is drifting with time and temperature, it is often necessary to adapt the predistorter to varying operating conditions. We propose the use of *model-based adaptation*, where a model of the drift as a function of amplifier load is used to speed up adaptation considerably.

I. Introduction

Today, it is common to digitally predistort (DPD) power amplifiers in order to compensate for undesired linear and nonlinear effects inherent in the circuitry. In order to find an appropriate pre-distorter, off-line identification can be performed. However, since the amplifier can be expected to show temperature and aging drift, it is usually necessary to adapt the predistorter to the changing conditions.

The state-of-the-art algorithms today are usually based on a feedback chain where the output of the amplifier is measured, and the measured data used in an adaptation algorithm to dynamically change the parameter values of the DPD. With such algorithms, the time constant of the adaptation may be in the order of several one-hundredths, or even one-tenths, of a second. The algorithms are *reactive*, in the sense that they react on a changed characteristic when it is already a fact.

We propose the use of *model-based adaptation* of pre-distorters. By studying the dynamic behavior of the amplifier as a function of temperature (and age), it is possible to introduce models for the behavior, and from the models fast adaptation algorithms can be derived. We focus mainly on the connection between the amplifier load conditions and the temperature changes that will introduce parameter drift in the predistorter, but it is straightforward to extend the theory to cases where processes other than load conditions cause temperature changes, or where external events directly affect the amplifier characteristics. The model-based approach allows the adaptation algorithm to be *proactive*, and adapt to changing operating conditions before they have lead to a change of amplifier characteristics. A block diagram of the proposed solution is illustrated in Figure 1, where we show a system where the adaptation is built on a linear combination of the model-based estimate T and the feedback z.

II. Simulation Results

In Figure 2, we show a simulated sequence of power spectrum densities of the output of an amplifier using a standard adaptation algorithm (top) and the proposed algorithm (bottom), when the output power is rapidly changed. In the standard case, the out-of-band distortion shows a considerable increase before the adaptation kicks in, while in the model-based case the out-of-band distortion remains quite small even during the sudden power shift.

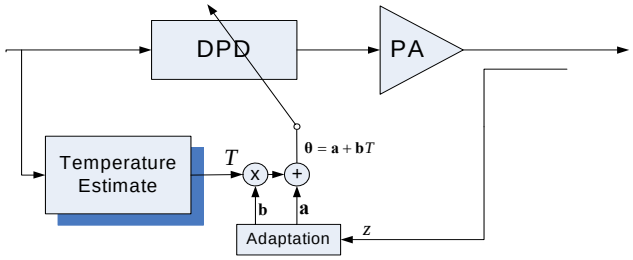

Fig. 1. A block diagram of a model-based adaptation algorithm, where a model of the temperature gives a proactive adaptation. Some adaptation from the feedback signal z is still needed, but to a lower degree.

III. Conclusion

We study model-based adaptation algorithms, and show that they can substantially improve the adaptation speed, mainly due to the possibility of proactive adaptation. Our simulations show that large gains can potentially be achieved, but measurements on real amplifier still remains to be done.

IV. Acknowledgement

This research has been carried out in the GigaHertz Centre in a joint research project financed by Swedish Governmental Agency of Innovation Systems (VINNOVA), Chalmers University of Technology, and Ericsson AB, Infineon Technologies, and NXP Semiconductors.

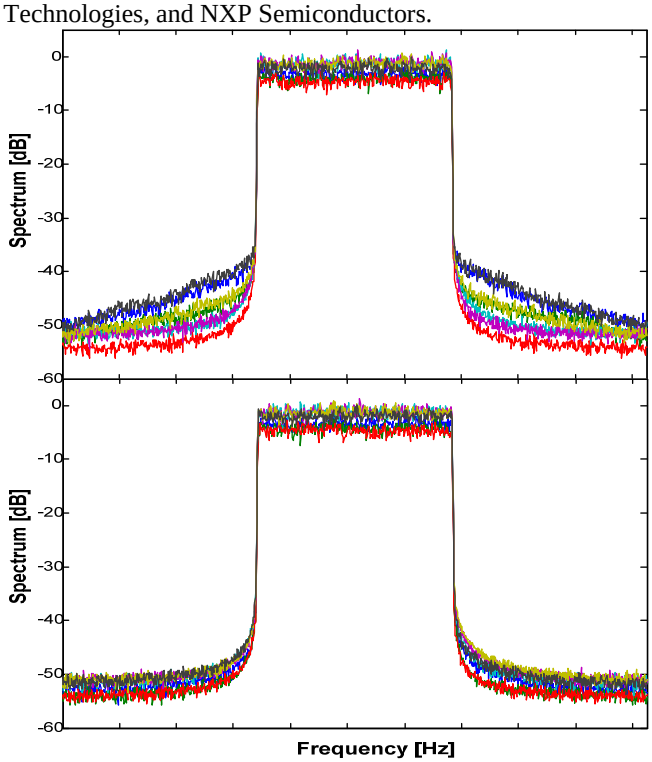

Fig. 2. A sequence of power spectrum density plots (different colors) for a signal where the input power level changes rapidly. We see a high out-of-band distortion for a while with the standard algorithm (top), while the distortion stays much lower for the model-based adaptation algorithm.

M-Sequence UWB Radar for Industrial Applications

Daniel Andersson[#], Kjell Wallin[#], Otar Javashvili[*] and Claes Beckman[*]

[#]*Radarbolaget*
Nobelvägen 1
801 76 Gävle, Sweden

[*]*Center for RF-Measurement Technology*
University of Gävle
801 76 Gävle, Sweden

Ultra Wideband Radar has the potential of dramatically improving the control and surveillance of industrial processes in confined areas. An example is the application of UWB radar for surveillance of furnaces for heath treatment of steel billets developed by Radarbolaget in Gävle.

In our installation at AB Sandvik Materials Technology, we have shown that by using a non-destructive UWB Radar technique it is possible to visualize in real-time the ongoing process inside the furnace behind a 0.5 m thick ceramic wall. Since the operating temperature inside the furnace is 1200 °C, there is today no other known method capable of visualizing the process for the operator of the furnace. The system is therefore designed to sustain high temperatures and powerful electromagnetic disturbances while performing measurement with wide dynamics and high stability.

The design of this radar is based on the idea of transmitting a continuous m-sequence and then detecting the correlated impulse response (see figure below). The wide bandwidth is a requirement for obtaining high spatial accuracy and resolution but puts further requirements on the design of the antennas and the electronics. Our results show that with this technique it is possible to determine the deformation of the steel billets inside the furnace with an accuracy of less than 5 mm. The radar system is also able to detect deformations in the furnace wall

The m-sequence radar has many advantages over other UWB radar technologies since it e.g. does not require many analogue components. Its performance is a result of the choice of code length, sampling rate and averaging. However, the resolution is still limited by the impulse response of the analogue antenna (ringing).

In this paper system parameters that affect the overall performance of an m-sequence radar are reviewed and means of enhancing its performance are discussed.

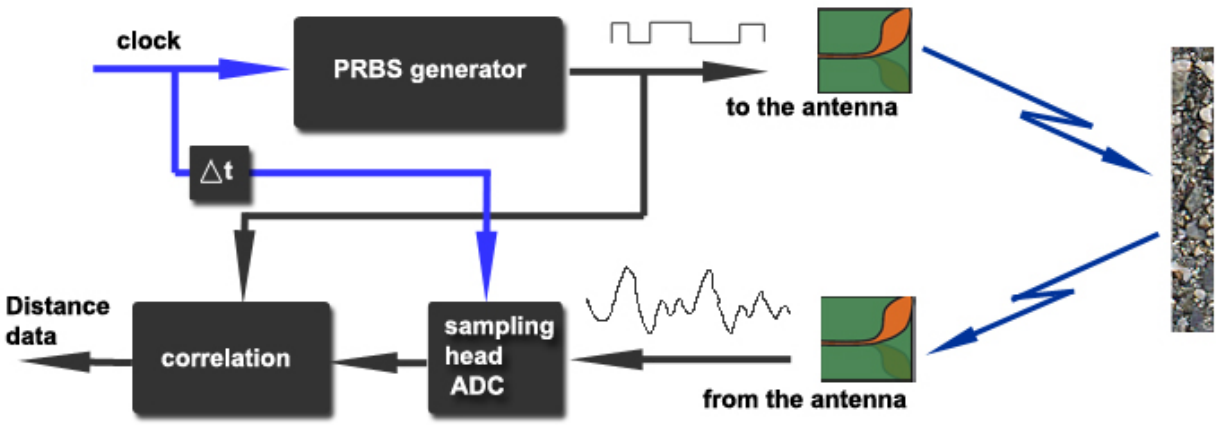

Fig. Schematic illustration of an m-sequence UWB radar

Wireless Body Area Networks (WBANs) and Efficient, Energy Conservative Designs

Magnus Jobs and Anders Rydberg
Uppsala University, Department of Engineering Sciences, Signals and Systems Group
Box 534, SE-751 21 Uppsala, Sweden

Recent technological advances in areas like wireless communication, mobile computing, electronics, sensing and information technologies have led to the emergence of low power miniaturized smart wireless sensor devices or “motes”. One important new field is in Wireless Body Area Networks (WBAN).

A WBAN prototype system has been evaluated consisting of 5 to 9 sensors using 802.15.4 ZigBee based sensor-nodes with 3-axis accelerometers and temperature sensors, coupled to knowledge of sensor placement. These were connected wirelessly to a Linux based personal server (PS) and allowed for an extraction of 80% of the subjects current posture [1].

Figure 1 displays data collected from a custom made ZigBee based WBAN. The data displays the current posture of the subject and is used to illustrate some of the data a WBAN system can provide. Even though some information like the direction of the shoulder joint is impossible to define exactly without known calibration of the accelerometer data the system can still provide useful data.

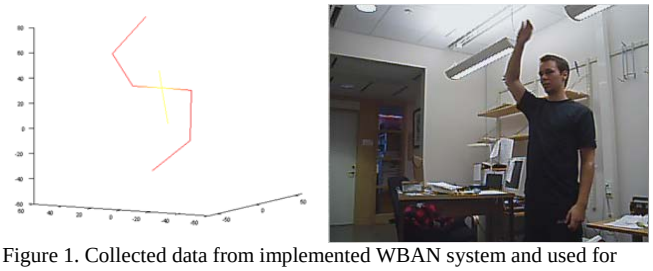

Figure 1. Collected data from implemented WBAN system and used for posture evaluation.

The receiver in a wireless module has a limit in sensitivity and thus the maximum amount of losses between output signal and received signal is important. Antennas that do not have an isotropic radiation pattern will introduce a potentially large variation into the system. A body worn system based on such an antenna will generate its own potentially fast fading channel. As seen in Fig. 2 these kinds of losses places the maximum distance in a range that could very well be reached in a WBAN system. Therefore, a WBAN system should avoid using antennas with a large directivity in order to reduce variation in receiver and transmitter gain. Some of the worst path loss scenarios can be counteracted by the use of diversity techniques. Using two or more antennas with good diversity gain fading dips due to multipath effects can be reduced as well as the possibility of combating sharp nulls from the receiver antenna.

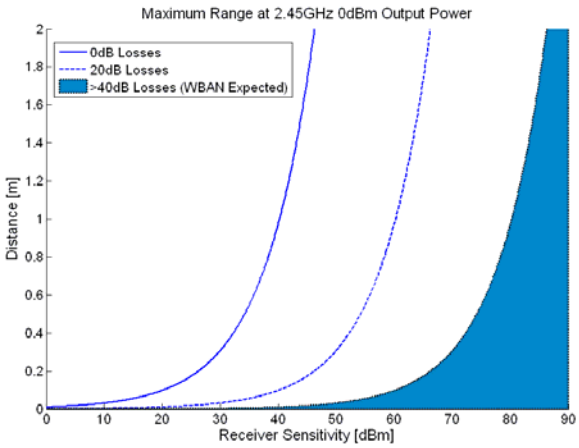

Figure 2. Maximum range between two nodes with 0dBm output power, losses include potential antenna gain variations.

The decision to include some form of diversity will have to be carefully weighed against the size constraints as well as the potential increase in power consumption. The increased power consumption due to diversity implementation cannot be set equivalent to simply increasing the transmitted output power or receiver sensitivity, as a receiver diversity implementation could combat deep fading dips which would have been too low to receive even with a higher transmitted power and receiver sensitivity.
If a multihop communication scheme is considered for implementation, it is important to consider the several factors covering including, but not limited to, the cost of transmitting over a relaying node from a pure transmission perspective [2].

References:
1. M. Jobs, B. Jaff, F. Lantz, B. Lewin, E. Jansson, J. Antoni, K. Brunberg, P. Hallbjörner and A. Rydberg, ”Wireless Body Area Network(WBAN) Monitoring Application System(MASS) for Personal Monitoring”, 6th edition of the International Workshop on Wearable Micro and Nano Technologies for Personalised Health (pHealth 2009), Oslo, Norway, 24 - 26 June, 2009
2. Erik Björnemo “Energy Constrained Wireless Sensor Networks: Communication principles and sensing aspects”. PhD Thesis, Uppsala University, ISBN 978-91-506-2043-6, January 2009.

Techniques for Communication Robustness in Train Environment

Anders Rydberg[1], Alexander Westman[1], Mathias Grudén[1], Janis Platbardis[2], Paul Hallbjörner[3].
[1]Uppsala University, Signals and Systems, Box 534, 751 21 Uppsala, Sweden (anders.rydberg@angstrom.uu.se)
[2]TNT Elektronik AB, Säter, Sweden
[3] SP Technical Research Institute of Sweden, Borås, Sweden

Introduction: At the moment there are only stationary detectors detecting warm ball bearings onboard trains in Sweden [1]. The detectors are placed next to the railway and is connected by wires to a surveillance central which in case of an alarm will stop the train. Even though there are detectors beside the track many of the railroad vehicles have problems with overheated bearings and emergent stops. Therefore it is of importance to mount wireless sensor network onboard the wagon to monitor the ball bearings continuously. If this is done there is also a chance to perform trend analysis to do proactive maintenance.

When applying a wireless network in a new environment it is important to know the radio propagation behavior. A long run test have been performed earlier to investigate the wave propagation and also to see if it is possible to have wireless sensors onboard the train [2]. The train environment is both a very harsh environment regarding the radio (much metal) and the physical with dirt and accelerations and shocks up to 300 G's [3]. The field trials have been performed during October and November in 2008. The wireless sensor network was consisting of 4 sensors which were mounted outside the wagon and one internet gateway inside the wagon. The wagon used in the experiment is owned by Banverket and is used to measure the wear and tear of the railway in Sweden and Denmark, see Fig. 1. During the measurements simple monopole antennas were used to obtain a well known radiation pattern. After the tests it was possible to extract all measured data from the database where everything was stored. It was found that many of the messages were lost during transmission. Depending of the sensor between 8% and 70% of the messages were lost which is too many lost messages if a stable and robust wireless connection is needed. Therefore it is necessary to improve this communication links. This can be performed by introducing diversity into the system. Mainly there are two different diversity types spatial, and polarization. In the case of the wireless sensor network onboard the train it is possible to have both spatial diversity and polarization diversity. By introducing diversity there is an expected throughput close to 100%.

Fig 1. Banverkets measuring wagon during a visit in Uppsala.

The drawback with a diversity system is the use of energy. There is generally a need for energy conserving sensor nodes. In the train environment it is a need for saving energy for each sensor node so battery change is not needed so often. However when a more robust wireless connection is needed more energy will be consumed.

This paper will show the latest technology for achieving a robust wireless connection in an environment where energy conserving is a key issue.

[1] "Detektorer, Förutsättningar för varmgångs-och tjuvbromsdetektering av järnvägsfordon", Banverket (Swedish Rail Administration), BVS 1592.0201
[2] M.Grudén, A.Westman "Microwave Propagation for Wireless Sensor Networks - Simulations and Empiric Models". M.Sc. Thesis Uppsala University, Uppsala, Sweden, 2009
[3] Railway applications - Rolling Stock Equipment - Shock and Vibration Tests, Reference: CEI/IEC 61373:1999, Commission Electrotechnique Internationale/International Electrotechnical Commission (CEI/IEC)

Session 3

13.15-15.15 Tuesday 9 March 2010

65nm CMOS SOI Circuit Design for a 100Gb/s Optical SCM Transceiver

Michael Salter, Duncan Platt, Lars Pettersson
Microelectronics Group
Acreo AB, Norrköping, Sweden

michael.salter@acreo.se, duncan.platt@acreo.se,
lars.pettersson@acreo.se

Lars Aspemyr, Mingquan Bao
Microwave and High Speed Electronics Group
Ericsson AB, Mölndal, Sweden

lars.aspemyr@ericsson.com,
mingquan.bao@ericsson.com

I. Introduction

Internet infrastructure capacity needs are driving the evolution of network architectures capable of 100Gbit/s Ethernet (IP) based traffic[1]. Within the 100GET-ER project[2], different data modulation techniques are being examined for improved bandwidth efficiency and reduced cost, one of which is sub-carrier multiplexing (SCM)[4]. The MEDEA+ project SIAM[3] is investigating the feasibility of a 65nm CMOS process on HR-SOI substrate for implementing an integrated SCM transceiver. This abstract presents the specification and design of key 100Gb/s SCM transceiver RF front end components.

II. 100 Gbit/s SCM System Simulation

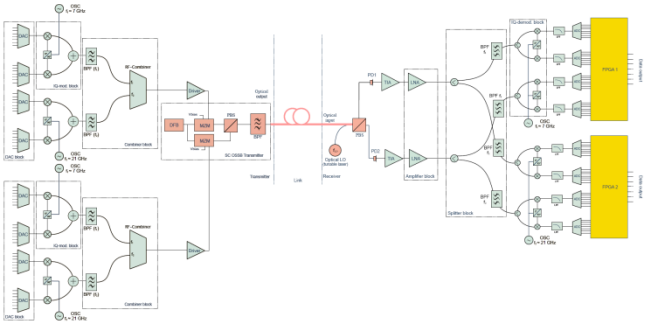

Figure 1. *100 Gb/s SCM transceiver architecture*

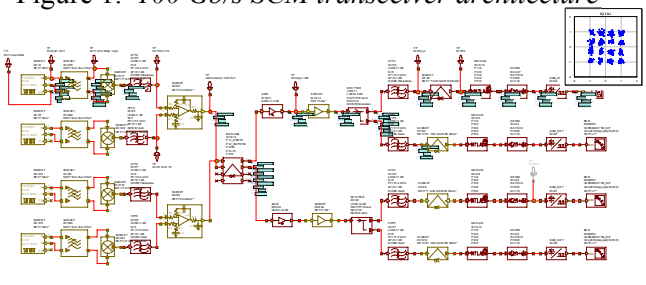

Figure 2. *100 Gb/s SCM transceiver VSS simulation block diagram*

The 100 Gb/s SCM transceiver architecture for a 16QAM, 7GS/s, 2-carrier system with optical polarization multiplexing is shown in Figure 1 with its equivalent simulation block diagram in Figure 2. The SCM system is modeled using AWR VSS together with MATLAB. The individual RF front end component requirements, necessary to achieve successful data transmission at a satisfactory BER level, are established from the system simulations.

III. Component Design in 65nm CMOS SOI

The simulation and design of key RF components is made using Cadence Virtuoso and ADS, together with the design kit for ST's 65nm CMOS SOI process.

IV. Summary

The RF component requirements for a 100 Gb/s SCM transceiver, established from system simulations, are summarized, together with the resulting component design simulation performance, in Table 1. The requirements have generally been met by the designs, which is promising for both the 65nm CMOS SOI and 100 Gb/s SCM transceiver technologies.

Component	*Component Requirements*	*Simulation Results*	*Chip area*
7 GHz mixer	BW 3.5 - 10.5 GHz CL< 7 dB, P1dBout > - 5 dBm LO level = 10 dBm S11 and S22 < -10dB	BW 3.5 - 10.5 GHz CL< 7 dB P1dBout > -5 dBm LO level = 10 dBm S11 and S22 < -10dB	1.05 mm^2
Sinc bun filter	5th order IL < 2 dB BW = 20kHz to 3.5 GHz S11 and S22 < -10dB	5th order IL < 1.96 dB BW = 0 to 3.5 GHz S11 and S22 < -10dB	0.11 mm^2
7 GHz band LP Filter	5th order IL < 2 dB fc = 10.5 GHz S11 and S22 < -10dB	5th order IL < 1.37 dB fc = 10.5 GHz S11 and S22 < -10dB	0.16 mm^2
21 GHz band HP Filter	5th order IL < 2 dB fc = 17.5 GHz S11 and S22 < -10dB	5th order IL < 1.38 dB fc = 17.5 GHz S11 and S22 < -10dB	0.08 mm^2
RF Combiner	BW 2.5 - 25.5 GHz Gain 12 dB S11 and S22 < -10dB Gain variation < 1 dB P1dB > - 5 dBm	BW 1 - 28 GHz Gain 10.4 dB S11 and S22 < -10dB Gain variation < 1.1 dB P1dB > - 4.5 dBm	1.10 mm^2
Active balun	Amplitude bal. < 0.3 dB Phase balance 180°±2 Insertion loss < 1.0 dB S11 and S22 < -10dB	Amplitude bal. = 0.0 dB Phase balance = 180.4° Insertion loss = 0.5 dB S11 and S22 < -10dB	0.07 mm^2
LNA	BW 2.5 - 25.5 GHz Gain > 15 dB NF < 5dB S11 and S22 < -10dB Gain variation < 1 dB P1dB > -12 dBm Group delay < 20 ps	BW 2.2 - 26.5 GHz Gain = 15.5 dB NF < 4.2dB S11 and S22 < -10dB Gain variation < 0.5 dB P1dB = -12 dBm Group delay < 15 ps	0.36 mm^2

Table 1. *SCM Component Design Summary*

V. References

[1] http://www.celtic-initiative.org/Projects/100GET/default.asp
[2] http://www.celtic-initiative.org/Projects/100GET-ER/default.asp
[3] http://www.medeaplus.org/web/medeaplus/projects.php
[4] Hui et. al, "Subcarrier Multiplexing for High-Speed Optical Transmission", Jnl. of Lightwave Tech., Vol. 20, No. 3, Mar. 2002

Broadband Mixer, LNA and Power Combiner in 65nm SOI CMOS

Michael Salter, Duncan Platt, Lars Pettersson
Microelectronics Group
Acreo AB, Norrköping, Sweden

michael.salter@acreo.se, duncan.platt@acreo.se, lars.pettersson@acreo.se

I. Introduction

A microwave optical transceiver with multiple broadband channels is being investigated within the SIAM project in collaboration with Ericsson Research. The optical transceiver being proposed requires broadband operation (2.5-25.5GHz) in addition to requirements for low noise, linearity, and especially low group delay variation. The simulation and design of key RF components is made using Cadence Virtuoso and ADS, together with the design kit for ST's 65nm CMOS SOI process.

II. 7 GHz I/Q Modulator Mixer

The 7 GHz TX IQ modulator mixer was implemented as a doubly-balanced resistive FET up-converter mixer as shown in Figure 1. Input LO matching circuit and IF filters are shown below together with the mixer core.

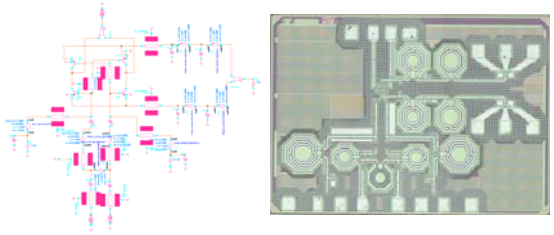

Figure 1. TX 7GHz IQ Mixer with Layout

The simulated up-converter mixer performance is given below in Figure 2 with a 7GHz LO signal.

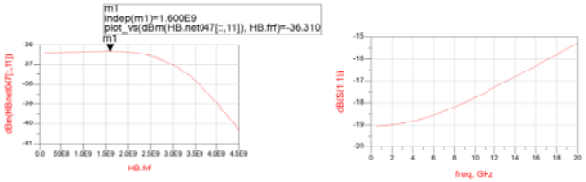

Figure 2. 7GHz IQ Mixer CL & RF input Match

Simulated CL of the mixer is roughly -6.5 dB with an RF input match better than 18 dB in the whole RF input band.

III. Low Noise Amplifier (LNA)

A common source feedback transistor LNA design topology was chosen. Three stages were used to achieve the specified gain with each stage having two parallel CS transistors to provide sufficient gain and to reduce gate resistance. The schematic and chip photo are shown below in Figure 3.

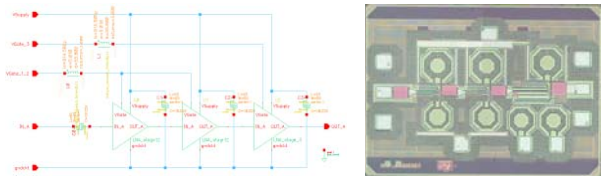

Figure 3. LNA Schematic and Layout

Simulated results are given below in Figure 4. Noise figure (< 4.2 dB), gain (> 15 dB), S11 and S22 (< -10 dB) are according to specification over the required bandwidth of 3.5-24.5GHz.

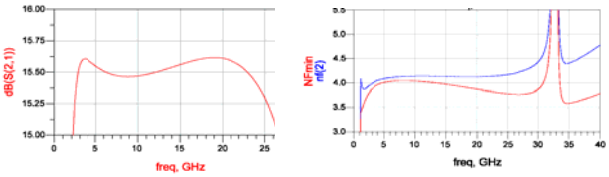

Figure 4. Simulated LNA gain, NF min and NF

IV. Broadband Active RF Combiner

An active wide-band power combiner was designed using a 4-stage traveling-wave amplifier (TWA) based architecture. The amplifiers in the combiner are implemented as cascode stages, with spiral inductors for gate/drain inter-stage impedances and MOM capacitors for matching and terminations. The schematic and chip photo is shown below in Figure 5. Simulated results in Figure 6. The RF combiner has S21>10.6dB S11<-10.4dB and 1.5dB gain variation over the 28GHz pass band.

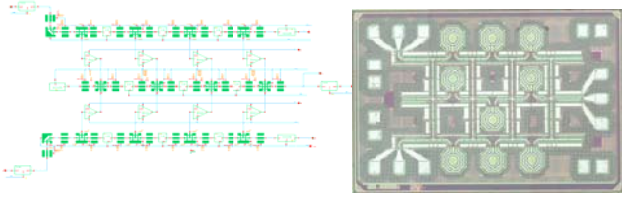

Figure 5. Combiner schematic and chip photo

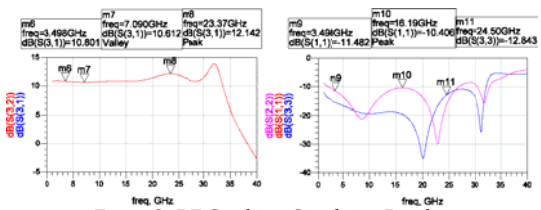

Figure 6. RF Combiner Simulation Results

E-band MMIC chipset for multi-Gb/s wireless links

Mattias Ferndahl[1], Marcus Gavell[1], Herbert Zirath[1,2]

[1] Gotmic AB, SE-411 33 Göteborg, Sweden

[2] Microwave Electronics Laboratory, Chalmers University of Technology. SE-412 96 Göteborg, Sweden

***Abstract*—This paper presents a MMIC chipset suitable for E$_a$-band (81-86 GHz) wireless link front ends. The chipset includes; LNA, buffer amplifiers, frequency octupler (x8), IQ image reject down conversion mixer, and a IQ direct modulator for the up conversion. This chip set is the first to the author's knowledge that supports direct conversion using more complex modulation formats, such as QAM.**

I. Introduction

In 2003 the US Federal Communications Commission (FCC) released 13 GHz of yet unused spectrum in the frequency bands 71-76, 81-86, and 92-95 GHz, dedicated for high speed wireless communications in the United States. These bands are usually referred to as the E-band [1] Several other regulating authorities, e.g. ETSI in EU, have or are expected to follow shortly. The upper band, 91-94 GHz is yet of limited use and the focus is mainly on the 71-76 and 81-86 GHz bands. The wide 2 x 5 GHz bandwidth opens up unprecedented possibilities of making wireless point to point links up to multi Gbit/s data rates [1]. These links can then be deployed to support the growing need for higher data rates in future mobile backhaul [2], [3] . But also in enterprize network replacing fiber connection.

The links are highly secure and links can be placed in close proximity of each other without any interference due to the narrow beamwidth. All these advantages, compared to today's microwave links, together with the light licensing requirements from the regulatory authorities make E-band point-to-point radios a very promising technology [4].

Despite the growing interest, with several commercial E-band radios on the market, both the number of scientific papers and commercially available front end components are very low. This paper presents an almost complete MMIC chipset well suited for E-band radio front ends.

II. E-band chipset

Today most systems are based on simple ASK or BPSK modulation, but as demand for better spectral efficiency increase a shift towards more complex modulation formats such as QAM is expected. The present chipset was made to support a direct conversion system using an IQ modulator and demodulator for the up and down conversion.

The measurements of all sub circuits show excellent performance, a short summary can be found in Table I, the full details will be presented at the symposium.

[1]The E-band generally denotes the waveguide band from 60 to 90 GHz. This paper propose a similar notation as for the K-band, with E$_u$ denoting the lower (71-76 GHz) band and E$_a$ denoting the upper (81-86 GHz) band.

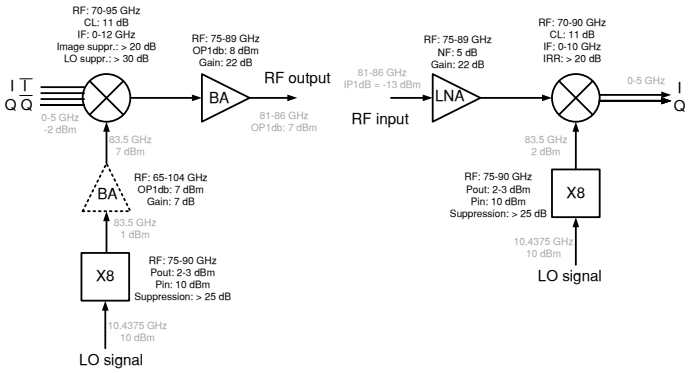

Fig. 1. Block diagram of proposed E-band front end.

TABLE I
PERFORMANCE BASED ON MEASUREMENTS OF EACH CIRCUIT.

Down converter

Parameter	Value	Comment
IF bandwidth	0 - 12 GHz	IQ IF output
RF bandwidth	75- 89 GHz	Full E$_a$ band coverage
Conversion gain	10 dB	1 dB interconnect loss
Noise figure	6 dB	
LO output bandwidth	75 - 90 GHz	USB and LSB possible
LO input bandwidth	9.4 - 11.25 GHz	P$_{LO}$ = 10 dBm
Input P1dB	-13	

Up converter

Parameter	Value	Comment
IF bandwidth	0 - 12 GHz	$IQ\bar{I}\bar{Q}$ IF input
RF bandwidth	75- 89 GHz	Full E$_a$ band coverage
Conversion gain	10 db	1 dB interconnect loss
Output P1db	8 dBm	Only buffer amplifier incl.
LO output bandwidth	75 - 90 GHz	USB and LSB possible
LO input bandwidth	9.4 - 11.25 GHz	P$_{LO}$ = 10 dBm
Input P1dB	7 dBm	
Input IP3	20 dBm	

References

[1] J. Wells, *Faster than fiber: The future of multi-G/s wireless*, IEEE, microwave mag. May 2009.

[2] *White paper: High-speed technologies for mobile backhaul*, Ericsson AB, available online: www.ericsson.com/technology/whitepapers, 2008.

[3] *White paper: The Economics of Gigabit 4G Mobile Backhaul*, Bridgewave Communicataions Inc. Available online: www.bridgwave.com, 2008.

[4] *Upper Millimeter microwave Radio Technology Poised to Take Off*, Report, Visant Strategies, May 2009.

SiGe Bipolar Limiting Amplifier with a Bit Rate of 50 Gbit/s for Optoelectronic Receivers

S. Klinger, M. Schmidt, M. Grözing, M. Berroth
Institute of Electrical and Optical Communications Engineering, Universität Stuttgart, 70569 Stuttgart, Germany
sandra.klinger@int.uni-stuttgart.de

Fast Ge on Si p-i-n photodiodes (PDs) suitable for a bit rate of 25 GBit/s have been presented [1]. In order to reduce the required optical input power, a differential limiting amplifier (LA) has been designed which will be placed between the PD and the flip flop (FF) used in [1]. The design of the LA is realized in a bipolar SiGe technology (B7HF200) from Infineon with a transit frequency f_T of 200 GHz.

At an optical input power of 1 mW, the output voltage of the PD is 1 mV at a 50 Ω load. To drive the FF, the LA has to provide a voltage gain of 300. The PDs have a 3 dB bandwidth of 49 GHz [2]. The minimum targeted bit rate for the LA is hence 50 Gbit/s.

Fig. 1 shows the circuit topology and layout of one amplifier stage. One driver (DRV) stage consists of a differential amplifier (DA) and an inductor for inductive peaking (INP) [3]. An emitter follower (EF) in front of the DRV prevents the DA from saturation. Six DRV stages with preceding EFs are used in total, each with a gain of 3. The first 4 stages work at 4 mA, the 5th at 6 mA and the 6th at 12 mA to drive 50 Ω-loads differentially with a voltage swing of ±300 mV.

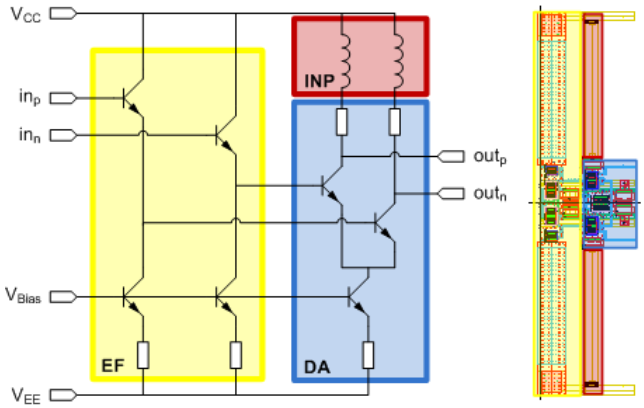

Fig. 1: Circuit topology and layout of one 4 mA-stage.

The whole chip in Fig. 2 has a size of 580 x 580 µm². Four times four pads with a pitch of 100 µm are used for RF-probe contacting.

The measurement setup is similar to the one described in [1]. The generated electrical high-speed pseudo random bit sequence (PRBS) is attenuated and then fed to the LA input.

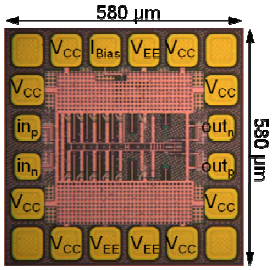

Fig. 2: Photograph of the overall chip.

Measurements with single-ended and differential input are done. One output of the LA is connected to a sampling oscilloscope to monitor the eye diagram as shown in Fig. 3. The circuit draws 100 mA at a supply voltage of -3.1 V. The input voltage swing of the LA is 45 mV and ±45 mV for single-ended and differential signals, respectively, which results in a differential output voltage swing of ±300 mV. A lower input voltage cannot be provided by the measurement setup due to bandwidth-limited attenuators.

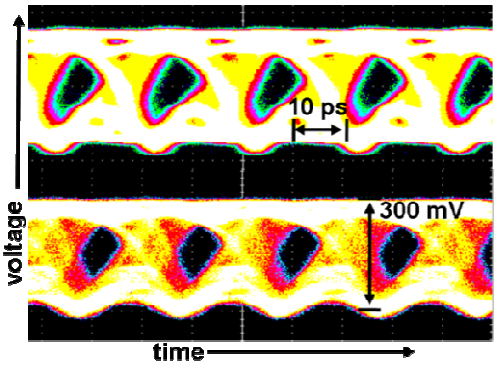

Fig. 3: Eye diagram of the LA output signal with single-ended (top) and differential (bottom) input at a bit rate of 50 Gbit/s.

50 Gbit/s are achieved for both, single-ended and differential input, with a PRBS length of 2^{31}-1. As a next step, the LA will be measured together with the PD.

[1] S. Klinger et al., *ECOC 2009*, Paper 9.2.3, Vienna/Austria, 20-24 September 2009.
[2] S. Klinger et al., *IEEE-PTL*, vol. 21, no. 13, pp. 920-922, July 2009.
[3] B. Razavi, "Design of Integrated Circuits for Optical Communications", McGraw-Hill New York, 2003.

Double Balanced Sub-Harmonic SiGe Mixer for the 79 GHz Automotive Band

Berthold Panzner[#], Lars Pettersson[*] ,Michael Salter[*], Darius Jakonis[*] and Mattias Ferndahl[‡]

[#]Otto-Von-Guericke-Universität
Institut fur Elektronik,
Signalverarbeitung und
Kommunikationstechnik
39106 Magdeburg, Universitätsplaz
203-313, Germany
Berthold.Panzner@ovgu.de

[*]Acreo AB, Innovative Electronics
Box 787, SE 601, Norrköping,
Sweden
lars.pettersson@acreo.se
michael.salter@acreo.se
darius.jakonis@acreo.se

[‡]Chalmers University of
Technology
SE 41296, Gothenburg, Sweden
mattias.ferndahl@acreo.se

I. Introduction

In this paper an active double balanced sub-harmonic mixer is presented and designed in 200 GHz SiGe technology. Sub-harmonic mixers offer a different solution compared to fundamental mixers as these mixers use local oscillators at low frequencies and therefore can provide better phase noise and higher output power.

II. Subharmonic Gilbert Cell

Figure 1 below shows the complete mixer with the mixer core which consists of two stacked switching quads, a transconductance stage and a load. For sub-harmonic mixer operation the two switching stages are fed 90° out of phase by a 40 GHz LO signal.

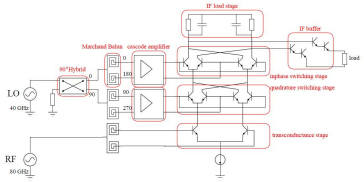

Figure 1. The complete double balance sub-harmonic SiGe mixer.

The most vital part with respect to operation and performance is the switching stage. Two quads are stacked to generate an internal 80 GHz signal out of two 40 GHz LO signals. main contributor. Figure 2 below shows a photo of the complete mixer. The size of the mixer chip is 750x550 µm.

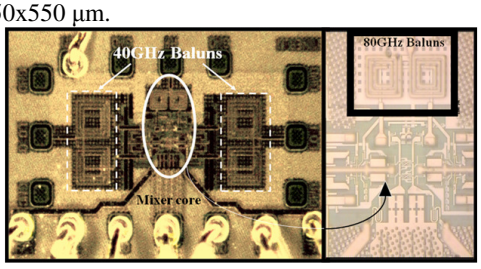

Figure 2. Photo of the mixer chip.

Integrated Marchand baluns on chip was also introduced in order to convert the balanced RF and LO ports to single ended ports. The 40 GHz and 80 GHz passive Marchand baluns have a size of 100x220 µm and 50x110 µm respectively.

III. Measured Results

The measurements where made using 80 GHz signal source with spectrum analyzer in the frequency band 77-81 GHz.

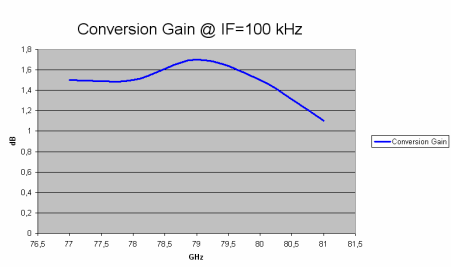

Figure 3. Measured conversion gain of the sub-harmonic SiGe mixer.

The measured conversion gain is 1.5 ± 0.2/0.3dB in the frequency band 77-81 GHz, see figure above.

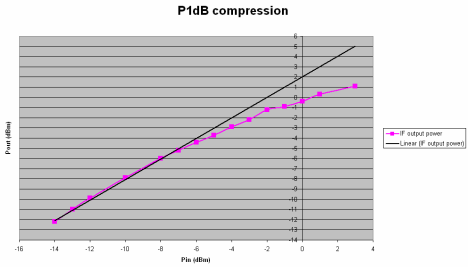

Figure 4. Measured P1dB point of the sub-harmonic SiGe mixer.

The measured input refereed P1dB compression point is -4 dBm.

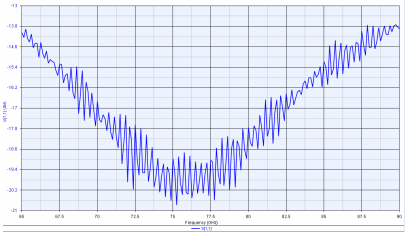

Figure 5. Measured RF input match of the sub-harmonic SiGe mixer.

The measured RF input match is better than 13 dB in the frequency band 65 GHz to 90 GHz.

Wideband GaN MMIC Development

Jonas Holmqvist[1], Niklas Billström[2]
[1]*Saab AB, Saab Avitronics, SE-175 88 Järfälla, Sweden*
[2]*Saab AB, Saab Microwave Systems, SE-412 89 Göteborg, Sweden*

This paper will focus on and summarize wideband 2–18 GHz low noise amplifier (LNA) and Transmit/Receive (T/R) switch results from MMIC demonstrators developed by Saab within programmes KORRIGAN and GHz Centre. The latter is a joint effort between Chalmers University of Technology and industry where GaN circuits are one of the research areas. These GaN activities have also been closely linked to the large-scale European GaN programme KORRIGAN, short for **K**ey **Or**ganisation for **R**esearch in **I**ntegrated Circuits in **GaN** Technology, where the main objective has been to prepare for independent European GaN foundries. As recently concluded, it marks the end of the largest research organisation so far assembled in the field of microelectronics.

The main design objective within the project was to realize GaN MMIC's for three key functions in a virtual T/R module applicable to an arbitrary active electronically scanned array (AESA) system: high power amplifier (HPA) for the transmitting channel, LNA for the receiving channel and a switch for channel selection. GaN has the potential of bringing HPA's to the next level, but LNA's and switches are also of great interest for these systems. Due to the robustness of the material, a GaN LNA could perhaps omit the need for a limiter or at least simplify the limiting circuitry in the receiver chain. Also, a high power switch could replace the bulky circulator used in most of today's modules.

Two LNA circuits denoted LNA-1 and LNA-2 are presented hereafter. They are both three stage designs based on 4×50 µm and 4×75 µm devices respectively. LNA-1 has parallel feedback on all stages while LNA-2 has inductive series feedback on the first stage and parallel feedback on the two following stages. Measured and simulated performance is presented in figure 1. Good gain agreement is shown at the lower part of the band, but then a roll off with frequency is noted, especially for LNA-2. The measured noise figure is generally a bit higher than expected. Both LNA's showed good power handling capabilities and catastrophic failure occurred at about 10 Watts of input power which is considerably more than any GaAs equivalent would withstand. The results can be considered encouraging for future efforts given the fact that the 0.25 µm gate length process used was optimized for high power densities rather than high frequency and low noise. However, future process improvements are necessary to really challenge wideband GaAs LNA's. Typical improvements are shorter gate length and specific low noise transistors.

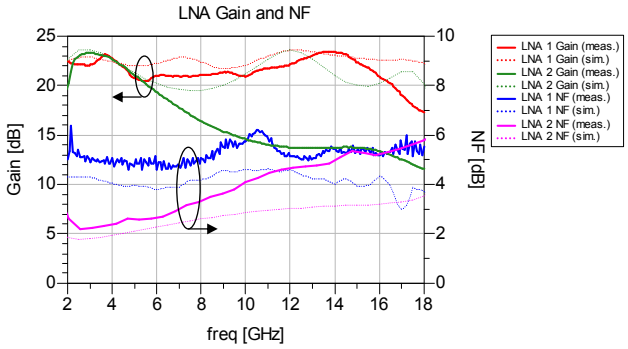

Fig. 1. Measured and simulated gain and noise figure for LNA-1 (red and blue) and LNA-2 (green and pink).

The wideband T/R switch designs were all based on a topology with a relatively large series device followed by several smaller shunt stages in each path. Initial designs suffered from high insertion loss at the high end of the frequency band. To improve the high frequency performance, specific switch devices were developed at Chalmers for the 0.25 µm process. The following presented switches, denoted SPDT-1 and SPDT-2, utilize these devices for a very efficient design. SPDT-1 is realized with a new optimized device layout. Both switches have similar device gate widths. Excellent measured performance is presented in table 1. These designs are very compact and much smaller than comparable ferrite circulators or PIN diode switches and are also well suited for use in 3×3 mm QFN packages.

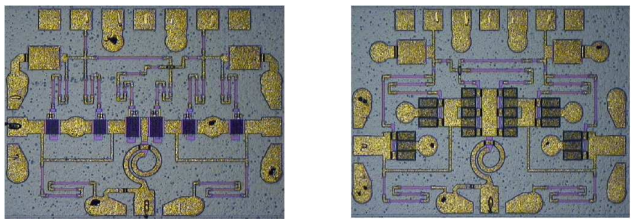

Fig. 2. SPDT-1 (left) and SPDT-2 (right). Chip dimensions are 1.4x1.1 mm^2 and 1.5x1.1 mm^2 respectively.

Parameter	**SPDT-1**	**SPDT-2**
Frequency range	DC–18 GHz	DC–18 GHz
Insertion loss	≤ 2.0 dB	≤ 2.0 dB
Isolation	≥ 28 dB	≥ 33 dB
Return loss	≥ 19 dB	≥ 15 dB
$P_{0.2dB}$ (input)	≥ 2 W	≥ 2 W
$P_{failure}$ (input)	≥ 15 W	≥ 15 W

Table 1. Performance summary for SPDT-1 and SPDT-2.

Low-phase noise InGaP HBT VCO design

Dan, Kuylenstierna, Herbert Zirath, Rumen Kozhuaharov, Bertil Hansson, Iltcho Angelov

Microwave Electronics Laboratory, Göteborg, Sweden, Chalmers University of Technology, GigaHertz Centre, Department of Microtechnology and Nanoscience

Introduction

InGaP HBT technology is known to be one of the best choices for low-phase noise MMIC VCOs [1]. However, there are yet several factors left to be better understood in order to maintain a low phase noise over wide tuning ranges. The bandwidth of a varactor-controlled LC oscillator is directly determined by the tuning range of its varactor. For hybrid VCOs hyperabrupt varactors with capacitance ratios, C_{max}/C_{min} in excess of 10 are used. In MMIC VCOs the varactor is constituted of the base-collector pn junction. Increased tuning range can be reached by customization of the collector doping-profile, but as the same collector is used also in the HBTs their performance will be affected as well.

This paper reports on advances in the design and modelling of of low-phase noise InGaP HBT VCOs with variation in the collector doping profile. Collectors with four different doping profiles have been evaluated for several different oscillator topologies, e.g., balanced Colpitts, cross-coupled, enhanced-gm, and Hartley. To evaluate whether the phase noise is generated in the varactor or in the HBTs, the same topologies are implemented also as fixed-frequency oscillators using MIM capacitors.

Results

In summary it is found that the phase noise in VCOs is roughly 6-12 dB higher than in corresponding oscillators using MIM capacitors. At least partly, the noise is coming from the varactor, as the phase noise of fixed-frequency oscillators is not varying equally much between different epis. Fig. 1 shows phase noise of fixed-frequency oscillators and VCOs in three different doping profiles. The widest tuning range is obtained in wafer 2, f_0=4.4-5.4 GHz with a phase noise <-107dBc/Hz at 100 kHz off-set.

Regarding the phase noise of VCOs in different doping profiles, it is found that the phase noise of wafer 2 (a type of hyper abrupt profile) is higher than for wafer 1 (a more abrupt profile). On the other hand wafer 2 provides tuning ranges that cannot be reached in an ordinary abrupt doping profile. Fig. 2 shows normalized phase noise vs tuning range for three different enhanced-gm VCOs (and corresponding fixed-frequency with MIM caps).

ACKNOWLEDGMENT

This work has been carried out in the GigaHertz Centre in a joint research project financed by Swedish Governmental Agency of Innovation Systems (VINNOVA), Chalmers University of Technology, Sivers IMA AB, and Ericsson AB.

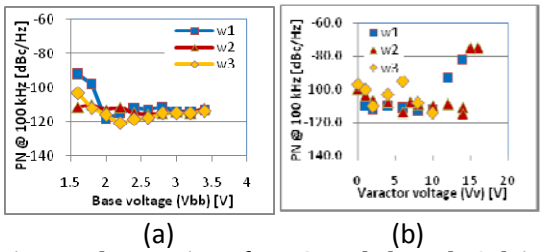

Fig. 1 Phase noise of 5 GHz balanced Colpitts oscillators (a) fixed-frequency vs base voltage (b) phase noise of VCO vs varactor voltage.

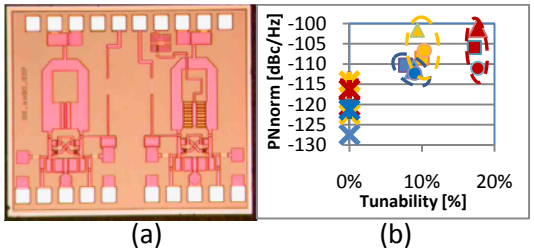

Fig. 2: Fixed-frequency and voltage-controlled Enhanced-gm oscillators

[1] H Zirath, R Kozhuharov, M Ferndahl, 'Balanced Colpitt Oscillator MMICs Designed for Ultra-Low Phase Noise', IEEE Journal of Solid-State Circuits, Vol 40, no 10, October 2005, pp. 2077-2086 .

Session 4

13.15-15.15 Tuesday 9 March 2010

24 GHz and 35 GHz RF MEMS Phase Shifters Fabricated in a Standard GaAs MMIC Process Technology

[1]R. Malmqvist, [1]C. Samuelsson, [2]W. Simon, [2]R. Baggen, [3]D. Smith, [4]J. Saijets and [4]T. Vähä-Heikkilä
[1]FOI Swedish Defence Research Agency, Olaus Magnus väg 42, SE-583 30, Linköping, Sweden
E-mail: robert.malmqvist@foi.se
[2]IMST GmbH, Kamp-Lintfort, Germany
[3]OMMIC, Limeil-Brevannes, Cedex, France
[4]VTT Technical Research Institute of Finland, Espoo, Finland

1. Introduction

RF Micro-Electro Mechanical Systems (MEMS) technology has matured over the last years and it has reached a level where MEMS switches have been successfully integrated into practical RF systems with proven long term reliability [1]. Hence, it is regarded as a promising technology for future reconfigurable antenna systems for communication and RF-sensing, particularly at microwave and mm-wave frequencies. The integration of MEMS switches and Monolithic Microwave Integrated Circuits (MMICs) is considered as a next logical step in process development and commercialisation of RF MEMS technology. In this paper, we report on initial results of fabricated test circuits (such as 24 GHz and 35 GHz phase shifters) made within the EC FP7 funded project MEMS-4-MMIC aiming at the merging of innovative MEMS switches and a well established and proven MMIC technology from the OMMIC foundry.

2. RF MEMS-MMIC Phase Shifters

Figure 1a shows a chip photo of a switched-line type of phase shifter circuit that has been fabricated using a standard GaAs MMIC process technology with on-chip integrated MEMS switches developed by OMMIC. The measured relative phase shift of this phase shifter bit is equal to 180° at 24 GHz (circuit area is 3 mm^2). The measured transmission losses (s_{21}) are equal to 1.2-2.3 dB at 24 GHz in the reference state and the delay state, respectively. The experimental results are also in a relatively close agreement with the simulations (see Fig. 1 b). A 35 GHz 3-bit RF MEMS-MMIC phase shifter has also been fabricated on a 600 µm thick GaAs substrate and it has a measured average loss of 5 dB. Lower phase shifter losses would be possible to achieve by using a µ-strip design on a thinner substrate [2].In our future work we will aim towards cost-effective packaging methods and monolithic integration of MEMS with active RF circuits (potentially as single-chip solutions) [3].

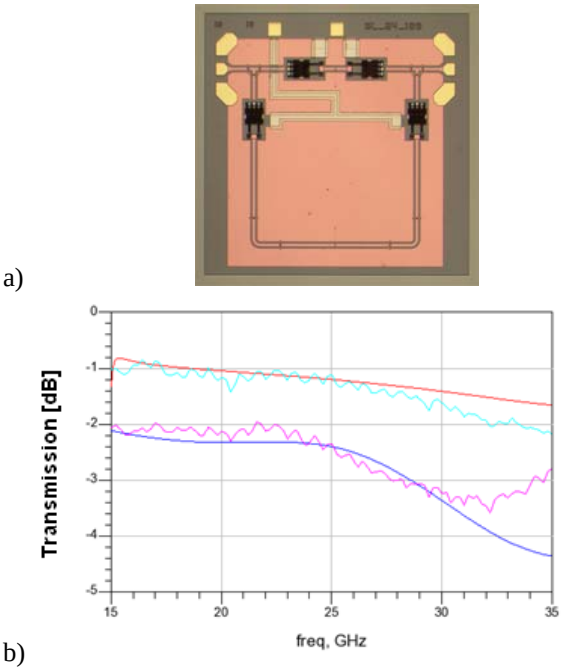

Fig. 1. Chip photo (a) and (b) measured and simulated transmission losses (s_{21}) of a 24 GHz RF MEMS phase shifter bit (180° of phase shift) fabricated using a GaAs MMIC process technology from OMMIC.

3. CONCLUSIONS

This paper describes some initial experimental results of fabricated test circuits obtained within a pan-European research activity aiming at a monolithic integration of RF MEMS switches into a standard GaAs MMIC process technology. Low-loss RF MEMS-MMIC phase shifters, switches and matching circuits have been realized indicating a potential usefulness of such circuits in various applications up to 40 GHz and beyond.

REFERENCES

[1] J.J. Maciel et al., "MEMS electronically steerable antennas for fire control radars," *IEEE Aerosp. Elect. Syst. Mag.*, vol. 22, no. 11, pp. 17 – 20, Nov. 2007.
[2] J. B. Hacker et al., "A Ka-band 3-bit RF MEMS true-time-delay network," *IEEE Trans. MTT*, Vol. 51, no. 1, Jan. 2003, pp. 305-308.
[3] M. Kim et al., "A monolithic MEMS switched dual-path power amplifier," *IEEE Microwave Wireless Comp. Lett.*, Vol. 11, no. 7, July 2001, pp. 285-286.

Millimeter-Wave Switch based on Air-Gap-MEMS Switched Capacitors

A. Enayati[1,2], X. Rottenberg[1], P. Ekkels[1], W. De Raedt[1] and G. A. E. Vandenbosch[2]
[1]IMEC, 3001 Leuven, Belgium
[2]K. U. Leuven, ESAT, 3001 Leuven, Belgium

ABSTRACT

One of the needed modules in RF transceivers is a single-pole-single-throw switch. It can be used as the basis for single-pole-double-throw switches which are used as the TX-RX switches in these transceivers. Like for other modules, the higher the frequency of operation is, the more complex the module design becomes. In this work, a millimeter wave switch based on air-gap variable capacitors [1] is introduced. The switch is formed by loading a CPW transmission line by two switched capacitors. The two capacitors are placed at two different points along the CPW line to improve the bandwidth characteristics of the switch.

A basic schematic of the air-gap variable capacitor used in this paper is shown in Fig. 1. A cross-sectional view, top view and a circuit model are shown in this figure. The moving electrode (named armature) is made up of nickel while the CPW is implemented in aluminum. As shown in this figure, instead of using a dielectric layer to prevent shorting of the capacitor electrodes, some dimples are fabricated beneath the moving electrode to prevent short circuit condition. Hence, for both up and down states, the dielectric filling the capacitor is air. That is why these capacitors are named air-gap capacitors.

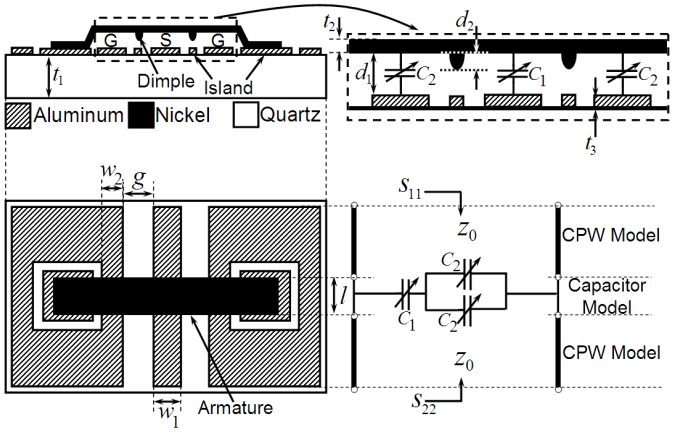

Fig. 1.Schematic and Model of an air-gap MEMS switched capacitor.

By putting two of these variable capacitors at a quarter wavelength distance from each other along a CPW line and optimizing different parameters of the structure, an SPST switch is designed for millimeter wave frequencies. Fig. 2 shows an SEM photo of the fabricated sample wile Fig. 3 and Fig. 4 show the simulatino versus measurement results for up and down states respectively. They show not only a good agreement between simulation and measurement results but also the switching behavior in the frequency range of [52-62]GHz.

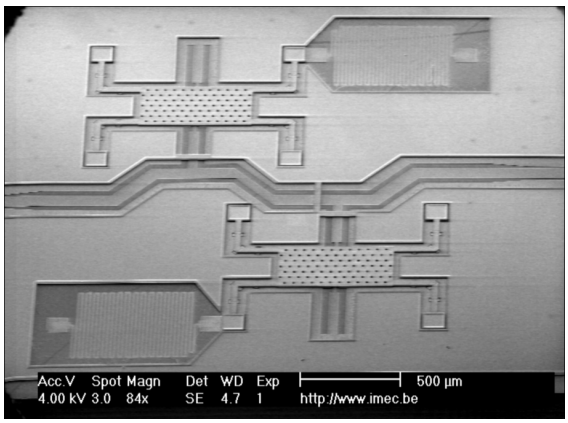

Fig. 2. SEM Photo of the Fabricated Switch.

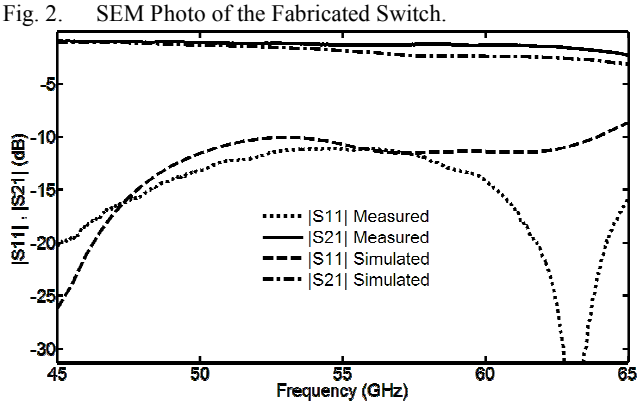

Fig. 3. Measurement vs. Simulation Results for the Up State.

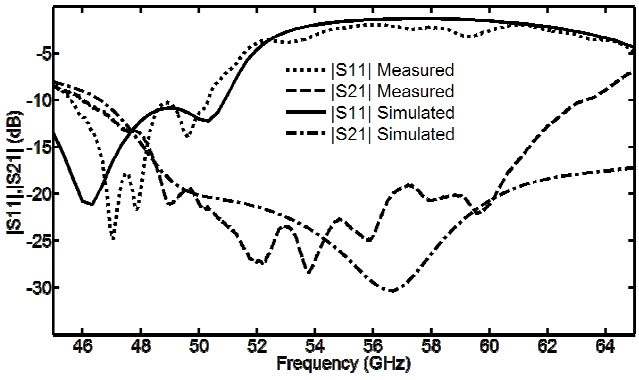

Fig. 4. Measurement vs. Simulation Results for the Down State.

References

[1] P. Ekkels, X. Rottenberg, P Czarnecki R. Puers, and H. A. C. Tilmans, "Simple and robust air-gap-based MEMS switch technology for RF application," *MEMS 2009,* pp. 856-859, January 2009.

Using Homogenisation Methods to Calculate the Effective Permittivity when Testing Microwave Properties of Carbon NanoTubes Grown in Alumina Membrane

Magnus Höijer[1] (magnus@foi.se), Lars-Gunnar Huss[1] (gunnar.huss@foi.se)
Niklas Wellander[1] (niklas@foi.se), Sandra Fontorbes (fontorbes@chimie.ups-tlse.fr) &
Laurent Arurault[2] (arurault@chimie.ups-tlse.fr)
1) Swedish Defence Research Agency FOI, SE-581 11 Linköping, Sweden
2) Université de Toulouse, CIRIMAT, UPS/INPT/CNRS, LCMIE, 118 Route de Narbonne, F-31062 Toulouse Cedex 9, France

CATHERINE is a 3 year project within the seventh Framework Programme of the European Union. CATHERINE has 11 partners from Italy, France, Romania, Netherlands, Latvia and Sweden. Consorzio Sapienza Innovatione is coordinator and Sweden has two partners, Smoltek AB and the Swedish Defence Research Agency FOI.

The miniaturization of electrical and electronic devices, together with the high integration level and the increase of the working frequencies and power density require the use of innovative solutions for the realizations of on chip interconnections and vias. One possible technology to use is Carbon NanoTubes (CNT) and Carbon NanoFibres (CNF). Within the CATHERINE project CNT are synthesized within the pores of properly designed alumina membrane, see Fig.1. One aspect particularly addressed by the CATHERINE project is to investigate the properties of the CNT in the microwave domain, including EMC and high electromagnetic power properties.

To be able to perform microwave testing, the test vehicle needs to be properly designed, see Fig.2. That is mainly depending on the structures connecting to the CNT and in our case also on the alumina membrane. As can be seen in Fig. 1, the alumina membrane is a mixture of air and alumina. To be able to calculate the effective permittivity of the membrane, different kind of mixing formulas can be used. They, however, give inaccurate results, and that justifies the use of more accurate methods.

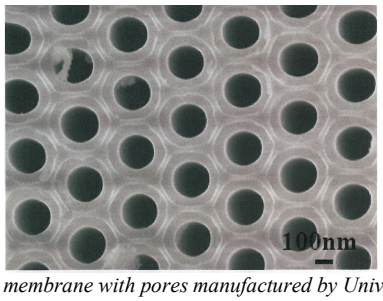

Fig 1: *Alumina membrane with pores manufactured by Université Paul Sabatier-CIRIMAT. (FEG-SEM plan view, side A, 10 mm disc.)*

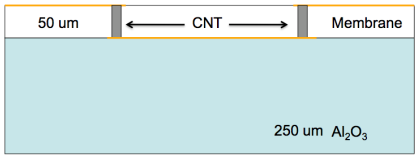

Fig 2: *Example of test-vehicle used in the CATHERINE-project.*

We use homogenisation methods, which are accurate and fast, compared to full numerical techniques. Homogenisation methods uses that the electromagnetic wavelength is much longer than the dimensions of a unit cell in e.g. the membrane of Fig.1. Hence the electromagnetic properties can be solved as an electrostatic equation,

$$\frac{\partial}{\partial y_i}\left\{\varepsilon_{ij}\left(\vec{y}\right)\left(\delta_{jk}-\frac{\partial}{\partial y_j}\chi^{(k)}\left(\vec{y}\right)\right)\right\}=0\,. \qquad (1)$$

Here, we only conclude that (1) is time independent and is to be solved for the electric potential χ, and once it is known the effective permittivity can easily be calculated. Figure 3 shows results calculated for different assumed permittivities of the bulk alumina. Clean alumina has a permittivity of close to 10.

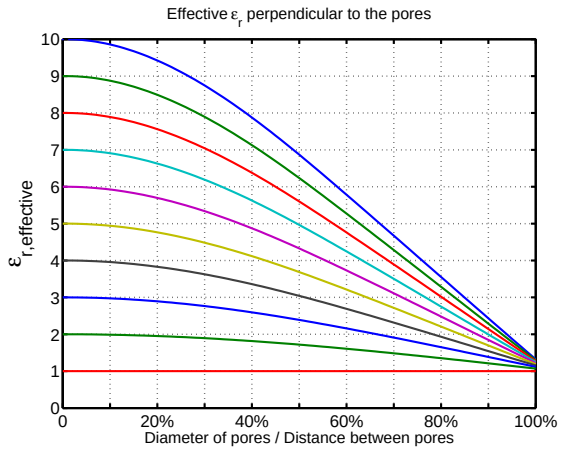

Fig. 3: *The effective relative permittivity as function of the diameter of the pores for different permittivities of the bulk material.*

Broadband Planar Balun

Tomas Windahl, Jan Grabs
Saab AB, Saab Avitronics, SE-175 88 Järfälla, Sweden

This paper presents a broadband planar balun, 2-6 GHz. A balun is a type of transformer that converts a balanced line into an unbalanced line and vice versa. It can be used in antenna feeding networks, balanced mixers, push-pull power amplifiers etc. Planar baluns have been the topic of many papers and the focus of this study is a low cost compact design for printed circuit board layout. The proposed balun is designed on a multilayer substrate consisting of FR4 and RO4350B.

The basic idea behind the balun is the insertion of a second floating ground, into a microstrip transmission line, see Figure 1.

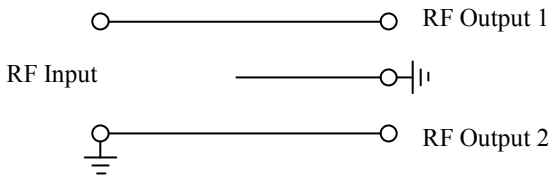

Figure 1. Principal operation.

To make this possible, a 4 mil RO4350B substrate has been used together with the top metal layer of the FR4 substrate. The prepreg used to join the different substrates acts as a dielectric.

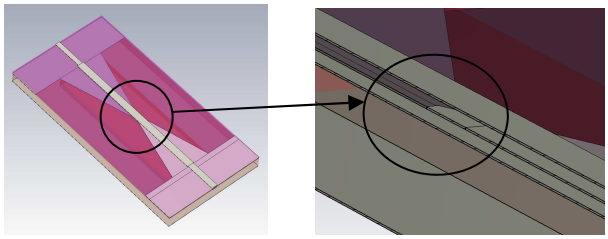

Figure 2. Simulated structure in CST Studio.

The 50Ω microstrip line at the input of the balun has a narrowing ground plane, creating a parallel transmission line. Between this parallel transmission line a new floating ground plane is inserted, dividing and phase shifting the microstrip quasi-TEM mode. To further increase the difference between the even and odd mode in the transition from a parallel line into two microstrip lines, a piece of the FR4 substrate has been machined away. The size of the balun is 14×5 mm.

Several simulations were performed since the actual height of the prepreg layer is difficult to predict. A nominal value of 0.1mm and ±20% was optimized.

Upon arrival, the PCB was cut and the height of the prepreg layer was measured.

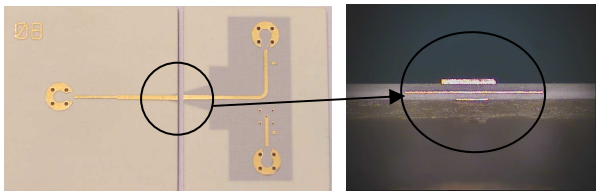

Figure 3. Picture of evaluation PCB.

The prepreg layer thickness was at the lower end of the nominal value.

The evaluation of the balun was made using SMP connectors on top of the PCB. Since the balun has 25Ω outputs, a 50Ω resistance was placed in parallel with the 50Ω impedance of the measurement system, creating 25Ω ports for the balun. By doing so, 3 dB losses are added to the measurements. The same is done to the simulation results for comparison of results.

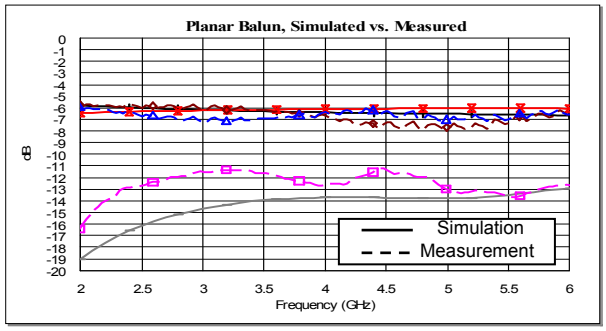

Figure 4. Simulated and measured S-parameters.

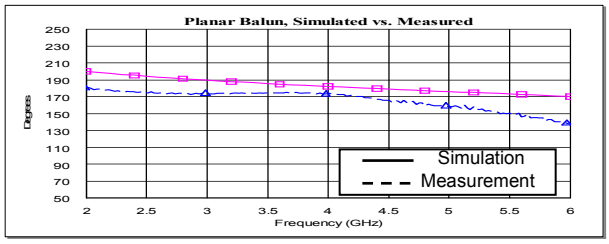

Figure 5. Simulated and measured phase imbalance.

Conclusion: A broadband planar balun has been presented and manufactured with standard manufacturing processes. The measured results show that the proposed balun has an insertion loss < 1 dB. The measured amplitude and phase imbalance between the outputs are < 1 dB and < 40°, respectively, over the entire operating frequency band. Good agreement between simulation and measurements has been achieved. The results indicate adequate performance for the intended application.

Acknowledgements: This work was partly financed by the Swedish Defence Materiel Administration.

Compact broadband directional coupler

Jan Grabs, Tomas Windahl
Saab AB, Saab Avitronics, SE-175 88 Järfälla, Sweden

In a broadband antenna array application a small and compact directional coupler is needed. The coupler should also be inexpensive and easy to produce with standard printed circuit board methods. The repeatability is also important which implies that a single layer coupler structure should be used with a ground plane. For this application a thin RO4350B RF substrate is selected which is placed on a thicker FR4 multilayer substrate.

With the requirements from the intended application, the coupling should be 28 dB with a directivity of about 20 dB in the frequency range of 2 – 6 GHz.
The insertion loss should be below 0.4 dB and the peak power handling capability should be 53 dBm.
The available space is 10 x 5.5 mm for two couplers. With the mentioned restrictions a standard ¼ λ coupler is not useful. A shorter version was investigated were the desired coupling and directivity was achieved but the frequency slope was too bad (10 dB) within the 2 – 6 GHz frequency range, i.e. low coupling at low frequency and high coupling at high frequency. A possible solution of this problem is to use an equalizer but the space needed is not available and the repeatability will be poor. A better solution is to divide each coupler in to two even smaller couplers and connect them with an appropriate length of transmission line, see figure 1.

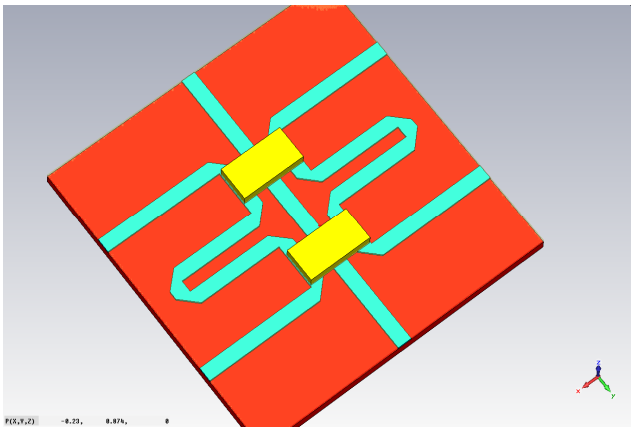

Figure 1. Outline of a dual directional coupler.

The length is chosen so that the signals are added almost in phase at low frequencies and partly cancelled at high frequencies so that a good flatness is achieved. With this design the desired coupling was achieved but the directivity was too low due to limited capacitive coupling. This was initially handled with small finger capacitors but this lead to small gaps between the transmission lines. These gaps where investigated regarding arcing at high power level and the conclusion was that the finger capacitors could not be used. Instead a small piece of dielectric material was glued on top of the couplers which solved both the problem with arcing and capacitance, see figure 1. This coupler has been manufactured with the dielectric piece mounted with an automatic pick and place machine. The measurements are shown in figure 2.

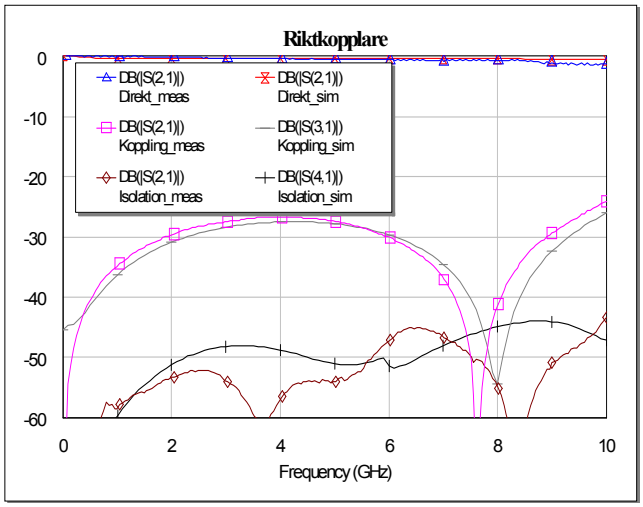

Figure 2. Simulation and measurement of a directional coupler

The coupling was 27 – 30 dB and the insertion loss < 0.4 dB. The directivity was > 20 dB for 2 – 5.5 GHz and > 17 dB from 5.5 – 6 GHz. Measurements showed good agreement with simulations and the repeatability was good.

Acknowledgements. This work was partly financed by the Swedish Defence Materiel Administration.

Q-FACTOR COMPARISONS BETWEEN NEW GAP WAVEGUIDE TECHNOLOGY AND STANDARD RECTANGULAR WAVEGUIDE

Elena Pucci[1], Ashraf Uz Zaman[1], E. Rajo-Iglesias[2], Per-Simon Kildal[1] and Ahmed Kishk[3]
[1]Department of Signals and Systems, Chalmers University of Technology, Sweden
[2]Universidad Carlos III de Madrid, Spain
[3]Department of Electrical Engineering, University of Mississippi, USA.
elena.pucci@chalmers.se, zaman@chalmers.se, eva@tsc.uc3m.es, per-simon.kildal@chalmers.se, ahmed@olemiss.edu

Introduction: Recently, a new type of waveguide technology, called ridge gap waveguide, has been presented [1], [2]. The new waveguide is created in the gap between two metal plates. The lower plate, which can contain metal ridges or strips, is surrounded by an artificial magnetic conductor (AMC), such as a bed of nails [3]. When the gap between the upper and lower plate is smaller than λ/4, the propagation is forbidden in any direction, except in the gap between the upper plate and the metal ridge, where only a quasi-TEM mode is allowed to propagate. Numerical studies and experimental validation have been established [3], [4]. The groove gap waveguide has also been studied. The benefit of this solution, compared to the standard rectangular waveguide, is that no metal contacts are needed between two metal plates, thus simplifying manufacturing issues.

The new gap waveguide technology is low loss and easy to manufacture which makes it suitable for application up to THz, integration of active components and packaging [5]. As said, one of the benefits of the new gap waveguide is its low loss, as shown in [4], [6]. However, losses are so small that it is quite difficult to quantify the exact amount, thereby motivating the present work.

This work presents a detailed study and quantification of losses in gap waveguide, compared to losses in standard rectangular waveguides. The study is performed by evaluating Q-factors of resonators made of ridge gap waveguide, groove gap waveguide and rectangular waveguide. The Q-factor approach is known to be very accurate for determining losses when they are small.

Quality Factor in Gap Waveguide: The Quality Factor $Q = f_0 / \Delta f$ where is the half power bandwidth Δf is an important parameter used to characterize the performance of a circuit resonating at f_0. Moreover, it becomes a fundamental requirement when designing filters. It is equal to the ratio between the average stored energy and the energy loss per second in a system [7]. The higher is the Q-factor, the lower are the losses in a resonant circuit.

Resonators Design: Design of ridge gap waveguide, groove gap waveguide and rectangular waveguide resonators are presented. Their computed and measured Q-factors will be shown. The simulations are carried out using CST Microwave Studio Eigenmode Solver. For a good comparison, all structures are designed with same width, height and same electrical length.

Results: Results will show that the gap waveguide has high Q-factor, quite close to the rectangular waveguide case. Moreover, it will be shown that when manufacturing rectangular waveguides many screws are needed in order to achieve the same Q-factor as in the ideal case, while the groove gap waveguide maintains very high Q-Factor without any need of metal contacts.

Acknowledgment: This work has been supported by the Swedish Foundation for Strategic Research (SSF) within the Strategic Research Center Charmant.

REFERENCES

[1] P.-S. Kildal, E. Alfonso, A. Valero-Nogueira, E. Rajo-Iglesias, "Local metamaterial-based waveguides in gaps between parallel metal plates", *IEEE Antennas and Wireless Propagation letters (AWPL)*, Volume 8, pp. 84-87, 2009.

[2] P.-S. Kildal, "Three metamaterial-based gap waveguides between parallel metal plates for mm/submm waves", 3rd European Conference on Antennas and Propagation *EUCAP 2009*, Berlin, Germany, 23-27 March 2009.

[3] Eva Rajo-Iglesias, Per-Simon Kildal, "Numerical studies of bandwidth of parallel plate cut-off realized by bed of nails, corrugations and mushroom-type EBG for use in gap waveguides", submitted to *IET Microwaves, Antennas & Propagation*, May 2009.

[4] P.-S. Kildal, A. Uz Zaman, E. Rajo-Iglesias, E. Alfonso, A. Valero-Nogueira, "Design and experimental verification of ridge gap waveguides in bed of nails for parallel plate mode suppression", submitted to *IEEE Transactions on Microwave Theory and Techniques*, August 2009.

[5] E. Rajo-Iglesias, A. Uz Zaman, P.-S. Kildal, "Parallel plate cavity mode suppression in microstrip circuit packages using a lid of nails", accepted for publication in *IEEE Microwave and Wireless Components Letters*, Aug. 2009.

[6] A. Uz Zaman, E. Rajo-Iglesias, E. Pucci, P.-S. Kildal, "Design of Transitions and Calibration Kit in New Wideband Metamaterial-based Gap Waveguide Transmission Line Technology for Millimeter and Submillimeter Waves", ESA Antenna Workshop on "*Millimetre and sub-millimetre waves - From technologies to systems*", 18-20 May 2009, ESTEC, Noordwijk, The Netherlands.

[7] D. Pozar, *Microwave Engineering 3rd edition*, Wiley, 2005.

[8] CST Microwave Studio 2009. www.cst.com.

Millimeter-Wave RF MEMS Reconfigurable High-Impedance Surfaces for Radar Applications

M. Sterner[1], D. Chicherin[2], A.V. Räisänen[2], G. Stemme[1], J. Oberhammer[1]
[1]Microsystem Technology Lab, KTH – Royal Institute of Technology, Stockholm, Sweden (msterner@kth.se)
[2]Dept. of Radio Science and Engineering, Aalto University (formerly TKK), P.O. Box 3000, 02015, Finland.

This paper presents MEMS tuneable metamaterial high-impedance surfaces (HIS). These miniaturized structures are designed for W-band beam steering applications, including automotive radar and reconfigurable high-capacity point-to-point communication links, and are able of replacing a multi-component subsystem by a single chip.

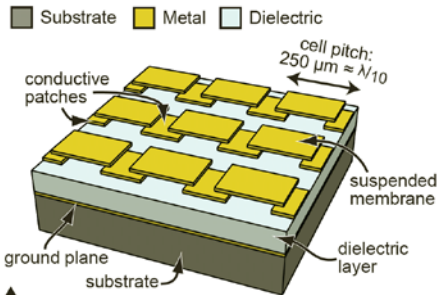

Fig. 1: Illustration of 3×3 elements of a periodic high-impedance metamaterial surface

Metamaterial surfaces are artificial periodic patterns with surface properties not available in nature. At their resonance frequency, high-impedance metamaterial surfaces (Fig. 1) have an effective surface impedance which is approaching $\pm j\,\infty$ and is thus very large as compared to the free space impedance [1,2]. This results in the phase of the reflection coefficient having a steep transition between –180° and 180°, wheras its amplitude ideally remains constant [3]. For a given frequency band, this can be utilized to create a tuneable phase-shift, which can be utilized for direct beam-steering by a single component, if a gradient in the phase of the reflection coefficient is created along the columns of the high-impedance surface array.

The high-impedance surface presented in this paper is composed of an array of electrostatically tuneable elements. The resonance frequency is determined by the element's geometry and by the capacitive coupling between the membrane and the patches. Fig. 2 shows SEM pictures of a large-scale high-impedance surface with 200×52 array elements with a pitch of 250 µm and a total size of 70×18 mm^2. The excellent repeatability and robustness of the actuator over 100 million cycles is shown in Fig. 3.

The microwave properties of the fabricated high-impedance surfaces are evaluated from 70 GHz to 114 GHz by backshort measurements with a rectangular WR-10 waveguide. The phase and amplitude of the measured reflection coefficient are shown for three structures in Fig. 4. The resonance frequencies are between 111.3 GHz and 111.8 GHz and the characteristic steep phase transition of over 245° clearly confirms the frequency-selective high-impedance surface behavior of the device. The losses of the first prototypes is worse than theoretically predicted and is attributed to imperfections in the fabrication.

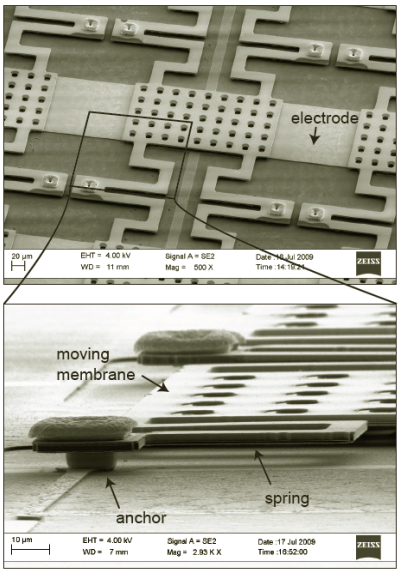

Fig. 2: SEM pictures of the fabricated high-impedance surfaces.

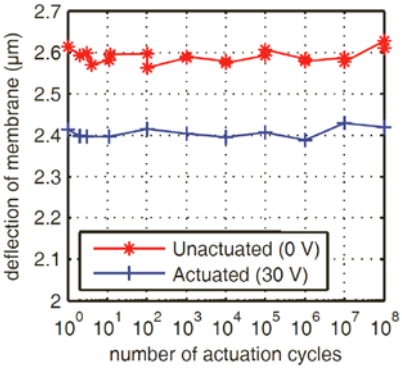

Fig. 3: Life-cycle measurement to over 100 million actuation cycles.

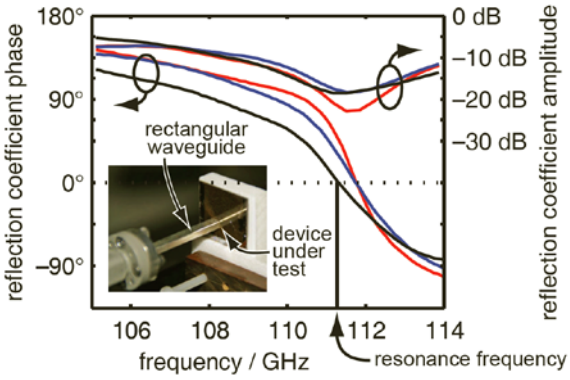

Fig. 4: Microwave characterization showing the steep phase transition around the resonance frequency.

[1] D. Sievenpiper, High-Impedance Electromagnetic Surfaces, Ph.D. dissertation, Dept. Elect. Eng., UCLA, 1999.
[2] D. Sievenpiper, et al., Dig. of 2001 IEEE Int. Symp. of Antenna and Propag. Soc., vol. 1, 2001, pp. 174–177.
[3] D. Chicherin, S. Dudorov, D. Lioubtchenko, V. Ovchinnikov, A.V. Räisänen, Proc. EuMC, pp. 372–375, 2006.

The research leading to these results has received funding from the European Community's Seventh Framework Programme FP7/2007-2013 under grant agreement n° 224197.

RF MEMS Matching Networks for Frequency Tunable SiGe LNA

[1]R. Malmqvist, [1]C. Samuelsson, [2]S. Cheng, [3]P. Rantakari, [3]T. Vähä-Heikkilä, [2]A. Rydberg, [3]J. Varis
[1]FOI Swedish Defence Research Agency, Olaus Magnus väg 42, SE-583 30, Linköping, Sweden
E-mail: robert.malmqvist@foi.se
[2]Uppsala University, Uppsala, Sweden
[3]VTT Technical Research Institute of Finland, Espoo, Finland

1. Introduction

Today, there is an increasing interest in making RF systems self-adjusting or "cognitive" [1]. Such a unique ability is expected to lead to very efficient RF systems with reduced size, weight, power and cost. Frequency-agile front-end architectures realised using RF Micro Electro Mechanical Systems (MEMS) technology is an enabling technology proposed to achieve those highly attractive benefits [1-2]. Reconfigurable MEMS matching networks could be utilized to implement tunable (multi-band) LNAs, PAs and filters that can be commercially very attractive since such devices could be useful for different frequency bands and applications [3]. For example, today's wireless RF systems for point-to-point communication can operate at many different frequencies (sub-bands) up to 40 GHz. Below, we will describe some initial results of fabricated RF MEMS based impedance matching networks that were designed in order to realize a frequency tunable SiGe LNA at 20 GHz

2. RF MEMS Matching Networks for Tunable SiGe LNA

Figure 1a shows chip photos of two differential tunable LNA matching networks that have been fabricated using RF MEMS processes from VTT and Fraunhofer ISIT, respectively. The centre frequency tuning range (Δf_c) of the fabricated tunable LNA matching networks is related to the MEMS capacitance ratio values realized in the two different process runs used. The first type of matching networks (using VTT process) were made with Δf_c=19.1-21.5 GHz (12%) and a return loss below -25 dB. Differential MEMS matching networks were later combined with a SiGe LNA with a measured gain of 17 dB at 23 GHz. The tunable LNA gain was quite low due to the parasitics of the relatively long bond-wires needed to connect the different chips together. Albeit, with the ISIT type of MEMS matching networks $\Delta f_c(s_{11})$=17.3-21.2 GHz (20%). Modified RF MEMS matching networks have been sent to be fabricated that will allow for flip-chip mounting and thus lower parasitics and improved performance to be achieved.

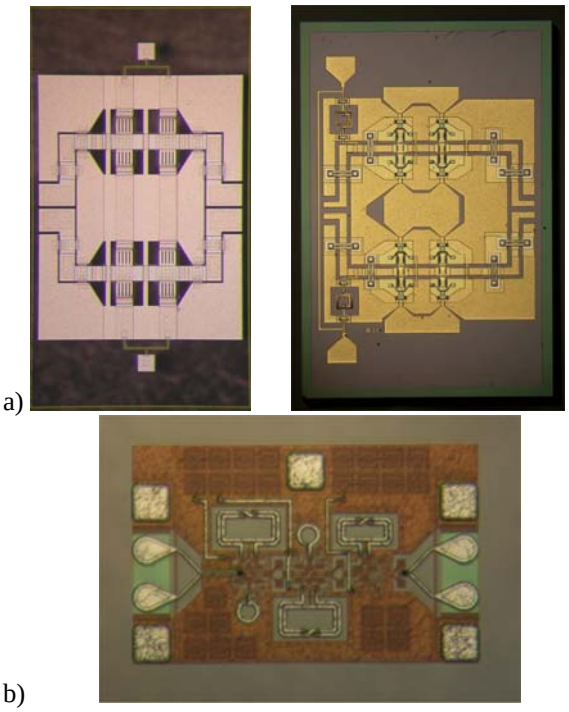

Fig.1. Chip photos of a) two reconfigurable impedance matching networks (made using RF MEMS processes from VTT and Fraunhofer ISIT, respectively) and b) a 24 GHz SiGe LNA (Atmel process).

3. CONCLUSIONS

This paper describes some initial experimental results of RF MEMS matching networks and a SiGe LNA that have been fabricated within the RF-PLATFORM and MOSART projects (funded by the EC FP6 and the NORDITE program). The MEMS based tunable LNA matching networks show up to 20% of tuning range at 20 GHz.

REFERENCES

[1] E.J. Martinez, "Transforming MMIC's," *Proc. of the Gallium Arsenide Integrated Circuits Symp*. 2002, 24th Annual Technical Digest, Oct. 2002, pp. 7-10.

[2] G. Kaminski, "Using RF-MEMS for a reconfigurable frequency agile frontend with a SW-radio architecture," *WS on reconfigurable RF-MEMS for optimum RF/microwave circuits, MTT-S Int. Microwave Symp.*, Fort Worth, USA, June 6-11, 2004.

[3] J.-P. Busquere et al., "MEMS IC concept for reconfigurable low noise amplifier," *Proc. of 36th European Microwave Conference*, Sept. 2006, Manchester, UK, pp. 1358-1361.

$Ba_xSr_{1-x}TiO_3$ Based Solidly Mounted Tunable FBARs

A. Vorobiev and S. Gevorgian
Department of Microtechnology and Nanoscience, Chalmers University of Technology, 412 96 Gothenburg, Sweden
Contact E-mail: andrei.vorobiev@chalmers.se

Abstract **— Integration possibilities of $Ba_xSr_{1-x}TiO_3$ (BST) based tunable Film Bulk Acoustic Wave Resonators (FBAR) using all-dielectric SiO_2/AlN and metal-dielectric SiO_2/W Bragg reflectors deposited on a high resistivity silicon substrate are considered. Both reflectors withstand the high deposition temperature (>600C) of the BST films. *Qf* products more than 1000 are achieved.**

I. Introduction

At present there is a strong push to make the FBARs tunable. Tunability allows taking care of the processing tolerances and makes FBARs useful in cognitive (software defined) radio. Practically AlN, ZnO and other piezoelectric material based FBARs are not tunable. $Pb_xZr_{1-x}TiO_3$ (PZT) based FBARs do provide substantial tunability. However due to the high losses and hysteresis the system applications of PZT (and $BaTiO_3$) resonators are very limited. In this work the induced piezoelectric effect in paraelectric phase BST is considered for high Q-factor electric field tuned and hysteresis free FBARs. Silicon substrate integration of the resonators is achieved by using SiO_2/AlN and *SiO_2/W* based Bragg reflectors.

II. Substrates and Bragg Reflectors

High resistivity (>10 kOhm cm) *p*-type 4" silicon wafer is used as substrate. The BST FBARs are acoustically isolated from the substrate using SiO_2/AlN and *SiO_2/W* based Bragg reflectors. The question was if these reflectors withstand high temperatures required for the deposition of the BST films?

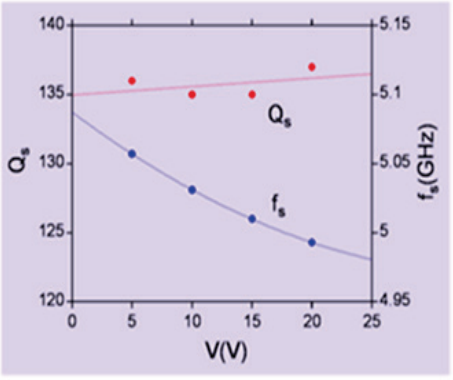

Fig.1 Motional Q-factor and tunability of SiO_2/AlN Bragg reflector based FBAR

In one set of the FBARs six pairs of SiO_2/AlN are used in Bragg reflectors. In the other set two pairs of *SiO_2/W* are used. SiO_2/AlN and *SiO_2/W* layers are deposited by magnetron sputtering. The BSTO film is deposited on non-patterned *Pt* bottom electrode by RF magnetron sputtering using a *$Ba_{0.25}Sr_{0.75}TiO_3$* target. The top *Al* electrodes have circular shape. The resonators are designed for center frequency 5.2 GHz.

III. Performance of the FBARs

The measured voltage dependent motional Q-factors and series resonant frequencies of the FBARs are shown in Fig.1 and Fig.2.

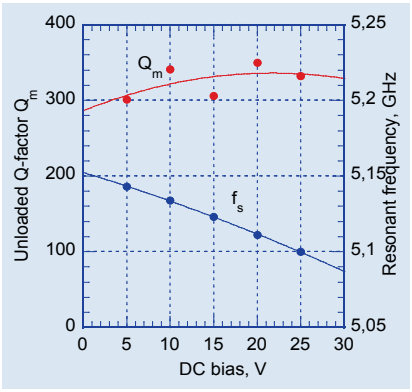

Fig.2 Motional Q-factor and tunability of SiO_2/W Bragg reflector based FBAR

IV. Conclusions

The experiments show that both SiO_2/AlN and SiO_2/W Bragg reflectors withstand the high deposition temperature of BST films. To assure good acoustic isolation and high Q-factor more (six) pairs of SiO_2/AlN layers are required. Still the SiO_2/AlN based FBAR yields lower Q-factors, Fig.1 as compared with the Q-factors of SiO_2/W based resonators, Fig.2 where only two pairs of SiO_2/W layers are used. Further improvement of the Q-factors and tunabilities require improvement of the film quality and the design of the resonator.

Acknowledgements

The work is partly supported by Swedish Research Council (project VR-FBAR) and EC (project NANOSTAR).

Growth and RF Characterization of Multiferroic $BiFeO_3$ Films

A. Vorobiev and S. Gevorgian

Department of Microtechnology and Nanoscience, Chalmers University of Technology, 412 96 Gothenburg, Sweden
Contact E-mail: andrei.vorobiev@chalmers.se

Abstract **— Multiferroic $BiFeO_3$ films are grown on silica substrates by pulsed laser deposition. Interdigital capacitors (IDC) are used to measure the electric and magnetic field dependences of the dielectric properties.**

I. Introduction

Multiferroics (e.g. $BiFeO_3$ BFO) are multifunctional materials combining both ferroelectric and ferromangentic properties. They are considered for sensors (magnetic field, bio- chemical etc.), ferroelectric memory etc. In this work their potential for agile microwave components, such as electrically controlled inductors, varactors, non-reciprocal devices, microwave photonics (optical phase modulators, tunable optical filters) is being explored.

II. Results and Conclusions

The $BiFeO_3$ films are grown on amorphous silica glass (SiO_2) substrates. Prior to deposition of the BFO films interdigital capacitors (IDC), made of Au films, are fabricated on the same substrate. The films grown on the surface of the amorphous SiO_2 substrate (in the gaps of the IDC) have highly oriented polycrystalline structure, Fig.1.

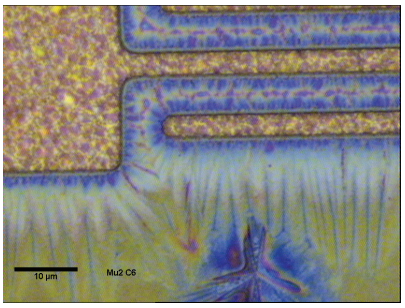

Fig.1 Micro photo of a BFO film in IDC structure

The C-V performance of the IDC including the BFO film is measured at room temperature under applied electric and magnetic fields. Fig.2a shows the C-V under applied electric field only. The "butterfly" shape of it indicates clearly that the film is in polar (ferroelectric) phase. The tunability of the capacitance is more than 7% under the field 20 V/µm. The superimposed magnetic field (limited by the experimental setup) causes a reduction in the capacitance, Fig.2b.

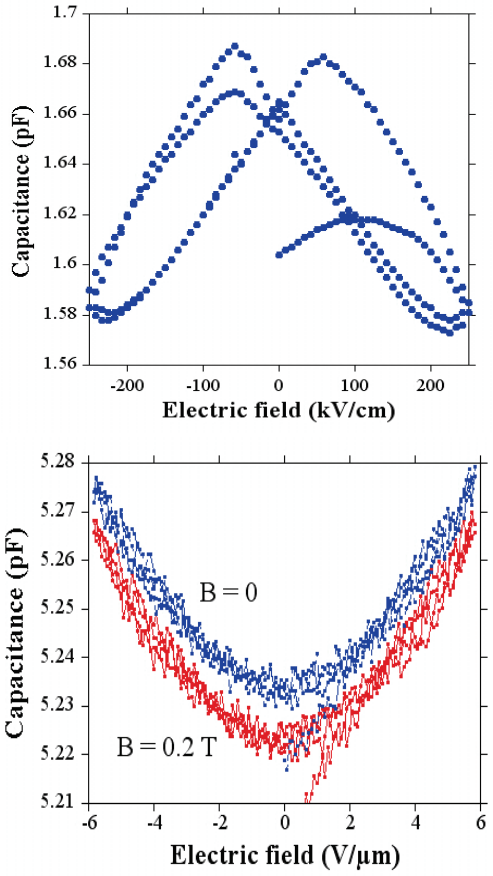

Fig.2 Measured C-V of the IDC including the BFO film without (a) and with (b) magnetic field

In conclusion, the preliminary experiments show the tunability (sensitivity) of the BFO film both on electric and magnetic fields. Further plans include optimisation of the film structure and measurements at microwave frequencies.

Acknowledgements

The work is partly supported by Swedish Research Council (project Metamaterials)

Session 5

13.15-15.15 Tuesday 9 March 2010

A Novel FPGA-based 2.5Gbps D-QPSK Modem for High Capacity Microwave Radios

Zhongxia (Simon) He† zhongxia@chalmers.se
Jingjing Chen‡
Yinggang Li‡
Herbert Zirath†‡

†Microwave Electronics Lab, Dept. of Microtechnology and Nanoscience, Chalmers University of Technology, Sweden
‡Microwave and High Speed Electronics Research Center, Ericsson Research, Sweden

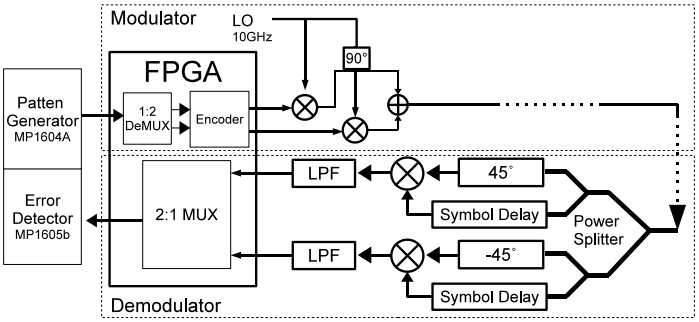

Fig. 1. The architecture of D-QPSK modem

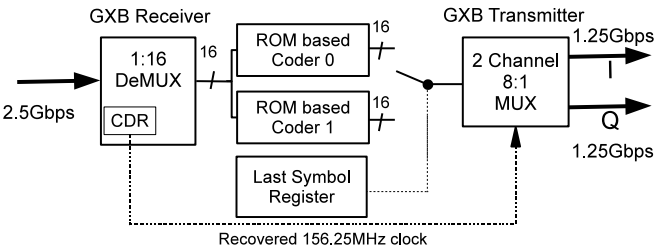

Fig. 2. The architecture of the FPGA-based D-QPSK encoder

As wireless technology evolves toward LTE and beyond, more and more mobile broadband services will roll out and consequently bandwidth demanding data traffic will grow rapidly. As a result, operators have to find the right technical and commercial approach to meet the increasing demand in network capacity as well as to manage the challenges of convergence, flexibility and cost-effectiveness. In terms of capacity, Giga-bit speed is required for LTE backhauling. Even high capacity is predicted for the LTE-Advanced.

Microwave links have been the obvious mobile backhaul choice for many operators [1]. Multi-Gbps capacity may be provided using the newly released E-band (71-76GHz and 81-86GHz) dedicated for Point-to-Point (PtP) application. In this band, 10GHz spectrum is available and spectrum efficiency is usually not of the highest priority. This allows the use of low-order modulation schemes and simple receiver implementation.

FPGAs are widely used in wireless communication and optical communication. However, in wireless communication ADCs and DACs are often employed for IF sampling and IF signal generation [2]. While in optical communication, due to the high data rate, external MUX/DeMUX is used to reduce the data rate in order to overcome the limitation of the FPGA throughput [3].

In this paper, we demonstrate a newly designed 2.5Gbps D-QPSK modulator and demodulator (modem) using a high-speed encoder implemented in FPGA without using ADCs and DACs. The encoder itself is not limited to 2.5Gbps and may be upgraded to well above 10Gbps if state-of-the-art FPGAs are used.

Fig.1 shows the architecture of FPGA based modulator and demodulator (modem). The D-QPSK modem is implemented in an Altera Stratix II GX FPGA together with microwave components such as mixers, phase shifter and 90-degree hybrids. The FPGA acts as an encoder in the modulator, also, in the demodulator, it acts as a 1:2 MUX combining two branches bit stream into a faster one. The fig.2 demonstrates the D-QPSK encoder. By adopting GXB receiver, high speed data is demuxed into 16 bit-width low speed bus. Two ROM based coders would providing coded data, a switch would select one of these coded data and put them onto the output buffer according to the status of the last symbol register.

Our test shows that the FPGA output eye is widely open and the modem can achieve error-free for transmitting different PRBS (from PRBS-7 up to PRBS-23). The utilization of FPGA logic is only 2% of the maximum resources. Only 3 of the 12 multi-Gbps transceivers are used in our application. The total power consumption is around 5W, which is sufficiently low for the FPGA to be included in a practical radio system.

REFERENCES

[1] Sandri, J.M, *Microwave backhaul as a business: taking the next step*, Microwave Magazine, IEEE, Volume 10, Issue 5, August 2009 pp.34 - 46

[2] Lee, D. Gray, A. Kang, E. Haiping Tsou Lay, N. Wai Fong Fisher, D. Hoy, S. *A gigabit-per-second Ka-band demonstration using a reconfigurable FPGA modulator*, Aerospace Conference, 2005 IEEE

[3] Serbay, M. Wree, C. Rosenkranz, W, *Implementation of differential precoder for high-speed optical DQPSK transmission*, Electronics Letters, IEEE, 2004.

Parabolic Synthesis Methodology

Erik Hertz and Peter Nilsson, *Member, IEEE*
Department of Electrical and Information Technology
Lund University, Box 118, 221 00 Lund Sweden
mail: {Erik.Hertz, Peter.Nilsson}@eit.lth.se

Abstract **This paper introduces a parabolic synthesis methodology for developing approximations of unary functions. Examples are trigonometric functions and logarithms as well as square root and division functions. They are extensively used and specialized for efficient hardware mapped VLSI design. The advantages with the methodology are, short critical path, fast computation and high throughput enabled by a high degree of architectural parallelism. The feasibility of the methodology is shown by developing an approximation of the sine function for implementation in hardware.**

Index Terms **Algorithms implemented in hardware, computer arithmetic, parabolic synthesis, parallel design style, VLSI.**

Introduction

UNARY functions, e.g. trigonometric functions, logarithmic, as well as square root and division, are extensively used in computer graphics, digital signal processing, communication systems, robotics, astrophysics, fluid physics, etc. For these high-speed applications, software solutions are in many cases not sufficient and a hardware implementation is therefore needed. Implementing a numerical function *f(x)*, by a single look-up table is simple and fast which is strait forward for low-precision computations of *f(x)*, i.e., when *x* only has a few bits. However, when performing high-precision computations a single look-up table implementation is impractical due to the huge table size and the long execution time.

Approximations only using polynomials have the advantage of being ROM-less, but they can impose large computational complexities and delays. By introducing table-based methods to the polynomials methods the computational complexity can be reduced and the delays can also be decreased to some extent.

The CORDIC (COordinate Rotation DIgital Computer) algorithm has been used for these applications since it is faster than a software approach. CORDIC is an iterative method and therefore slow which makes the method insufficient for this kind of applications.

This paper proposes a parabolic synthesis methodology to develop functions that performs an approximation of original functions in hardware. The architecture of the processing part of the methodology is based on parallelism to reduce the execution time. For the development of approximations of functions, a novel parabolic synthesis methodology is used. Only low complexity operations that are simple to implement in hardware are used.

Methodology

The methodology is developed for implementing approximations of unary functions in hardware. The approximation part is of course the important part of this work but there are sometimes two other steps that are necessary, a preprocessing normalization and postprocessing transformation. The computation is therefore divided into three steps, normalizing, approximation and transforming.

A. Normalizing

The purpose with the normalization is to facilitate the hardware implementation by limiting the numerical range.

B. Developing the Hardware Architecture

When developing a hardware architecture that approximate an original function, only low complexity operations are used. Operations such as shifts, additions and multiplications are efficient to implement in hardware and therefore searched for.

As in Fourier analysis the proposed methodology is based on decomposition of basis functions. The proposed methodology is not, as in Fourier analysis, a decomposition method in terms of sinusoidal functions but in second order parabolic functions [1]. Second order parabolic functions are used since they can be implemented using low complexity operations. The proposed methodology also differs from Fourier synthesis process since the proposed methodology is using multiplications in the recombination process and not additions as in the Fourier case.

C. Transforming

The postprocessing part transforms the value to the output result.

If the approximation is implemented as a block in a system the postprocessing part can be taken into consideration in the following blocks which implies that the postprocessing part can be excluded.

[1] Erik Hertz and Peter Nilsson, Parabolic Synthesis Methodology Implemented on the Sine Function , in Proceedings of the 2009 International Symposium on Circuits and Systems (ISCAS'09), Taipei, Taiwan, May 24-27, 2009.

A/D Conversion for Software Defined Radio

F.Qazi, T.Sundstöm, S.Ahmad, J.Wikner, C.Svensson, J.Dąbrowski
Department of Electrical Engineering, Linköping University
e-mail: jdab@isy.liu.se

For the concept of software defined radio (SDR) the A/D conversion is vital. Placed close to the receive antenna an ADC is exposed to strong interference and as a consequence it requires very high dynamic range and linearity. Noise performance and power consumption are the accompanying design constraints. To follow the SDR concept the RF sampling technique was introduced where SC circuits serve as decimation filters [1-3]. In this way, signal prefiltering flexible with RF frequency is achieved (including antialiasing) and the rate of samples is reduced to match A/D conversion with a clock around 100 MHz. The requirements for the antialiasing filtering can be largely mitigated when using much higher clock frequencies, feasible with contemporary CMOS technology. In this case the ADC and the decimation block in the receiver are swapped and the latter is digital rather than analog.

In this work we investigate sigma-delta ADCs clocked at GHz frequencies thus providing large oversampling ratios to common signals used in personal RF communication systems. The inherent noise shaping is useful both in terms of receiver noise performance and dynamic range. We present simulation and measurement results of a current mode, first order, 4-bit ΣΔ converter implemented in 90 nm CMOS (Fig.1). The RF signal downconverted to zero or low IF is used as the input after simple filtering to mitigate interference. In simulation this circuit achieves SINAD = 83 dB (ENOB = 13.5) for 20 MHz signal bandwidth in zero-IF architecture. The maximum clock frequency is close to 3 GHz and the power consumption is 17 mW. A digital decimating filter, which could include linearity correction, is needed to enable further baseband processing.

Another sigma-delta converter suited for direct RF sampling is also presented. The second-order one-bit architecture is chosen for possibly best linearity and sufficient dynamic range. A preliminary implementation is a passive SC circuit (Fig.2) that allows to save power. Also the problem of settling time, typical of active integrators, is avoided in this way. The circuit designed in 65 nm CMOS can operate at frequency up to 4 GHz and achieves SNDR = 75 dB for conditions similar to the previous circuit. By incorporating the "noise coupling" technique [4] a further improvement of 10dB or so can be expected.

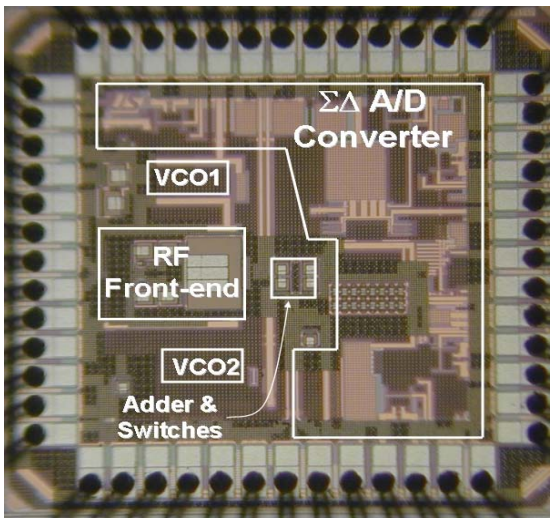

Fig.1. Chip micrograph of ΣΔ ADC and wideband Rx frontend implemented in 90 nm CMOS.

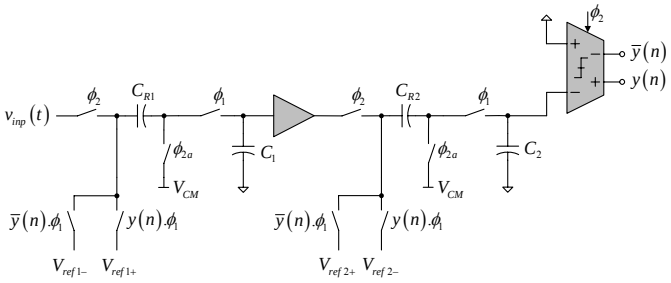

Fig.2. Schematic of second-order passive ΣΔ ADC.

[1] Muhammad K. et al., "The First Fully Integrated Quad-Band GSM/GPRS Receiver in a 90-nm Digital CMOS Process," *IEEE JSSC*, Vol. 41, No 8, Aug. 2006, pp. 1772 – 1783.

[2] Andersson S. et al., "SC Filter for RF Sampling and Downconversion with Wideband Image Rejection," *ALOG Springer*, Vol. 49, 2006, pp. 115-122.

[3] Bagheri, R. et al., "An 800-MHz–6-GHz Software-Defined Wireless Receiver in 90-nm CMOS," *IEEE JSSC,* Vol. 41, No 12, Dec. 2006, pp. 2860 – 2876.

[4] Lee K., et al., "A noise-coupled time-interleaved ΔΣ ADC with 4.2MHz BW, -98dB THD and 79dB SNDR," *IEEE ISSCC Digest*, Feb 2008, pp 494-495.

Power Consumption in Digital Filter Architectures in 65 nm CMOS Technology

S.M. Yasser Sherazi, Joachim N. Rodrigues, and Peter Nilsson
Department of Electrical and Information Technology, Lund University
Box 118, SE-221 00 Lund, Sweden

I. Introduction

This paper focuses on the digital baseband part for ultra low power radio devices. In the digital baseband section, the main circuits are filters and in our application we need decimation filter. This manuscript presents the comparison between two architectures of a half band digital filter, a bit-serial implementation and a parallel implementation in 65 nm CMOS technology. In order to evaluate the power consumption, designs are synthesized in 65 nm low leakage-high threshold CMOS technology.

II. Power Consumption Basics

In a digital circuit the dominant power consumption source is either dynamic or leakage power, where they are specified as

$$P_{dynamic} = \alpha f_{clk} C_L {V_{DD}}^2, \quad (1)$$

$$P_{leak} = I_{leak} V_{DD}, \quad (2)$$

In (1) α is the activity or switching factor of a node, f_{clk} the switching frequency, C_L the total node capacitance. In (2) I_{leak} is the leakage current in static mode and V_{DD} is the supply voltage. It is evident that by reducing the supply voltage the power consumption may be reduced quadratically. For static or leakage power the scaling effect is more exponential. However, the down side of reducing the voltage is that the delay of the device will increase, causing the devices to leak for longer durations. However, leakage will be decreased by the order of 1000 per operation compared to super-threshold regime [1].

III. Half Band Digital Filter

An optimized third order filter structure is used to show the power consumption for the both parallel and bit-serial architectures. The filter structure for parallel implementation, shown in Figure (1a), is a third order bi-reciprocal lattice wave digital filter [2], also called a half-band filter. Half-band filter, are highly suitable as decimators or interpolators, with the factor of two. The benefit of using such type of filter is that all the filtering may be performed at lower sample rate. When compared to FIR filters, recursive half-band filters have low arithmetic complexity, therefore, yielding low power consumption and low chip area cost [3].

The recursive structure originally has four adders and three registers. There is also one multiplication with the coefficient 0.5, which corresponds to a shift. This filter is optimized in such a way that we get three adder circuits instead of four adders but instead we include two more delay elements as shown in Figure (1a). The benefit of applying such optimization is threefold, firstly it may reduce the hardware cost, secondly it may reduce the critical path, and thirdly it may help in reducing the energy dissipation. We have used a word length of 12-bits for the parallel implementation of the filter [4]. For the sake of fairness and comparability we have used the libraries provided by the vendor. In order to attain correct functionality a small controller circuitry is needed for bit-serial implementation. The serial architecture of HBD filter is shown in Figure (1-b).

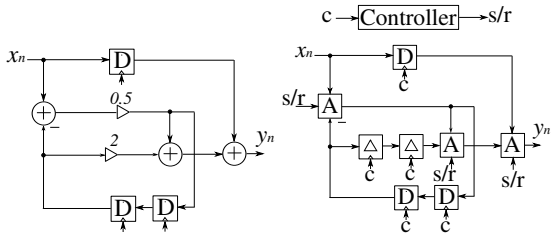

Fig. 1. **a:** Optimized Parallel HBD Filter. and **b:** Serial HBD Filter

TABLE I
Circuitry Performances at EMV

Circuit	Supply [V]	f [MHz]	P/Cyc [W]	P/smp [W]	Area
parallel	1	100	$1.4\,e^{-5}$	$1.4\,e^{-5}$	1123
serial	1	100	$6.3\,e^{-6}$	$8.8\,e^{-5}$	653

A. Implementation

For implementation purposes, the two architectures of HBD filters were modelled in VHDL. The functionality of the filters were verified by doing simulations in *ModelSim*. The full adder and DFF cell were instantiated from the *Low Power High Threshold* cell libraries provided by vendors in order to create the complete design. Once the design were verified, they were synthesised using *Design Vision*, it created netlist in a *.v* file and back-annotated toggle information in *.sdf* file. These files were used in generating the *.vcd* that containing the switching information of all nets, this file is acquired by doing simulations in *ModelSim*. The power consumption results are generated through power analysis tool *Prime Time*.

IV. Result and Conclusion

Table I, indicates the characteristics of the two architectures. Theoretically, the bit-serial architecture should be clocked at a frequency that is *n* times higher than the frequency of parallel architecture to have a same throughput. In these simulations, the time it requires to process a complete sample is larger in a bit-serial implementation, making the devices switch for longer period of time, that overcomes the advantage of device reduction. Hence, the over all power consumption per sample is higher.

References

[1] C. Neau and K. Roy, "Optimal body bias selection for leakage improvement and process compensation over different technology generations," in *ISLPED '03*. New York, NY, USA: ACM, 2003, pp. 116–121.
[2] P. Nilsson and M. Torkelson, "Method to save silicon area by increasing the filter order," in *Electronic letters*. ACM, NY, USA, 1995.
[3] H. t. Ohlsson, "Arithmetic transformations for increased maximal sample rate of bit-parallel bireciprocal lattice wave digital filters," in *The 2001 IEEE International Symposium on Circuits and Systems*, vol. 2, May 2001.
[4] P. Nilsson, "Arithmetic and architectural design to reduce leakage in nano-scale digital circuits," in *Proceedings of 18th European Conference on Circuit Theory and Design*, 2007.

On MB OFDM-UWB Channel Estimation

Johan Löfgren and Peter Nilsson
Dept. of Electrical and Information Technology, Box 118, Lund University, Sweden
Email: {Johan.Lofgren, Peter.Nilsson}@eit.lth.se

I. Introduction

In this paper, different channel estimation strategies for the MB OFDM-UWB are investigated and compared based on complexity and error performance. The applied algorithms are the Least Square (LS) and different simplifications based on the Minimum Mean Square Error (MMSE) estimator [1], [2]. The algorithms are known, but there is no published numbers on the cost of implementing them in a UWB system. This paper fills that gap.

II. System and Channel Model

The standard proposes $N = 128$ sub-carriers, where 100 carry data, 12 pilots, 10 are guards and the final 6 are empty. In addition, the cyclic prefix is $1/4th$ of the number of sub-carriers, or $L = 32$ samples. on top of this there is a frame structure containing a number of OFDM symbols in each frame. The frame pre-amble contains synchronization information and 6 all-pilot symbols for an initial channel estimation. Following the pre-amble there is a data stream with varying length. [3]

In this work, the channel is assumed to be quasi-stationary and only change between different frames. That allows for channel estimation to be performed using only the initial all-pilot symbols and ignoring the continuous pilots in the data stream, which otherwise is used for tracking a changing channel. In addition, it is assumed that the channel delay is no longer than the cyclic prefix, which means that the orthogonality criterion between the different sub-carriers hold.

III. Channel Estimation

As stated above, the pilots in the initial all-pilot symbols are used to estimate the channel. Since the channel is quasi-constant, it is possible to average the estimates from the different symbols and thereby improve the SNR by a factor of 6 (7.7 dB).

The simplest channel estimation is then to just calculate the channel coefficient for each sub-carrier not considering the correlation with the neighboring sub-carriers. This is the LS estimation and the operation require one complex multiplication per sub-carrier and pilot. To get a better estimate it is possible to also consider the correlation to the neighboring sub-carriers, using an MMSE approach. The correlation can be pre-calculated, using a robust approximation [4]. Still the complexity is too high and to further reduce the complexity it is possible to use a subset of the correlation information, either with a Wiener filter with a limited number of taps [1], or using the SVD reduction [2].

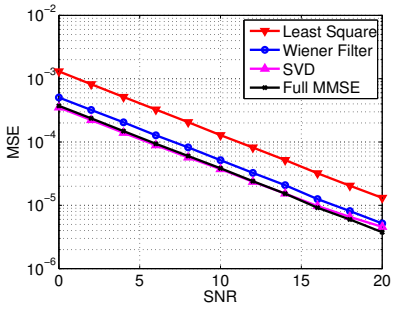

Fig. 1. MSE for different Channel Estimators

TABLE I
Complexity per tone for the different estimators

Estimator	Total complex multiplications
Least Square	768
Wiener 11 taps	2,176
SVD Estimator	9,728
Full Matrix	17,152

IV. Results

In fig. 1, the Mean Square Error (MSE) for the different approaches are shown. The complexity of the different approaches for estimating the channel for one frame are seen in table I.

V. Conclusion

Due to the relatively long cyclic prefix many coefficients need to be calculated in the SVD approach. That makes this impractical in the UWB case. Also the averaging of six independent OFDM symbols indicates that the LS approach is sufficient. If better performance still is asked for, Wiener filtering seems to be the better option, especially for high SNRs.

References

[1] P. Hoeher, "Tcm on frequency-selective land-mobile fading channels," *Proc. 5th Tirrenia International Workshop on Digital Communications*, pp. 317–328, 1991.

[2] O. Edfors, M. Sandell, J.-J. van de Beek, S. Wilson, and P. Borjesson, "OFDM channel estimation by singular value decomposition," *Communications, IEEE Transactions on*, vol. 46, no. 7, pp. 931–939, Jul 1998.

[3] (2009) Multiband OFDM proposal update - january 2005. [Online]. Available: http://www.docstoc.com/docs/15592882/MultiBand-OFDM-Proposal-Update—January-2005

[4] Y. Li, J. Cimini, L.J., and N. Sollenberger, "Robust channel estimation for OFDM systems with rapid dispersive fading channels," *Communications, IEEE Transactions on*, vol. 46, no. 7, pp. 902–915, Jul 1998.

Digital Cross-Correlators: Two Approaches

Ryman E.[*†], Emrich A.[*], Embretsen J.[*], Riesbeck J.[*], Andersson S.[*], Larsson-Edefors P.[†] and Svensson L[†].

[*]Omnisys Instruments AB
Gruvgatan 8, SE-421 30, Västra Frölunda, Sweden
Email: er@omnisys.se

[†]Dept. of Computer Science and Engineering
Chalmers University of Technology
SE-412 96 Gothenburg, Sweden
Email: erirym@chalmers.se

Abstract

Cross-correlation is a signal processing method that requires immense amounts of calculations. One way to achieve this is to use specialized digital circuits, either in the form of ASICs or FPGAs. This paper describes two cross-correlators, one based on an FPGA and the other one implemented as an ASIC.

The FPGA-based cross-correlator unit performs complex cross-correlations on 2x32 inputs (I and Q). It has a detection bandwidth of 300 MHz centered at 3.71 GHz. A series of tests and measurements have been made on the unit for verification. The noise isolation is measured to exceed 50 dB. The total power consumption of the correlator system is below 130 W, including significant analog signal processing parts and analog to digital conversion. The digital correlator core is estimated to have a power dissipation between 5 W and 10 W, which would equal 7.5-15 mW/ch/GHz. While the compactness and power requirements of the FPGA-based correlator is an achievement, it is still constructed as a ground-based correlator.

Figure 1: The FPGA based correlator

An ASIC-based cross-correlator has the potential to further reduce power dissipation and size. This is ideal for applications in space where power and size are major issues. Two satellite-borne correlator projects are currently being planned; Geo MS (ESA/Eumetsat) and GeoSTAR (NASA). A single-chip cross-correlator which could be appropriate for these projects is being developed; a first test chip is currently under fabrication and is planned to return from the foundry by March 2010. The chip has around 3 million transistors, in a low-power 65-nm CMOS process. This cross-correlator has 64 single-bit digital inputs. Simulation results suggest that operation at up to 4 GHz bandwidth could be achievable, and this at a power dissipation of just above 1 W. With a total of 2016 output channels this would equal around 0.13 mW/ch/GHz. As a comparison, a state-of-the-art cross-correlator being developed for Geo STAR is estimated to have a total power dissipation of less than 20 W when performing 20 trillion 1-bit multiplications per second [1]. This would equal a power dissipation of less than 1 mW/ch/GHz. Currently an effort is put into making a suitable breadboard test bench for the circuit. Some of the challenging requirements on the test bench are high clock frequencies and low skew between inputs. The 65-nm correlator will be verified for functionality, speed and power dissipation.

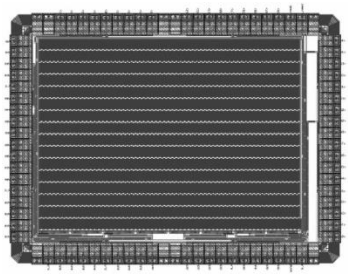

Figure 2: The ASIC correlator

REFERENCES

[1] A. B. Tanner, S. T. Brown, S. J. Dinardo, T. M. Gaier, P. P. Kangaslahti, B. H. Lambrigtsen, and W. J. Wilson, "Initial results of the GeoSTAR Prototype (Geosynchronous Synthetic Thinned Array Radiometer)," in *Proceedings of IEEE Aerospace Conference*. Jet Propulsion Laboratory California Institute of Technology, 2006.

High-Resolution Digital Backend for Superconducting Microresonators

Johan Riesbeck

Omnisys Instruments AB

Email: jr@omnisys.se

Abstract

The MKIDCam which is currently being constructed for the Caltech Submillimeter Observatory is an instrument based on 2304 Microwave Kinetic Inductance Detectors (MKIDs). In order to measure the instantaneous resonance frequency dissipation of the these detectors a digital back-end with high noise requirements has to designed.

The noise requirement of the back-end is specified so that the system noise must be limited by that of the cryogenic HEMT amplifiers that follow the MKID detectors.

Omnisys is designing an FPGA-based back-end which utilizes 16-bits DACs for resonance frequency generation and low-noise 14-bits ADCs for data sampling. Both DAC and ADC operates with a 400MHz sample clock and uses IQ sampling.

Between the A/D conversion stage and the MKIDs is an IF system with modulator and demodulator. The LO frequency of the IF system can be tuned between 1GHz and 4Ghz in 10kHz steps. The signal path also includes amplifiers and attenuators for fine-tuning of signal power.

The high-end FPGA performs an FFT transform which produces a complex spectra with 3kHz spectral resolution over 400MHz bandwidth.

The back-end development is currently in the last phase of the breadboard state where functionally and performance of the hardware is tested. So far the results have been very promising both with respect to hardware functionality and noise performance.

The system developed for CSO will be based on 16 modules with one FPGA and 400MHz bandwidth each. Each module will measure 144 MKIDs at a 100Hz rate and the corresponding data will be sent to a host PC or server via an Ethernet interface. Omnisys is focusing on buildning a powerful and flexibel solution which can be used in different applications. The FPGA can be configured with different signal processing algorithm in order acommodate different uses. The data rate is limited by the Ethernet port on the system, but each module can also be equipped with either a separate Ethernet port or a serial gigabit transceiver for even higher data rates.

Session 6

15.45-17.10 Tuesday 9 March 2010

Carrier Aggregation - Another RF Design Challenge

Lars Sundström – lars.s.sundstrom@ericsson.com
Ericsson AB, Ericsson Research
Lund, Sweden

Mobile communication standards continuously evolve to accommodate more users and more demanding services. Various technologies are introduced in the standards as soon they are expected to become cost-efficient. The dominating WCDMA-based 3G standard, specified by 3GPP, continue to evolve and the most recent version (Release 8), usually referred to as HSPA evolution, provides more than two orders of magnitude higher data rate compared to the first release. With Release 8 a new radio access technology, Long-Term Evolution (LTE), was introduced as a parallel track to HSPA evolution to provide a springboard to future 4G mobile communication. LTE is not held back by the backward compatibility requirements of HSPA evolution and therefore could be designed, for example, to address more complex spectrum scenarios. It introduces an air-interface technology different from WCDMA to allow for more flexible and graceful deployment. The downlink transmission is based on OFDM and the uplink transmission on SC-FDMA and should support a scalable channel bandwidth from 1.4MHz to 20MHz. The requirements on a fourth generation standard are specified in IMT Advanced by ITU-R and LTE Release 10 is expected to meet or exceed these requirements. Several enablers need to be introduced to reach this target that have a direct implication on transceiver design including multi-antenna techniques, higher order modulation, and wider bandwidth. The multi-antenna techniques included ranges from basic antenna diversity to beam-forming and MIMO and translate to having several transceivers operating simultaneously. Higher order modulation means more stringent linearity requirements on transmitter power amplifiers. Wider bandwidths will be supported by means of carrier aggregation, i.e. rather than simply increasing the channel bandwidth, more carriers can be added on a per-user need basis. This approach is backward-compatible with LTE Release 8 and therefore allows for a graceful introduction in existing bands and a more flexible frequency planning of virgin bands.

Carrier aggregation (CA) constitutes a major RF design challenge from a complexity point of view. Inter-band CA means that at least two transceivers need to be operated simultaneously and each region will have at least one such standardized combination of bands. Intra-band carrier aggregation will most likely be contiguous in Release 10 but non-contiguous in a future release to support even more complex spectrum situations. Contiguous intra-band CA means that transceivers should support an even larger range of bandwidths to accommodate different combinations of channel bandwidths while maintaining the stipulated per carrier performance requirements. With non-contiguous intra-band CA the choice of transceiver architecture is less obvious. It is tempting to continue using a single transceiver for several carriers within the same band. But since the distance between carriers is variable there will be even more scenarios for which the transceiver must be standard compliant.

This presentation will discuss these challenges in more detail, in particular with respect to architectures, complexity, power efficiency, performance requirements, and not least the increased test space.

Ultra-Wideband Low-loss All-Silicon MEMS Phase Shifters for High-Performance Electronic Beam-Steering Applications

N. Somjit, G. Stemme and J. Oberhammer
Microsystem Technology Lab, KTH – Royal Institute of Technology
KTH-Royal Institute of Technology, 10044 Stockholm, Sweden
contact: nutapong.somjit@ee.kth.se

This paper introduces a novel concept of an ultra-broadband low-loss mechanically reconfigurable digital-type dielectric-block microwave MEMS shifter with best performance optimized for 75-110-GHz W-band applications. This phase shifter concept does not involve any air-suspended thin moving metallic membranes which are employed in the conventional distributed MEMS phase shifters and MEMS switched true-time delay line phase shifters. Thus, it is suitable to operate under larger signal power, providing excellent robustness and reliability.

Figure 1 shows conceptional drawings of a single stage phase shifter. The relative phase shift between up and down state is achieved by vertically movable a high-resistivity silicon dielectric block above a 3D micromachined coplanar waveguide (CPW) by electrostatic actuation which results in different propagation constants of the microwave signal. The length of the silicon block is chosen to λ/2 for a specific frequency of 75 GHz to minimize return loss caused by reflected electromagnetic waves from both ends. The monocrystalline-silicon block is suspended above the 3D micromachined CPW by four serpentine flexures. The phase shift of a single stage is tailor-made to 45°, 30° and 15° by artificially tuning the effective dielectric constant of the silicon block by varying the size of the etch-holes. For full 360º phase-shift capabilities, 15°+30°+5×45° phase shifters are required, providing 19×45° phase-shift resolutions. For digital-type operation, the optimized operation point of high phase-shift sensitivity and medium deflection is chosen to be 5 µm.

Fabrication process starts with sputtering and patterning 1-µm-thick gold CPW on top of a 500-nm SiO_2 layer. Above the gold, 100-nm thick Si_3N_4 bumps are deposited as distance keepers to prevent DC short circuiting. The slots of the CPW are further etched by DRIE into the silicon substrate to decrease substrate loss and to increase the sensitivity of the propagation speed to changes in the displacement of the dielectric block. An SOI wafer is bonded to this wafer by adhesive polymer bonding, and the SOI handle wafer is afterwards removed by plasma etching. The 35-µm thick device layer is patterned by two DRIE steps to shape the thick dielectric block with its release-etch holes and the 9-µm thick serpentine flexures. Finally, the patterned structure is released by O_2-plasma etching process. Fig.2 shows a SEM picture of 45°, 30° and 15° stages, and Fig.3 shows a microscope picture of a full 15°+30°+5×45° phase-shifter.

Fig. 4 and 5 show the RF measurement results of the binary-coded 15°+30°+5×45° phase shifter for one to all seven stages actuated. At the design frequency of 75 GHz, maximum return and insertion loss are -17 dB and -3.5 dB, respectively, which are corresponding to a loss of -0.82 dB/bit, and a phase shift efficiency of 71.1°/dB and 490.02°/cm. The phase shifter behaves exceptionally broadband over the whole *W*-band with the maximum return loss better than -12 dB and the maximum insertion loss of less than -4 dB (98.3°/dB; 715.6°/cm at 110 GHz). The binary-coded MEMS phase shifter presented in this paper has better insertion loss per bit and better maximum return loss than any phase shifter ever reported, both for their respective nominal frequency and for the whole W-band. The pull-in behavior of the electrostatic actuator voltage was characterized to be 29.9 V with the effective spring constant of 36.67 N/m.

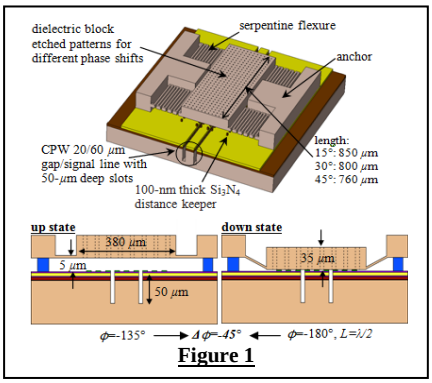

Figure 1

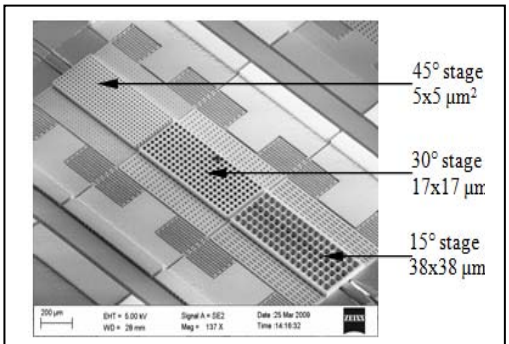

Figure 2

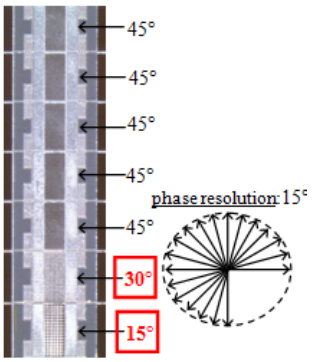

Figure 3

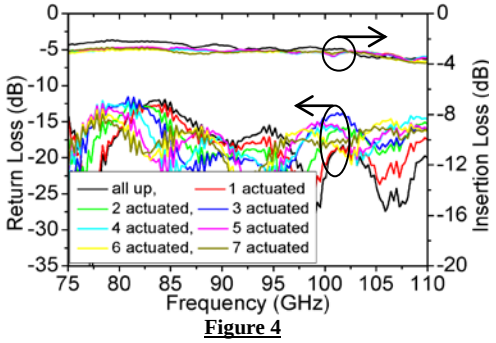

Figure 4

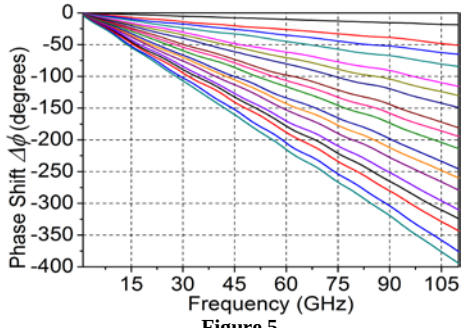

Figure 5

A PLL based 12GHz LO Generator with Digital Phase Control in 90nm CMOS

Andreas Axholt, Henrik Sjöland
Electrical and Information Technology, Lund University
Box 118, SE-221 00 Lund, Sweden
{andreas.axholt,henrik.sjoland}@eit.lth.se

Abstract—A 12 GHz PLL with digital output phase control has been implemented in a 90 nm CMOS process. It is intended for LO signal generation in integrated phased array transceivers. Locally placed PLLs eliminate the need of long high frequency LO routing to each transceiver in a phased array circuit. Routing losses are thereby reduced and design of integrated phased array transceivers become more modular. A chip was manufactured, featuring two separate fully integrated PLLs operating at 12 GHz, with a common 1.5 GHz reference. The chip, including pads, measures 1050x700 um^2. Each PLL consumes 15 mA from a 1.2 V supply, with a typical measured phase noise of -110 dBc/Hz at 1 MHz offset. The phase control range exceeds 360^0.

System architecture

The presented circuit, Fig. 1, eliminates the need of cumbersome high frequency routing by allowing the high frequency local oscillator signal to be generated close to the mixer of each transceiver. The only signal that needs distribution is the relatively low frequency 1.5 GHz reference. The elimination of complex distribution networks makes the design of a phased array transceiver more modular.

System architecture

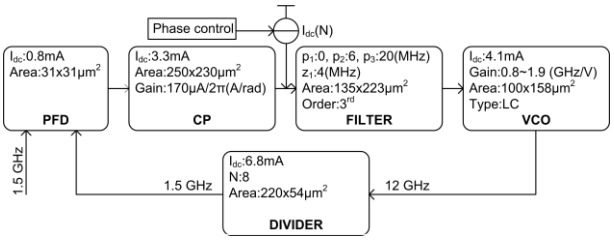

Fig. 1: Blockdiagram

The principle of the phase control is rather intuitive. Assuming the loop to be locked, the PFD and CP operate to align the rising edges of the reference and feedback signals by injecting charges into the loop filter, adjusting the VCO frequency. Once the edges are aligned the net charges injected into the filter is zero, maintaining a constant VCO frequency control voltage. By introducing a static current injection into the loop filter, the loop must counteract by injecting the inverse current to maintain zero net charging, keeping the frequency constant. Since the phase difference between the reference and feedback signal and net charges injected are correlated (proportional), an injected static current corresponds to a static phase difference.

Experimental results

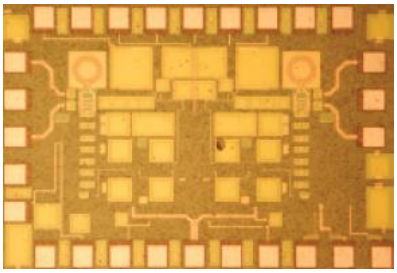

Fig. 2: Die photo

The die photo is shown in Fig. 2. Phase shift versus 6-bit control word was obtained by simultaneously measuring both PLL output signals with Agilent VNA E8316A, Fig 3. The phase range is full 360 degrees with a resolution of 6 degrees. The reference spur is lower than -55dBc for all phase settings. Phase noise versus phase setting is shown in Fig. 4.

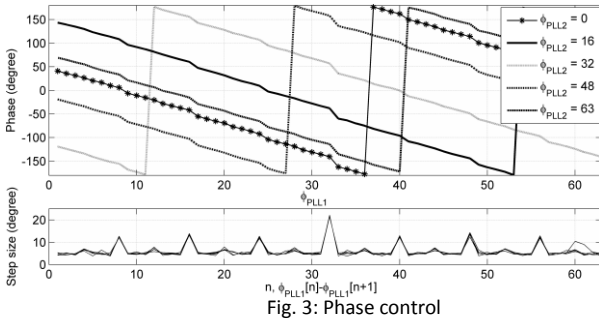

Fig. 3: Phase control

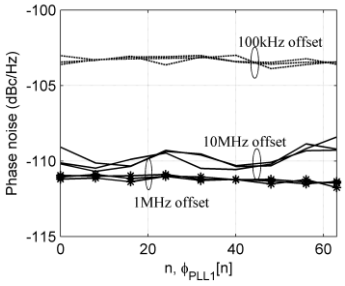

Fig. 4: Phase noise

References

Andreas Axholt and Henrik Sjöland "A PLL based 12GHz LO Generator with Digital Phase Control in 90nm CMOS" Proc. IEEE Asia Pacific Microwave Conference , Dec. 2009.

Highly Efficient Dynamic Load Modulation Transmitter

C. Fager*, H. Nemati*, H. Cao*, A. Soltani+, T. Eriksson+, R. Jos¤, and H. Zirath*

GigaHertz Centre, Departments of Microtechnology and Nanoscience* and Signals and Systems+
Chalmers Tekniska Högskola, SE-41296 Göteborg, Sweden,
E-mail: {christian.fager, mashadne, haiying, asoltani, thomase, herbert.zirath}@chalmers.se

¤NXP Semiconductors, 6534 AE Nijmegen, The Netherlands, E-mail: rik.jos@nxp.com

I. INTRODUCTION

The energy consumption and thus operating expenses of radio base stations is dominated by the RF power amplifier (PA). Much research has therefore been devoted to PA efficiency enhancement methods for such applications. Dynamic load modulation (DLM) is one of the most promising methods, potentially offering wider bandwidth compared to other methods used, e.g. envelope tracking or Doherty amplifiers. Challenges in designing load modulation networks and accompanying linearization schemes for this architecture in high power RF applications have, so far, limited the performance of the results presented.

In this work we show that a DLM transmitter can be successfully implemented using a modular approach where an existing highly efficient 1 GHz LDMOS PA is combined with a dedicated varactor based electrically tuneable load network. The transmitter is finally combined with an efficiency optimized linearization scheme.

II. TRANSMITTER DESIGN

The load modulation properties of the existing PA were first investigated using load-pull measurements, sweeping the load impedances (Z_L) and input power (P_{in}) independently. The results in terms of power added efficiency (PAE) vs. output power (P_{out}) are shown in Fig. 1. Clearly, the efficiency can be significantly improved at low power if optimized impedance and input power are provided.

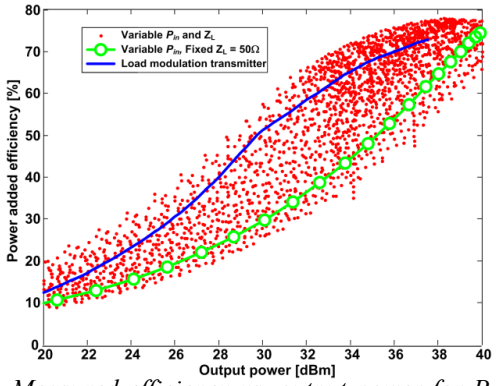

Fig. 1. Measured efficiency vs. output power for PA load pull and implemented load modulation transmitter.

The PA load-pull measurements were then used as a basis for the design of a dedicated varactor based load modulation network that is used to approximate the desirable PA load impedance at each output power level. A picture of the complete DLM transmitter demonstrator is shown in Fig. 2

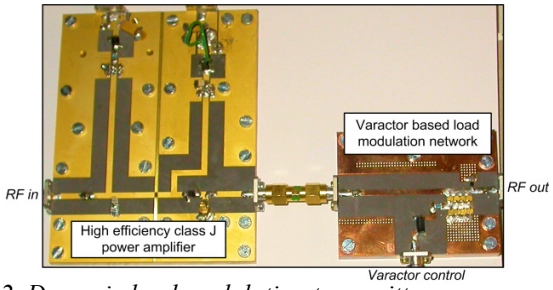

Fig. 2. Dynamic load modulation transmitter.

III. RESULTS

The DLM transmitter has RF and baseband varactor voltage inputs that are dynamically controlled in the measurements. A dual input inverse model was therefore derived from static measurements where, for each P_{out}, the efficiency optimizing combination of P_{in} and varactor voltage was recorded. This model was then combined with a conventional digital pre-distortion scheme and careful time alignment between the two signal paths. The linearized results in terms of measured output spectrum are shown in Fig. 3 when a WCDMA signal (7dB PAPR) is transmitted. The average PAE is in this case 53%, which is the highest efficiency reported for DLM transmitters at RF.

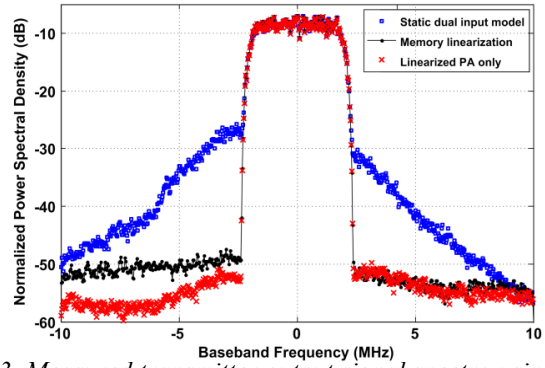

Fig. 3. Measured transmitter output signal spectra using different linearization methods.

IV. CONCLUSIONS

A linearized highly efficient DLM transmitter has been demonstrated using an existing PA and commercially available Si varactors. The results show that DLM is a feasible method to improve the efficiency of power amplifiers for future radio base station applications.

ACKNOWLEDGMENT

This research has been carried out in the GigaHertz Centre in a joint research project financed by Swedish Governmental Agency of Innovation Systems (VINNOVA), Chalmers University of Technology, and Ericsson AB, Infineon Technologies, and NXP Semiconductors.

Session 7

08.30-09.40 Wednesday 10 March 2010

THz in Space Science, Biology and Medicine

Peter H. Siegel, Caltech
phs@caltech.edu

Historically THz applications have focused on the identification and mapping of light weight gases and molecules present in the cold, low pressure environments in and around regions of new star formation, gas and dust in the galaxy, the sphere encompassing the early universe, the atmospheres of planets and small solar system bodies (moons and comets), and the upper atmosphere of the Earth. Seventeen space missions have already completed observations in this energy rich region of the electromagnetic spectrum which boasts 98% of all the photons in the universe. In more recent times, especially after the advent of THz pulsed time domain spectroscopy, applications of this far infrared wavelength regime have spread into many new areas of technology. Most prescient is the recent interest in THz imaging and spectroscopy for security applications. The largest commercial driver for THz however is likely to be in communications, and if early results are proven to hold up, THz radiation may have substantial impact on biological function.

In this talk we will review traditional THz applications being pursued in the Submillimeter Wave Advanced Technology (SWAT) group at the US National Aeronautics and Space Administration Jet Propulsion Laboratory and then turn to this new application area in the life sciences: millimeter and submillimeter-wave interactions with cells. A simple setup is demonstrated for remote temperature monitoring of water, water-based media, and cells exposed to millimeter wave energy. The technique relies on recording changes in the shape of a stretching band of the hydroxyl group in liquid water at 3100 to 3700 cm^{-1}. Temperature changes of 1°C are readily distinguished over a range consistent with cellular processes (25-45°C) using integration times below 10 seconds. The instrument was used to successfully determine the temperature rise of a cluster of H1299 derived human lung cells adhered to polystyrene and immersed in PBS under exposure of RF millimeter wave radiation (60 GHz, 1.3, 2.6 and 5.2 mW/mm^2). Following this, our first measurements of low levels of RF power on cell function were performed using a FRET (Forster resonance energy transfer) technique on lung and neuronal cells tagged with GFP (green fluorescent protein) to look at the formation of membrane nanopores. Most recently, some very exciting results have been observed with power levels 1000 times below the recommended safe exposure levels at 60 GHz on in vitro cortical slices from mouse pups. We have recorded both inhibition and enhancement of action potential firing rates in individual neurons and controllable neuronal membrane depolarization, which may have applications in pain control, drug delivery and control of neural prosthetics.

Millimeter wave design in bulk and SOI CMOS

Baudouin Martineau, Andreia Cathelin, STMicroelectronics, Crolles Cedex, France
Baudouin.martineau@st.com

Invited Paper

The presentation will start with a short notice about mmW applications targeting CMOS integration: high data rate WLAN/WPAN communications, low data date sensor applications, THz imaging and car radar applications. A discussion about the available standards to address these demands is also included. Then, an overview of deep submicron CMOS technologies (bulk and SOI) will be presented. Insights on the SOI specific devices will be given. The HF behaviour of active devices will be out lighted via the well-known figures of merit: f_T, f_{max} and NF_{min}. The design of passive devices for mmW will also be presented, taking into account all the constraints coming from the BEOL of digital deep-submicron technologies. Active and passive devices design hints for mmW will finalise this section. The following section presents mmW building blocks on CMOS: LNA, mixer, VCO, Rx Front-End, ... Design techniques will be discussed, based on the information presented in the previous section, together with technical implementation details and measurement results.

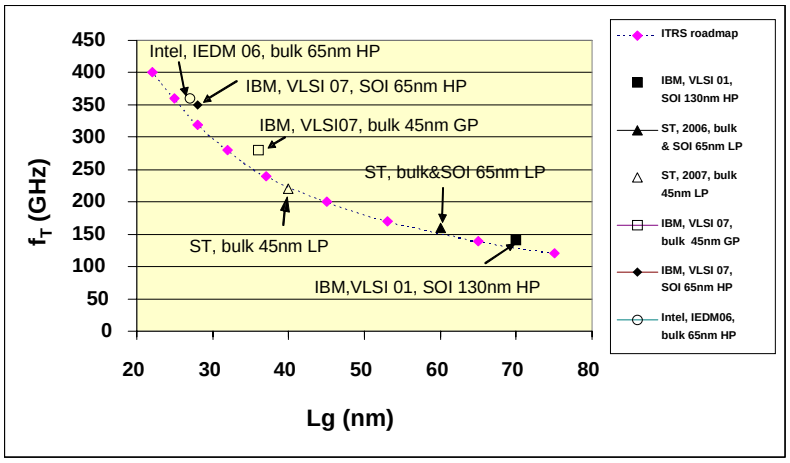

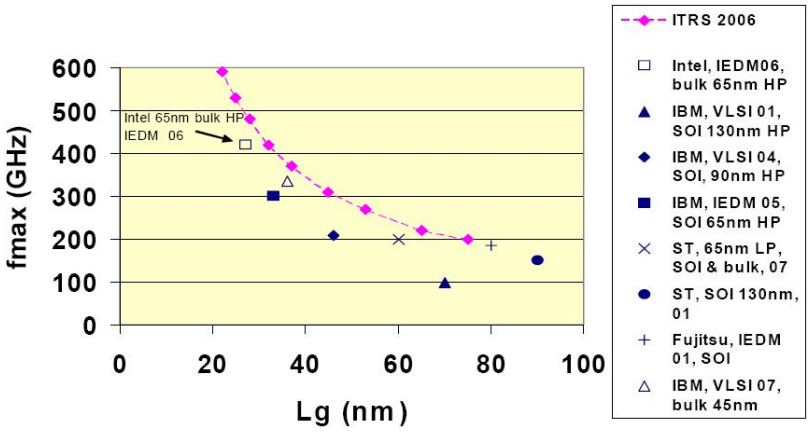

Session 8

10.10-12.10 Wednesday 10 March 2010

An electrically tuned probe for noncontacting microwave measurements

K. Yhland[1], J. Stenarson[1] and K. Andersson[2]

[1] SP Technical Research Institute of Sweden, email: klas.yhland@sp.se

[2] GHz Centre, Microwave Electronics Laboratory at Chalmers University of Technology, Sweden.

Introduction

Noncontacting probes allow measurement of power and reflection coefficient at internal nodes in planar microwave circuits; nodes which may be unavailable when using galvanically contacting techniques such as coplanar probes or coaxial connectors.

In the past years several probe techniques have been presented [1-5]. The probes in [1-3] lack directivity. Therefore they require complicated error correction to allow measurement of waves or reflection coefficient. The probes in [4, 5] have inherent directivity and can be used with simpler error correction, i.e. scalar measurements as with a power meter or a spectrum analyzer.

However, to obtain good directivity, the probes in [4, 5] need mechanical tuning for each individual substrate type and conductor width. To solve this problem we present an electrically tuneable probe in this paper.

Principle of operation

The directivity of the loop coupler probe, Fig. 1a, is caused by the balance between the capacitive and inductive coupling to a wave traveling in one direction on a transmission line below the probe. By adjusting the loop geometry the capacitive and inductive coupling can be made to cancel at one port and add at the other port. The coupling balance is, however, also dependent on the dielectric constant of the substrate and the conductor width. This forced earlier probe types [4, 5] to be mechanically tuned for the individual substrate type.

One way to offset the coupling balance is to split the probe into two and to terminate the loop ends in mismatched resistors as in Fig. 1b. This way the substrate effect on the directivity can be tuned out. We use PIN diodes as adjustable resistors.

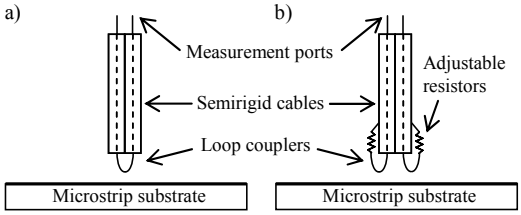

Fig. 1 a) Earlier loop coupler probe. b) Tuneable probe.

This research has been carried out in the GigaHertz centre in a joint research project financed by Swedish Governmental Agency of Innovation Systems (VINNOVA), Chalmers University of Technology, Comheat Microwave AB, Ericsson AB, Infineon Technologies Austria AG, Mitsubishi Electric Corporation, NXP Semiconductors BV, Saab AB, and SP Technical Research Institute of Sweden.

Measurements

We have designed and measured a pair of tuneable probes. They were made from a 1.2 mm diameter semirigid cable with wire loops extending from their ends. Two packaged PIN diodes of the size 0.2x0.2x1 mm were soldered according to Fig. 1b. The probes were placed 0.5 mm above a 1.11 mm wide 50 Ω microstrip line on a substrate with $\varepsilon_r = 2.33$. The directivity was measured with a VNA. Fig. 2a shows the directivity versus frequency and Fig. 2b shows the directivity versus PIN diode dc bias current.

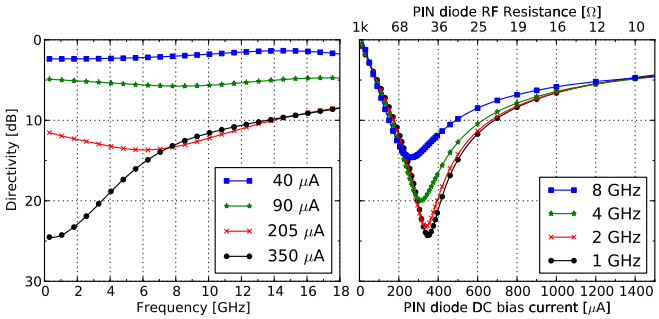

Fig. 2 Probe directivity versus: a) frequency, b) current

Discussion and conclusion

We have presented an electrically tuneable probe with good tuneability when tested on a substrate with $\varepsilon_r = 2.33$. Due to the parasitics of the packaged diode the operation is limited to a few GHz. The probe remains to be tested for other conductor widths and substrate dielectric constants.

References

[1] S. S. Osofsky, et al., "Design and performance of a noncontacting probe for measurements on high-frequency planar circuits," *IEEE Transactions on Microwave Theory and Techniques*, vol. 40, no. 8, pp. 1701-8, 1992

[2] G. Yingjie, et al., "Measurements of field distributions and scattering parameters in multiconductor structures using an electric field probe," presented at IEEE International Microwave Symposium Digest, 1997.

[3] J. Stenarson, et al., "An In-Circuit, Non-Contacting, Measurement Method For S-parameters And Power In Planar Circuits," *IEEE Transactions on Microwave Theory and Techniques*, vol. 49, no. 12, pp. 2567-2572, 2001

[4] K. Yhland, et al., "Noncontacting measurement of reflection coefficient and power in planar circuits up to 40 GHz," presented at 69th ARFTG Conference, Honolulu Hawaii, 2007.

[5] T. Zelder, et al., "Contactless Vector Network Analysis With Printed Loop Couplers," *IEEE Transactions on Microwave Theory and Techniques*, vol. 56, no. 11, pp. 2628-2634, 2008

Oscillator for 60 GHz Super Regenerative Receiver

Mats Ärlelid, Mikael Egard, Erik Lind, and Lars-Erik Wernersson

***Abstract*—An oscillator is designed for a super regenerative receiver with a gated tunnel diode and investigated with Cadence. We demonstrate the first qualitative performance of this receiver type for on-off keying modulated non coherent impulse radio with a pulse rate of 100 Mpulses/s at 60 GHz.**

I. Introduction

THE super regenerative receiver is considered to be a candidate for non-coherent impulse radio receivers. Receivers implemented for the 3-10 GHz band shows that the method of sampling the energy received at the antenna for each presumed pulse is feasible for on-off keying modulation (OOK). The ability to control the output conductance of the gated tunnel diode (GTD) from positive to negative values and also to operate it at high frequency has been presented in the implementation of a pulse generator for impulse radio [1-2]. The results presented here also show the possibility to use the GTD in a super regenerative oscillator (SRO).

II. Super Regenerative Oscillator

The operation of a super regenerative oscillator is basically an analogue sampling procedure, where a RF tank with small negative total conductance is excited with energy supplied from the antenna which sets the initial condition of the oscillator. An oscillation builds up exponentially until it reaches its steady-state, and the supplied energy effectively changes the start-up time of the oscillator. When the oscillator has reached its steady-state, it's quenched in order to redo the sampling procedure. In Fig. 2, the oscillator is excited with a pulse in the first sampling period. The energy of the pulse is equal to -99 dBm in 50 ohm based on the rms value of the pulse and repetition rate.

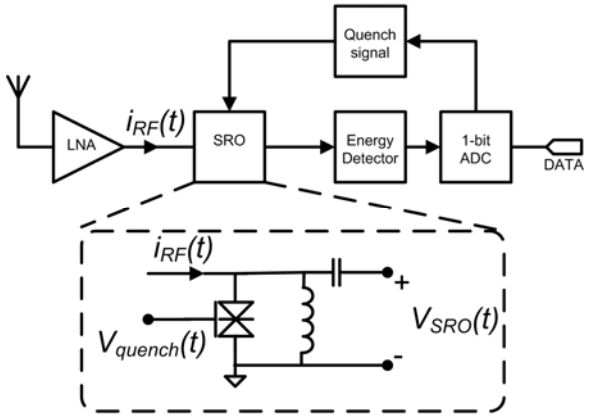

Fig. 1. Block diagram of a super regenerative receiver, with the gated tunnel diode SRO.

M. Ärlelid and L.-E. Wernersson are with the Department of Electrical and Information Technology, Lund University, Lund S-22100, Sweden (e-mail: mats.arlelid@eit.lth.se).

M. Egard, and E. Lind are with the Department of Solid State Physics, Lund University, Lund S-22100, Sweden.

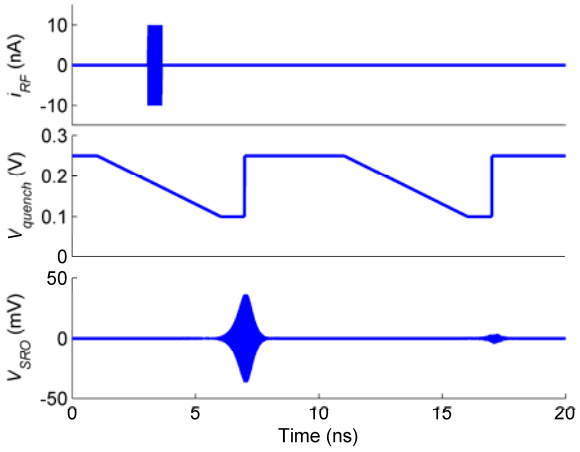

Fig. 2. Two sampling periods of a SRO, one period with excitation and one without. The input signal is described by $i_{RF}(t)$ which is a 500 ps long rectangular pulse with carrier frequency at 60 GHz. The energy supplied to the tank is sampled by the SRO with a rate of 100 MHz.

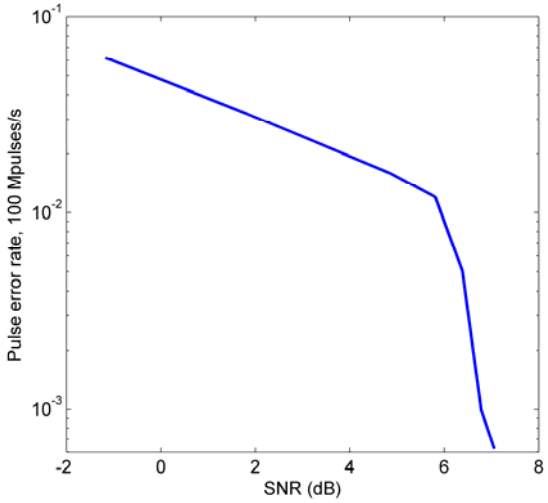

Fig. 3. Pulse error rate of a SRO modulated with OOK at 100 Mbps.

The effect of noise is investigated in Fig. 3, where the pulse error rate is investigated for different noise levels. The received pulses are modulated with OOK at a rate of 100 Mpulses/s.

III. Conclusion

The first report on a super regenerative receiver for impulse radio communication at 60 GHz is presented and the result from the simulation environment is useful for future investigation of the gated tunnel diode RF properties and functionality.

References

[1] M. Ärlelid, L.-E. Wernersson, M. Egard, and E. Lind, "60 ghz ultrawideband impulse radio transmitter," in *Ultra-Wideband, 2009. ICUWB 2009. IEEE International Conference on*, Sept. 2009, pp. 185–188.

[2] M. Egard, M. Ärlelid, E. Lind, G. Astromskas, and L.-E. Wernersson, "20 ghz wavelet generator using a gated tunnel diode," *Microwave and Wireless Components Letters, IEEE*, vol. 19, no. 6, pp. 386–388, June 2009.

60 GHz Wavelet Generator for Impulse Radio Applications

M. Egard, M. Ärlelid, E. Lind, and L.-E. Wernersson

***Abstract*—We report on a 60 GHz wavelet generator, which operates by switching the differential output conductance of a gated tunnel diode between positive and negative values. This makes it possible to generate sub-100 ps long wavelets. It is also shown that it is possible to generate bi-phase signals by applying different bias conditions to the generator.**

I. Introduction

WIRELESS communication in the 60 GHz band is considered a candidate for short range Gbps data transmission. Possible applications are simple docking solutions for laptops (3-5 Gbps) and high definition multimedia interfaces (5-10 Gbps). One technique, which is considered for these applications, is ultra-wideband (UWB) impulse radio (IR). This technique offers low power consumption and the ability to co-exist with other communication standards.

We report on a wavelet generator for implementation in an UWB-IR transmitter [1]. The wavelet generator operates at 60 GHz and produces sub-100 ps long pulses. The implementation is based on a LC-tank circuit, which is integrated on-chip together with a gated tunnel diode (GTD). High frequency wavelets are generated from this circuit by switching the differential output conductance of the GTD between negative and positive values [2]. A schematic view of the layout is shown in Fig. 1(a). The GTD is integrated in parallel to a co-planar waveguide (CPW), which may be modelled by an inductance. The CPW is terminated with a large metal-insulator-metal capacitor and a Schottky diode, which acts to stabilize the operating point of the GTD wavelet generator.

II. Measurement results

Figure 1(b) shows the baseband signal that is used to trigger the wavelet generator, the corresponding output signal is shown in Fig. 1(c). The input signal switches the output conductance of the GTD from a positive value to a negative value, hence the circuit oscillates during a time that is set by the length of the input signal. In this particular experiment, the input pulse length is 87 ps and the output pulse length is 97 ps, the oscillation frequency is 60 GHz and the voltage swing is 206 mV_{pp}, after de-embedding measurement losses. Figure 1(d) shows that it is possible to generate bi-phase signals. This is achieved by reversing the polarity of the input signal.

M. Egard and E. Lind are with the Department of Solid State Physics, Lund University, Lund 221 00, Sweden, e-mail: mikael.egard@ftf.lth.se

M. Ärlelid and L.-E. Wernersson are with the Department of Electrical and Information Technology, Lund University.

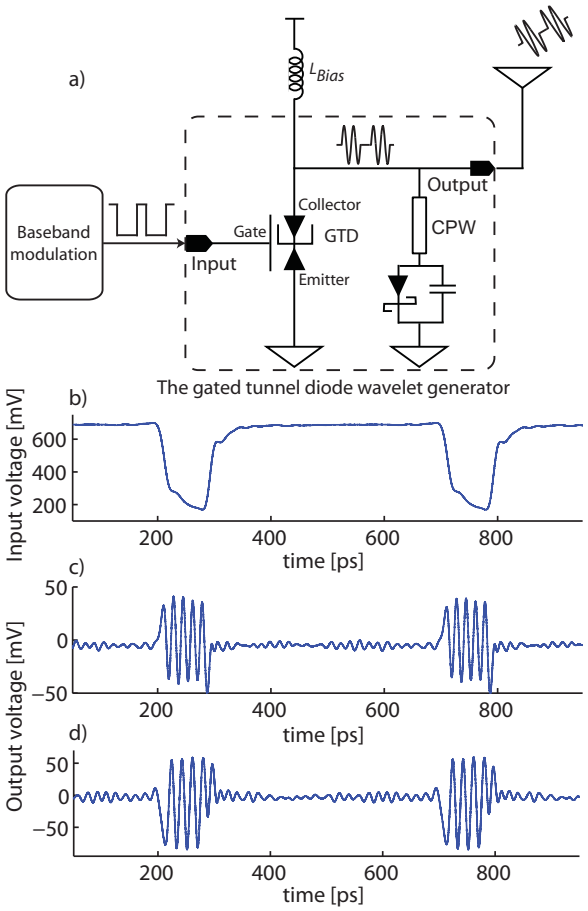

Fig. 1. (a) Schematic layout illustrating the GTD wavelet generator and its implementation in an UWB-IR transmitter circuit. (b) Baseband input signal used to generate the 60 GHz wavelets in (c). (d) Output signal generated from an input signal with opposite polarity as to the one shown in Fig. 1(b).

III. Conclusion

We have demonstrated the generation of 60 GHz wavelets using a gated tunnel diode. The measurement results show that it is possible to control the length, phase, and position of the wavelets with the baseband input signal.

References

[1] M. Ärlelid, L.-E. Wernersson, M. Egard, and E. Lind, "60 ghz ultra-wideband impulse radio transmitter," in *Ultra-Wideband, 2009. ICUWB 2009. IEEE International Conference on*, Sept. 2009, pp. 185–188.

[2] M. Egard, M. Ärlelid, E. Lind, G. Astromskas, and L.-E. Wernersson, "20 ghz wavelet generator using a gated tunnel diode," *Microwave and Wireless Components Letters, IEEE*, vol. 19, no. 6, pp. 386–388, June 2009.

A large-signal GaAs InGaP HBT model optimized for design of low phase-noise VCOs

Szhau Lai, Iltcho Angelov, Dan Kuylenstierna, Rumen Kozhuharov, Herbert Zirath

Department of Microtechnology and Nanoscience, Microwave Electronic Laboratory, Chalmers University of Technology, Göteborg, Sweden

Summary: The work presents a compact GaAs InGaP HBT model optimized for low phase-noise oscillator design. A large number of HBTs with different sizes and process variations in terms of collector doping profile have been modeled and they all show good agreement between simulations measurements.

Model extraction: The purpose of the paper is to develop a HBT LS model for transistors in an InGaP HBT process, optimized for VCO applications. To design wide-tuning range VCOs, hyper-abrupt doping profiles are used. In VCO design, difficulties as frequency and output power inaccuracy often appear. Even worse, phase noise is never easy to predict. A LS model able to describe small signal and large signal behavior accurately is essential to estimate VCO performance, power, frequency, phase noise, etc. Next, VCO phase noise is well known to be dominated by 1/f noise up conversion and mixing. The HBT LS model used in this work is extended version of [1] enhanced with RF and LFN noise modeling features. The HBT model was evaluated for three different collector doping profile designed for various varactor-tuning range. The model is compact, simple to extract and in addition, it converges very well when used for VCO design in ADS.A simple noise model including 1/f noise and burst noise at the base side and shot noise at the collector side is adopted in the LS model. Parameters of 1/f noise in HBTs have been extracted by measurement with ICCAP will be presented. Finally, a few simulation of VCO gives reasonably good agreement with measurement.

Results: On-wafer DC and S-parameter measurements were implemented and parameters were extracted. Fig. 1 shows good agreement between simulated and measured S-parameters. Finally the large-signal model, being extracted from DC measurements and small signal S parameters, is verified with LSNA measurements. Fig. 2 shows excellent agreement between simulated and measured waveforms, at 6GHz, input power= -5 to 5 dBm, Vce=4V. The dynamic load line measurement is important because it has relation with VCO waveform. 1/f noise was measured and parameter is extracted. VCO measurement and simulation have good agreement in terms of power, frequency and phase noise is shown in Fig.3.

Conclusion: Accurate models for describing small signal and large signal behavior have been created for 5 different sizes of HBT on 3 processes. The Angelov HBT model has been verified to be efficient VCO phase-noise simulations.

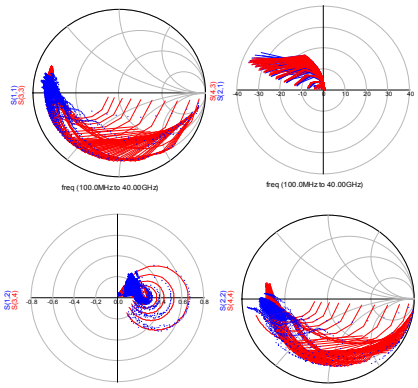

Fig. 1 S-parameter measurement (blue), simulation (red)

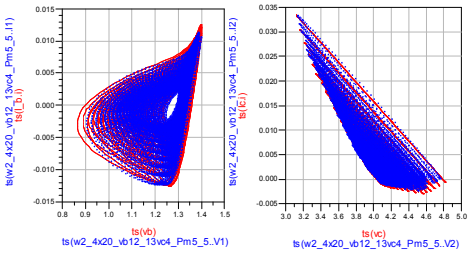

Fig. 2 LSNA measurement (blue) and simulation (red)

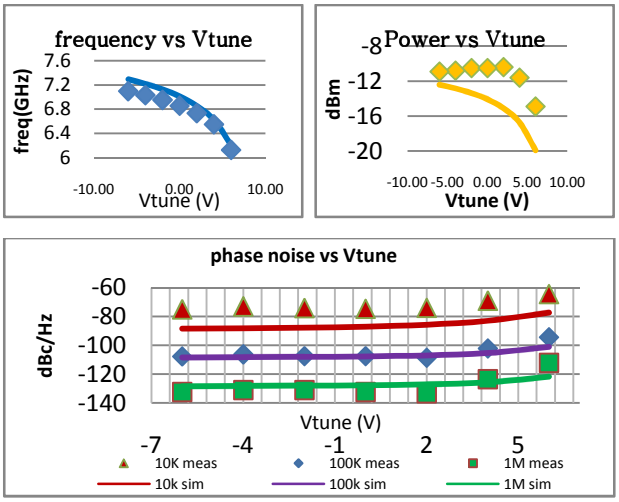

Fig. 3 VCO measurement and simulation

Reference

[1] I. Angelov, K. Choumei, A. Inoue **"An empirical HBT large-signal model for CAD** Int. J. of RF and Microwave Computer-Aided Engineering Vol. 13, N 6,Nov. 2003, Pp: 518-533

Low-Frequency Noise in Vertical InAs Nanowire FETs with L_g=35nm

Karl-Magnus Persson[1], Erik Lind[2], Anil W Dey[1], Claes Thelander[2], Henrik Sjöland[1], and Lars-Erik Wernersson[1]

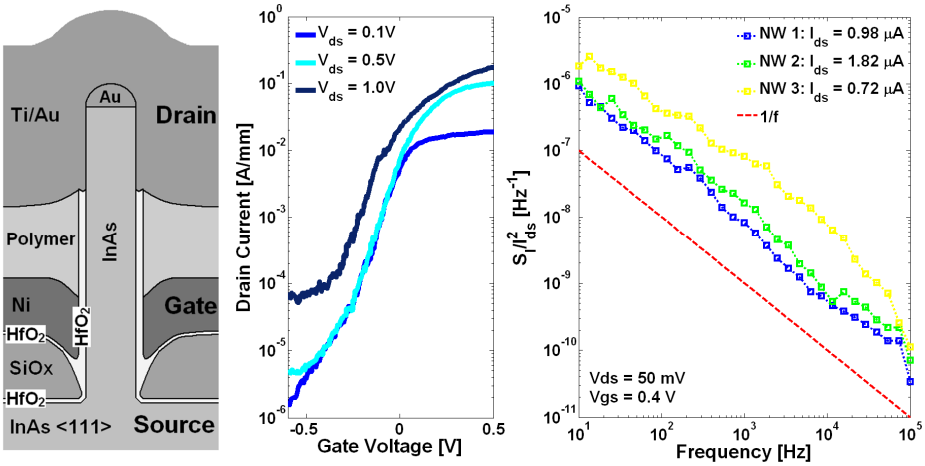

Fig. 1. (a) Schematic cross-section of a NW FET. (b) Device transfer characteristics of an individual NW FET (40 nm diameter, 35 nm gate length) at V_{ds} = 0.1 V, 0.5 V, and 1.0 V. (c) CNSD for three individual NW FETs. *1/f* is plotted for reference.

We present DC characteristics and low-frequency noise (LFN) measurements on single epitaxially grown vertical InAs nanowire MOSFETs with 35 nm gate length and HfO_2 high-κ dielectric. The nanowire has a diameter of 40 nm. A schematic cross-section is shown in Figure 1a. The nanowire geometry offers electrostatic advantages using a wrap-around gate, providing better control of the channel potential. We present data of the DC and *1/f* characteristic, shown in Figure 1b and 1c respectively, for FETs based on individual vertical InAs NWs. Up to now, several papers of FETs based on individual lateral NWs have been published, but only a few in the vertical geometry. We report an average transconductance and an average two-decade subthreshold slope of 160 mS/mm and 130 mV/decade respectively.

LFN of MOSFETs tends to increase linearly with the scaling factor, making it a major concern for analog and RF applications. Ultra-scaled devices not only suffer from high noise levels, but also large disparity between devices processed in parallel [1]. In our measurements we note a $1/f^{\gamma}$ dependence with the frequency exponent γ being close to unity, indicating an even distribution of slow and fast traps. The *1/f* behavior was unchanged for V_{gs} smaller than 0.4 V, even in the subthreshold region (V_{gs} = -0.2V), with γ close to unity. This indicates that several traps are involved in the noise process. The noise power correlates well with $(gm/Id)^2$, indicating for small bias currents that the 1/f noise is originating from number fluctuations. At 10 Hz a minimum current noise spectral density (CNSD) of 7.3×10^{-7} Hz^{-1} was reached for a drain current of 1.2 µm. This can be compared to a study of lateral Si nanowire devices which showed a CNSD of 1×10^{-7} Hz^{-1} for a drain current of 6 µm [1]. As a reference, we also measured the LFN for matrices with varying number of nanowires (7-19), where we observed a roughly constant CNSD level as the current level was increased.

At high gate overdrive voltage mobility fluctuations or correlated mobility-number fluctuations must be considered. Mobility fluctuations are commonly characterized using Hooge's parameter, which depends on material and crystal quality and is a good measure to evaluate the properties of advanced structures and exotic materials. We computed the average Hooge's parameter for two devices, (for V_{gs} = 0.2 and 0.4 V at 10 Hz) and could determine it to 4.2×10^{-3}. This can be compared with the minimum obtained room temperature value for the study of a lateral InAs NW FET device, corresponding to 8.4×10^{-3} [2].

This work has been supported by the Swedish Foundation for Strategic Research, the Swedish Research Council, the Knut and Alice Wallenberg Foundation, and EU through the NODE project, No. 015783.

1) Department of Electrical- and Information Technologies, Lund University, Box 118 S-221 00, Lund, Sweden.

2) Department of Solid State Physics, Lund University, Box 118 S-221 00, Lund, Sweden (email: karl-magnus.persson@eit.lth.se).

References

[1] C. Wei, et al., "Impact of Gate Electrodes on 1/f Noise of Gate-All-Around Silicon Nanowire Transistors," *Electron Device Letters*, vol. 30, no. 10, pp. 1081-1083, Oct. 2009.

[2] M. R. Sakr and X. P. A. Gao, "Temperature dependence of the low frequency noise in indium arsenide nanowire transistors," *Applied Physics Letters*, vol. 93, no. 20, pp. 203503-203503-3, Oct. 542008.

Characterization of graphene-based field-effect transistors

Stella Bevilacqua, Per-Åke Nilsson, Kristoffer Andersson, Niklas Rorsman, Jan Grahn, Herbert Zirath
Microwave Electronics Laboratory, Department of Microtechnology and Nanoscience (MC2)
Chalmers University of Technology, SE-412 96 Göteborg, Sweden, stellab@exfwd.chalmers.se

Rositza Yakimova, Erik Janzen
Linköping University, SE-581 83 Linköping, Sweden

Abstract
We report fabrication and measurements of field effect transistors based on epitaxial graphene on a SiC substrate. The current-voltage characteristics and transconductance of top-gated graphene FETs (GFETs) have been measured. The drain-current density and peak transconductance were 200 mA/mm and 16 mS/mm, respectively, at V_{ds}=3V. The cut-off frequency f_t was 0.78 GHz.

Introduction
Graphene is an atomically thin form of hexagonal carbon and has attracted a lot of attention in the research community over the last few years. Carrier mobility in graphitic forms of carbon, such as nanotubes and thin graphene sheets can be very high, on the order of 100000 $cm^2 V^{-1}s^{-1}$ at room temperature [1]. This is at least 100 times greater than that of Si but also 10 times greater than InP. The saturation velocity of graphene has not been determinate clearly, but it is estimated to be 6-7 times greater than that for Si MOSFETs. These material parameters points to the possibility to use graphene for high frequency devices. However, since graphene is a semimetal with a zero band-gap, it is difficult to achieve good on-off current ratio (I_{on}/I_{off}).

Experimental
The measured graphene FET was grown on a SiC substrate. Graphene forms the channel of the device. The ohmic contacts, the gate and the metallic pads were fabricated with a Ti/Au layer. The gate dielectric (Al_2O_3) is 50 nm thick. Transistors with gate lengths down to 250 nm were made.

Results and discussion
The drain current (I_{DS}) as a function of source-to-drain voltage (V_{DS}) was measured (Fig. 1.). The source-to-gate voltage (V_{GS}) changes from 3V (top) to 0V (bottom) in 0.5 V steps. The drain current at V_{DS}=3V is 200 mA/mm for a 500 nm gate length device. The extrinsic transconductance (g_m) is about 16 mS/mm (Fig. 2). The gate leakage current is very low, in the order of 10^{-12} A. S-parameter measurements gave an f_t of 0.78 GHz for a 250 nm gate length device.

Conclusions
We have fabricated and investigated graphene field-effect transistors. In the experiment, we achieved clear gate control of the transistors, and have made a first step to investigate the high frequency performance.

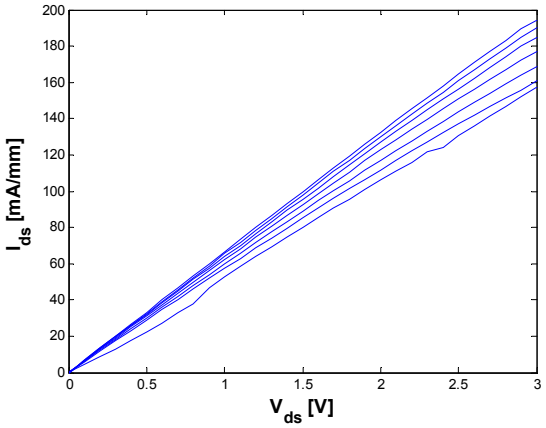

Figure 1. Current-voltage characteristics of a 500 nm gate length GFET.

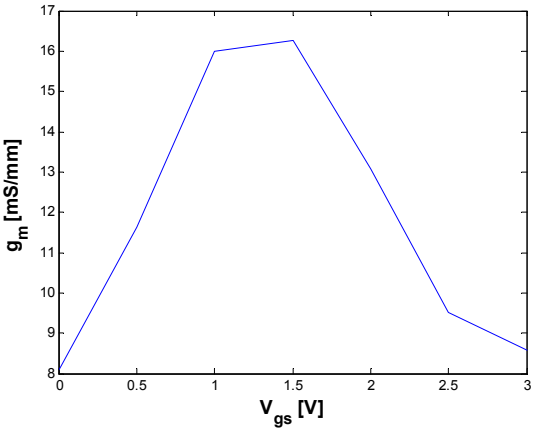

Figure 2. Transconductance (g_m) as a function of gate-source-voltage for V_{ds}=3V for a 500 nm gate length GFET.

References
[1] Moon, J. S., D. Curtis, et al. (2009). "Epitaxial-Graphene RF Field-Effect Transistors on Si-Face 6H-SiC Substrates." Electron Device Letters, IEEE **30**(6): 650-652.

Cryogenic behaviour of InAs/AlSb HEMTs for low-noise amplifiers

G. Moschetti[#1], P-Å Nilsson, Y. Roelens*, F. Danneville*, S. Bollaert*, G. Dambrine*, L. Desplanque*, X. Wallart*, H. Zirath and J. Grahn
Microwave Electronics Laboratory, Department of Microtechnology and Nanoscience (MC2)
Chalmers University of Technology, SE-412 96 Göteborg, Sweden
**Institut d'Electronique de Microélectronique et de Nanotechnologie (IEMN), UMR CNRS 8520, Université de Lille I, BP 60069, 59652 Villeneuve d'Ascq Cedex, France*
[#1]giuseppe.moschetti@chalmers.se

Abstract
We demonstrate that DC and RF properties of InAs/AlSb HEMTs are improved at 77 K compared to 300K. Upon cooling the device shows lower R_{on}, gate leakage I_G and output conductance g_{ds} together with a more distinct knee in the $I_{DS}(V_{DS})$ characteristics. Furthermore, the device exhibited higher g_m, higher f_T and f_{max} at low drain bias (V_{DS} up to 0.3V) upon cooling. These results point to the potential of InAs/AlSb HEMT in cryogenic low-noise amplifiers with very low power dissipation.

Introduction
Cryogenic operation of LNAs is crucial in space communication systems and radio astronomy where the antenna temperature is about one order of magnitude less than for terrestrial application [1]. InAs/AlSb HEMTs are very promising devices in millimetre-wave, low-power and low-noise applications since the narrow bandgap in AlSb provides a large conduction mobility and high peak velocity of electrons in InAs [2]. The DC and RF performance are very sensitive to the operating temperature, especially in 2DEG based devices, due to the electron transport improvements and reduction of thermal noise generated by parasitic elements. In this paper we have studied the DC and RF performance at cryogenic temperature by measuring the same InAs/AlSb HEMTs at 300 K and 77 K.

Results
The device reported here is a two fingers HEMT with a total gate width of 100µm. The drain current as a function of drain voltage at 300K and 77K is shown in fig. (1a). The gate voltage V_{GS} was varied between 0V to -1.2V. At 300K $I_{DS}(V_{DS})$ showed an output conductance g_{ds} of 1591mS/mm (V_{DS}=0.2V and V_{GS}=0V), a transconductance g_m of 371mS/mm at V_{DS}=0.1V and 808mS/mm at V_{DS}=0.3V. The gate leakage I_G was 100µA at V_{DS}=0V and V_{GS}=-1.2V. The on-resistance, calculated as the linear fit of the I_{DS} at V_{GS}=0V, was 0.52Ωmm at 300K. Small-signal measurements were then performed and the extrinsic f_t/f_{max} ratio was 99/117GHz at 300K using a bias of V_{DS}=0.3V and V_{GS}=-1V. The same characterization was carried out at 77K using a cryogenic probe station. At this temperature the device behaviour was clearly different showing a lower R_{on} of about 0.45Ωmm, a peak transconductance g_m 44% higher (536mS/mm) at V_{DS}=0.1V and a lower gate leakage of 47µA. The output conductance g_{DS} decreased to 1208mS/mm at 77K for V_{DS} up to 0.2V. Small-signal measurements were performed at 77K as well showing an extrinsic f_t/f_{max} ratio of 132/155GHz at V_{DS}=0.3V and V_{GS}=-1.08V; See fig. (1b).

Conclusions
At cryogenic temperature, the DC and RF performance of the device were clearly improved. In particular, the on-resistance decreased while the cut-off frequency f_T increased for V_{DS} below 0.3V. These improvements for both DC and RF performance make the InAs/AlSb HEMT a possible device candidate for cryogenic low-noise amplifiers.

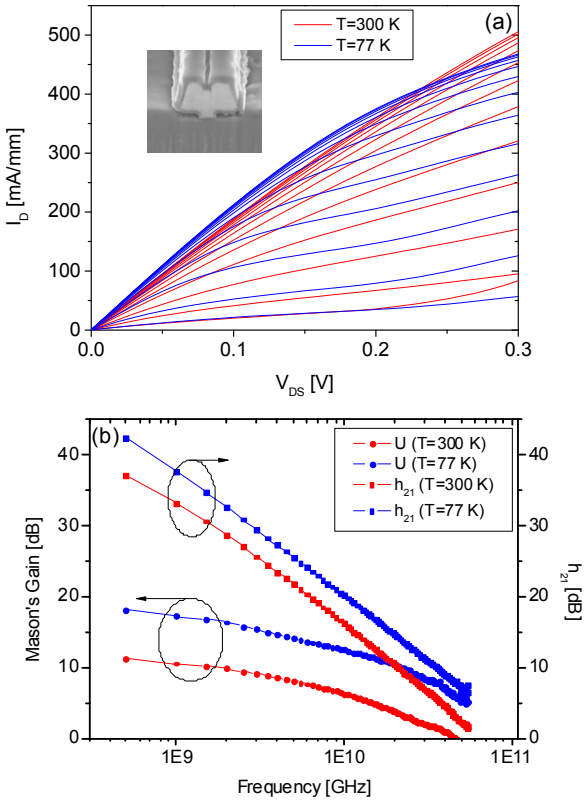

Fig.1a: $I_{DS}(V_{DS})$ with V_{GS} ranging from 0.1 V to -1.2 V at 300 K (red lines) and 77 K (blue lines) for a 110-nm gate length InAs/AlSb HEMT. The device gate width is 2x50µm.
Fig. 1b: Mason's gain U and current gain $|h_{21}|$ at 300 K (red lines) and 77 K (blue lines) with V_{DS}=0.1 V.

References
[1] Pospieszalski, M.W., *Extremely low-noise amplification with cryogenic FETs and HFETs: 1970-2004.* Microwave Magazine, IEEE, 2005. **6**(3): p. 62-75.
[2] Bennett, B.R., et al., *Antimonide-based compound semiconductors for electronic devices: A review.* Solid-State Electronics, 2005. **49**(12): p. 1875-1895.

Linear and non-linear frequency modulation up to 3.2 GHz in nanocontact spin torque oscillators

P. K. Muduli[1], Ye. Pogoryelov[1], S. Bonetti[1], G. Consolo[2], F. Mancoff[3], and J. Åkerman[1,4]
[1]Materials Physics, Royal Institute of Technology, Sweden
[2]Department of Physics, University of Ferrara, 44100 Ferrara, Italy
[3]Everspin Technologies, Inc., 1300 N. Alma School Road, Chandler, Arizona, USA
[4]Physics Department, Göteborg University, 412 96 Göteborg, Sweden, email: *johan.akerman@physics.gu.se*

Spin torque oscillators (STO) are nanoscale devices capable of generating signals in the GHz frequency range with wideband frequency tunability and high signal quality. These devices are believed to be used in the next generation microwave sources, because of their lower cost and smaller size compared to conventional YIG oscillators. Since a pure microwave resonance of the STO doesn't carry any information, the standard modulation techniques have to be applied to these devices to test their suitability for communicating information. Modulation is the process of varying the characteristic parameters of a periodic high-frequency wave ("carrier"), in accordance with a low-frequency information signal ("modulating"), to obtain a "modulated" signal.

In this work, we report the frequency modulation of a nano-contact based STO. The devices presented here are 130 nm point contacts made from $Co_{81}Fe_{19}$(20 nm)/Cu(6 nm)/$Ni_{80}Fe_{20}$(4.5 nm) pseudo spin valve stacks.[1] The frequency modulation experiment was performed by injecting a signal from the microwave source to the STO through a broadband circulator. The measurements were performed with a magnetic field of 10 kOe applied at an angle of 70° to the film plane,[2] which ensures that we operate the STO around its maximum output. We have studied frequency modulation of a nano-contact spin torque oscillator for three principally different cases of frequency non-linearity: d^2f/dI^2_{dc} being zero, positive and negative. The sign of d^2f/dI^2_{dc} determines the sign of the frequency shift during modulation as shown in Fig.1. Asymmetry in sideband power is found to depend upon both frequency and amplitude non-linearity. The asymmetry of the modulated sideband power agrees with calculations based on a recent theory of combined non-linear frequency and amplitude modulation.[3]

We have achieved continuous gigahertz frequency modulation up to at least 3.2 GHz, around a carrier frequency 19-26 GHz. The previous and only experimental literature available on frequency modulation of STO on a similar device was performed at a much lower frequency of 40 MHz.[4] Hence to our knowledge, this is the fastest ever achieved analog modulation in an STO. The 3-dB modulation bandwidth of the STO is measured to be 110 MHz for an operating frequency at 22 GHz, which is a promising value for applications.

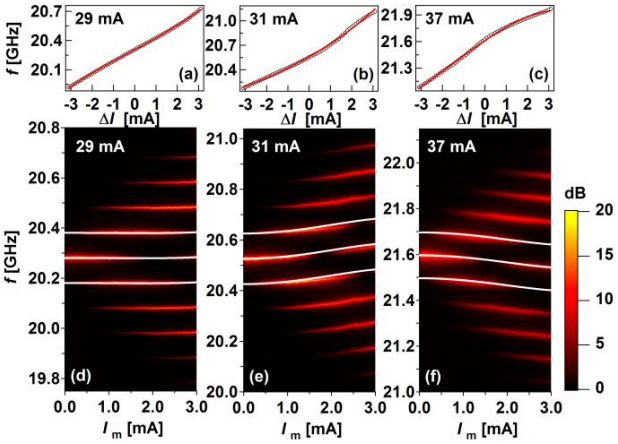

FIG 1 (a-c) Frequency of the free-running STO around the drive current values of 29 mA, 31 mA and 37 mA with corresponding 4th-order polynomial fit. (d-f) Frequency modulation (f_m=100 MHz) of the STO showing the progressive development of sidebands with increasing modulating amplitude I_m. The white lines show the calculated frequency of the carrier and the first-order sidebands according to the combined non-linear frequency and amplitude modulation theory.

[1]F. B. Mancoff, N. D. Rizzo, B. N. Engel, and S. Tehrani, Appl. Phys. Lett. **88**, 112507 (2006)
[2]S. Bonetti, P. K. Muduli, F. Mancoff, and J. Åkerman, Appl. Phys. Lett. **94**, 102507(2009)
[3]G. Consolo1, V. Puliafito, L. Lopez-Diaz, F. Nizzoli1, L. Giovannini, G. Valenti, and B. Azzerboni, arXiv:0902.4901.
[4]M. R. Pufall, W. H. Rippard, S. Kaka, T. J. Silva, and S. E. Russek, Appl. Phys. Lett. **86**, 082506 (2005)

Session 9

10.10-12.10 Wednesday 10 March 2010

Microwave breakdown in space borne rf equipment

J. Rasch[a], D. Anderson[a], J. Johansson[b], M. Lisak[a], J. Puech[c],
E. Rakova[d], V. Semenov[d]
Contact person J. Rasch (joel.rasch@chalmers.se)
[a] Department of Radio and Space Science, Chalmers University of Technology, Göteborg, Sweden
[b] RUAG Space AB, Göteborg, Sweden
[c] Centre National d'Etudes Spatiale (CNES), Toulouse, France
[d] Institute of Applied Physics (IAP), Nizhny Novgorod, Russia

Microwave breakdown in rf components is a potentially serious failure mechanism in space borne rf equipment. Breakdown is manifested by an avalanche-like growth of the free electron density in the device and is created by rf heated electrons which either cause secondary electron emission when hitting the wall of the device (vacuum breakdown - multipactor) or cause ionizing collisions with neutral particles in a gas-filled device (corona breakdown). Microwave breakdown may generate rf noise, change the device impedance, heat the device walls, and may even permanently damage the hardware inside the device. The development of modern space borne microwave technologies, e.g. the new generation of multimedia satellites involving more and more users, all demanding access to higher bit rates, tends to increase the power densities in the rf equipment with a concomitantly enhanced risk for system failure due to microwave breakdown. Thus, an important part of the development of rf components is to establish the critical rf power at which the breakdown process is initiated. The basic physics involved in the breakdown phenomenon is well known, e.g. the multipactor phenomenon has been known for more than 70 years. However, new applications and designs continuously give rise to situations where microwave breakdown is a potential risk and where previous results and predictions concerning breakdown are not applicable. In particular, previous studies have mostly been carried out for the simplest geometry of two metallic parallel plates with a homogeneous rf electric field between the plates and for CW operation, i.e. the average power density has been assumed constant in space and time. Since many modern microwave devices involve both more complex geometries leading to inhomogeneous electric fields and in addition e.g. multi-carrier operation where the signal power varies significantly in time, space industry has been forced to base breakdown predictions on more or less well-founded extrapolations and generalizations of the plane parallel CW results. This situation is very unsatisfactory and leads to uncertainties in predicted breakdown power levels, thus making it necessary to allow for large safety margins in device specifications and/or to use expensive test and validation procedures.

In order to remedy this situation, a sustained applied research effort, involving a close collaboration between Chalmers, CNES and IAP, has been done since 2001 with the aim to develop a better understanding of microwave breakdown phenomena in modern microwave devices. This effort was last year extended further with a new collaboration between Chalmers, IAP and RUAG aimed at studying microwave breakdown in open antenna systems such as e.g. helix antennas.

The purpose of this contribution is to present some recent research results obtained within the collaborations e.g. the effects on the breakdown thresholds caused by the inhomogeneous electric fields and time varying power as characteristic of e.g. rectangular and cylindrical wave guides, irises in waveguides, microstrip lines and multi-carrier signals. Some recent representative publications are:

1. J. Rasch, D. Anderson, M. Lisak, V. E. Semenov, J. Puech, "Microwave corona breakdown in inhomogeneous electric fields", J. Phys. D: Appl. Phys. 42, 205203 (2009)
2. V. E. Semenov, E. I. Rakova, A. G. Sazontov, I. M. Nefedov, V. I. Pozdnyakova , I. A. Shereshevskii, D. Anderson, M. Lisak, and J. Puech, "Simulations of multipactor thresholds in shielded microstrip lines", J. Phys. D: Appl. Phys. 42, 205204 (2009)
3. V. E. Semenov, E. Rakova, R. Udiljak, D. Anderson, M. Lisak, and J. Puech, "Conformal mapping analysis of multipactor breakdown in waveguide irises", Physics of Plasmas 15, 033501 (2008)
4. V. E. Semenov, E. Rakova, N. Zharova, D. Anderson, M. Lisak, and J. Puech, "Simulations of the multipactor effect in hollow waveguides with wedge-shaped cross section", IEEE Transactions of Plasma Science 36, 488-493 (2008)

Concept of Gap Waveguide and Measured Results for First Demonstrator

A.U. Zaman[1], P.-S. Kildal[1], E. Rajo-Iglesias[2], A. Kishk[3]

[1] Chalmers University of Technology; [2]Universidad Carlos III de Madrid; [3]University of Mississippi.
Email: zaman@chalmers.se; per-simon.kildal@chalmers.se; eva@tsc.uc3m.es; ahmed@olemiss.edu

Introduction:

Recently a new type of metamaterial waveguide has been introduced on the concept of two parallel metal plates [1], [2]. The waveguide consists of a smooth upper plate and a lower metal ridge surrounded by the metal pins. The pins surrounding the ridge acts like an artificial magnetic conductor. This artificial magnetic conductor stops wave propagation in all directions except along the direction of the ridge when the gap between the ridge and upper metal plate is smaller than λ/4. The ideal case and realized case is shown below in fig.1

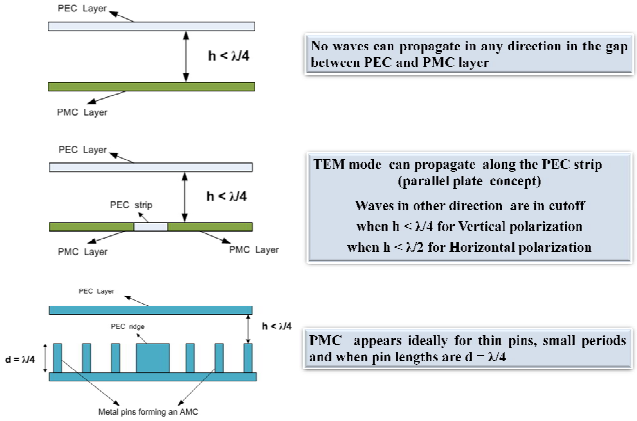

Figure:1 Concept of Gap Waveguide

First Prototype Design and Measurement Results:

Surfaces formed by metal pins standing vertically on a ground plane, i.e. like a bed of nails or Fakir's bed have properties close to ideal impedance boundaries. That is why bed of nails was chosen as a PMC realization for this initial study. The prototype of Gap-waveguide was designed with the following dimensions and arrangements as is seen in fig.2.

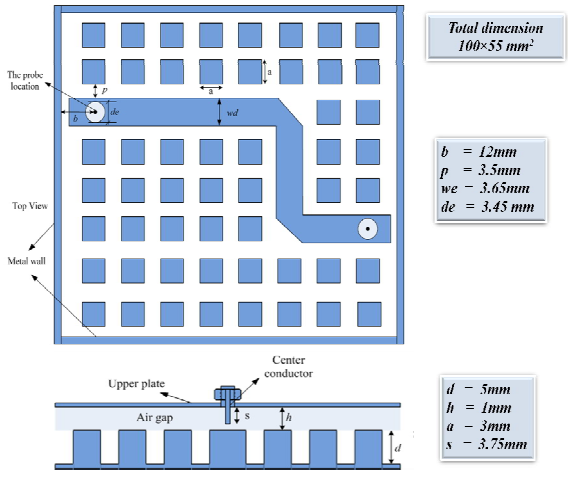

Figure:2 Prototype Dimensions

Measured S-parameters are shown in fig. 3(a). The calculated loss is shown in fig. 3(b).

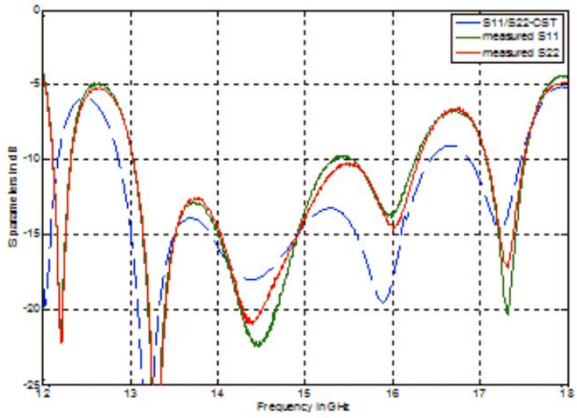

Figure: 3(a) Simulated and Measured S11

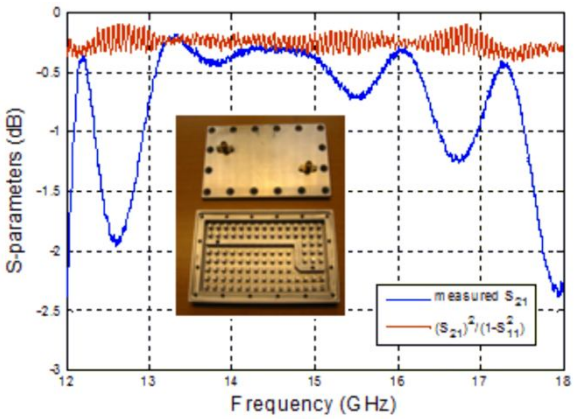

Figure: 3(b) Measured S21 and loss

Conclusion:

The ridge-gap waveguides are expected to contribute significantly towards the design of high frequency system components in future due to its flexibility in manufacturing , low loss and high power handling capability. In this work, the basic working principle for ridge-gap waveguide has been presented. Also, measured results for the first ridge-gap waveguide demonstrator has been shown. The initial results show good agreement between simulations and measurements.

References:

[1] P.-S. Kildal, E. Alfonso, A. Valero-Nogueira, E. Rajo-Iglesias, "Local metamaterial-based waveguides in gaps between parallel metal plates", IEEE Antennas and Wireless Propagation letters (AWPL), Volume 8, pp. 84-87, 2009.

[2] P.-S. Kildal, ''Three metamaterial - based gap-waveguides between parallel metal plates for mm /submm waves,'' *3rd European Conference on Antennas and Propagation*, Berlin, March 2009.

Comparison of Diversity Gains of Wideband Antennas Measured in Anechoic and Reverberation Chambers

Xiaoming Chen, Nima Jamaly, Jan Carlsson, Jian Yang, Per-Simon Kildal, Ahmed Hussain
Dept. of Signals and Systems, Chalmers University of Technology, Sweden
xiaoming.chen@chalmers.se

MIMO (multiple-input multiple-output) is the use of multi-port antennas at both the receiving and the transmitting sides of a radio communication link to enhance performance by exploiting multipath fading environments. The MIMO terminals can be characterized by diversity gains. Different methods have been developed to measure diversity antennas. In this paper, two wideband antennas, Eleven antenna and LINDGREN antenna (see Fig. 1) have been measured in anechoic chamber (AC) at DTU, and reverberation chamber (RC) at CTH (see Fig. 2), which is basically a large metal cavity stirred to create a Rayleigh fading environment. Diversity parameters are calculated based on different methods corresponding to different measurements. In AC, the embedded element pattern is measured. Then correlation is calculated from the embedded antenna pattern, and then diversity gains are calculated from the correlation based on approximation formulas. In RC, since the antennas are measured in isotropic rich scattering fading, correlation are calculated based on measured envelope between different antenna ports, and diversity gains are calculated based on the cumulative distribution function (CDF) of received signals between different antenna ports. The corresponding diversity parameters obtained from both methods will be carefully compared and analyzed in the presentation.

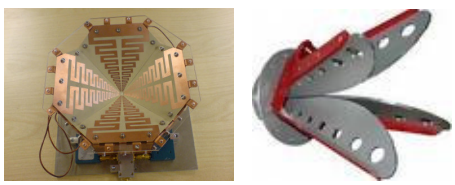

(a) (b)

Figure 1: Photos of Eleven antenna (a) and LINDGREN antenna(b)

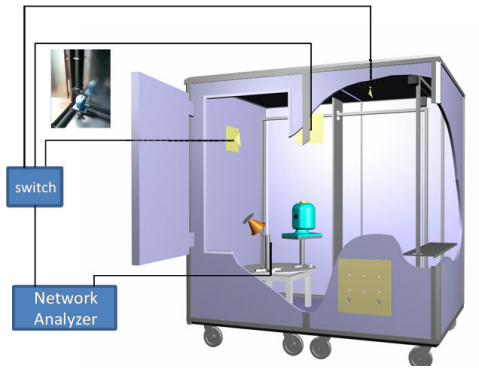

(a)

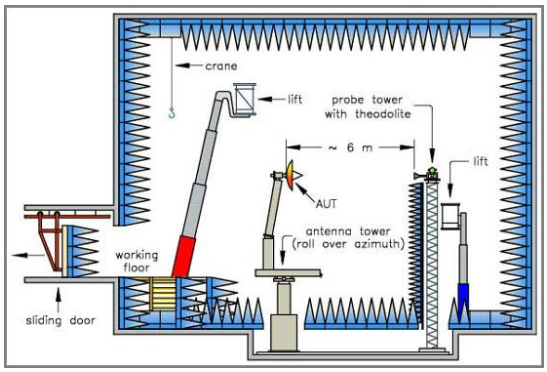

(b)

Figure 2: Sketches of CTH Bluetest reverberation chamber (a) DTU anechoic chamber (b)

Design of Cryogenic 2-14 GHz Eleven Feed for Reflector Antennas for Future Radio Telescopes

Jian Yang[1], Miroslav Pantaleev[2], Per-Simon Kildal[1], Yogesh Karadikar[1], Leif Helldner[2], Benjamin Klein[3], Niklas Wadefalk[4], Ashraf Zaman[1], Mojtaba Zamani[1]
[1]Dept. of Signals and Systems, Chalmers University of Technology, Sweden
[2]Onsala Space Observatory, Sweden
[3]School of Electrical and Information Engineering University of the Witwatersrand, and Hartebeesthoek Radio Astronomy Observatory (HartRAO) , South Africa
[4]Dept. of Microtechnology and Nanoscience, Chalmers University of Technology, Sweden

The design of the cryogenic 2-14 GHz Eleven feed for reflector antennas in future wideband radio telescope involves electrical design of the Eleven antenna, design of center puck, different alternative solutions for integrating with low noise amplifiers (LNAs), mechanical and cryogenic design and tests, system noise temperature estimation and so on. All these design aspects will be described in the paper. A large quantity of simulated and measured data has been obtained in order to verify the electrical, mechanical and cryogenic performance, and the system noise temperature. The objective of this work is to provide a good feed candidate for reflector antennas in VILB 2010 and US SKA projects.

The system configuration of the Eleven feed can be represented by the block diagram shown in Fig. 1, which consists of three parts: the Eleven antenna, center puck and the LNA-integration circuit board.

Fig. 2 shows a photo of the Eleven feed. The reflection coefficient measured at Caltech (California Institute of Technology) is shown in Fig. 3, and the aperture efficiency and other sub-efficiencies measured at DTU (Denmark University of Technology) are shown in Fig. 4. Fig. 5 shows Steady state analysis of the thermal distribution along the feed with head load of 20W/m2.

More simulated and measured data will be shown in the paper. In conclusion, the Eleven feed has good performance in the frequency range of 2 – 14 GHz, and has gone through several cryogenic tests.

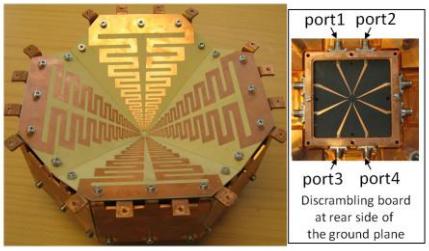

Figure 2 Photo of the Eleven feed

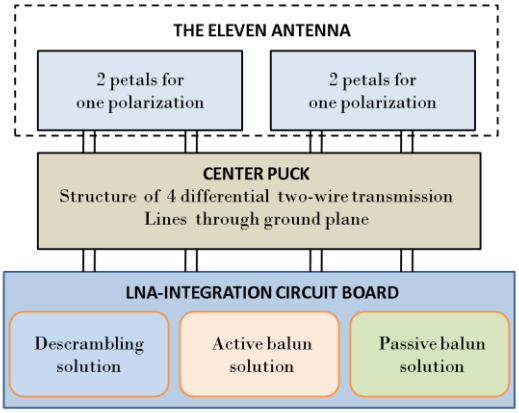

Figure 1 System configuration of the Eleven feed

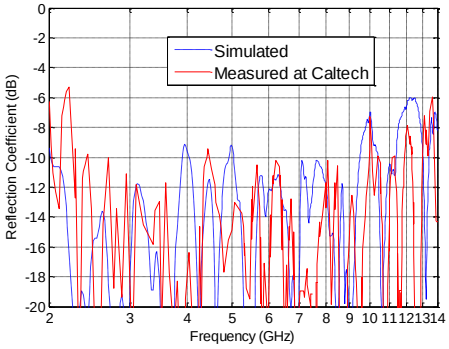

Figure 5 Simulated and measured reflection coefficient of the Eleven feed

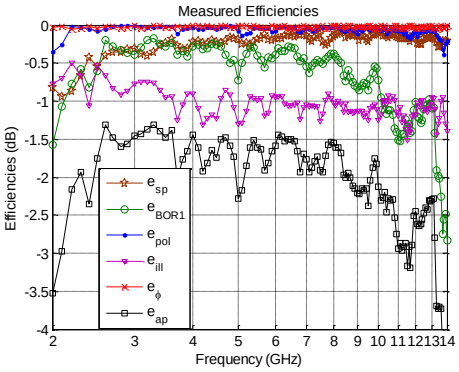

Figure 4 Measured efficiencies

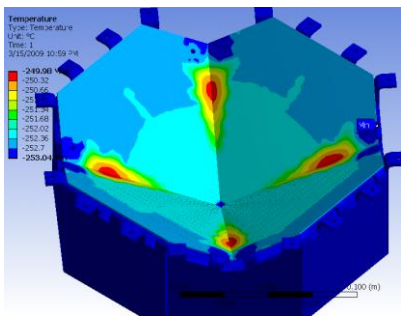

Figure 3 Steady state analysis of the thermal distribution. The temperature gradient is about 5K.

This work has been supported in part by The Swedish Foundation for Strategic Research (SSF) within the Strategic Research Center Charmant, and by The Swedish Governmental Agency for Innovation Systems (VINNOVA) within a VINN Verification project.

Vulnerability of Radio Technologies Used in Wireless Industry Automation

José Chilo[1] and Peter Stenumgaard[1,2],

[1]*Center for RF Measurement Technology, University of Gävle*
SE-80176 Gävle, Sweden
jose.chilo@hig.se

[2]*Swedish Defence Research Agency*
P.O Box 1165, SE-581 11, Sweden
peter.stenumgaard@foi.se

Abstract— Several commercial-off-the-shelf radio technologies currently used in wireless industry automation are not optimized to deal with electromagnetic interference in these kinds of radio-hostile environments. An important issue is the choice of wireless solutions for critical applications sensitive for delay in the radio link. Several wireless solutions use MAC- and link-layer solutions that react with delay if electromagnetic interference is present on the channel, see figure 1. Therefore, it is necessary to have good knowledge of the electromagnetic environment for certain applications so that vulnerability analyses can be done for different candidates of wireless solutions.

From the viewpoint of design and performance analysis of a radio system in an industrial environment, a trade-off between robustness and capacity must be considered. In order to for a radio system to have high robustness to disturbances in harsh environments, data redundancy, which would result in a low data rate, is required. A low data rate in turn leads to system reliability, safety, and security, which are desirable in industrial applications but other factors are loose, i.e. quick response. Further, the following parameters are also important and should be considered: a) delay, i.e. the amount of tolerable delay in packet delivery; b) loss, i.e. the tolerable degree of packet loss; and c) jitter, i.e. the amount of tolerable variation in packet delay.

Because several wireless technologies can be used in industrial applications, more research is required for understanding their advantages and limitations. This would provide an opportunity to derive full benefits from wireless technology while preventing problems due to misapplication.

The first step towards understanding environments surrounded by electromagnetic radiation—both natural and artificial—is to characterize them. A research project to this end is currently underway with the Center of RF Measurement Technology at the University of Gävle as project manager. The main aim of this project is to develop improved technologies that ensure high reliability of wireless applications in industrial environments.

Between 2008 and 2009, electromagnetic interference measurements were performed in three different industrial environments [1-2]. In this paper, we present some conclusions on the vulnerability of some existing wireless technologies to such environments.

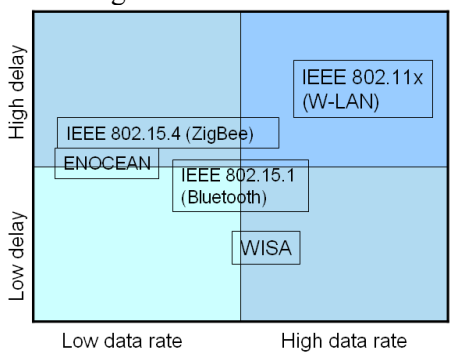

Figure 1. Schematic comparison between short-range wireless technologies. Data from [3]

From the results of the study, we can conclude that it is necessary to be aware of the basics of wireless technology, particularly the type of technology used in industry. This will determine which technologies should be considered for a particular application.

References

[1] J. Chilo, C. Karlsson, P. Ängskog and P. Stenumgaard, ”EMI disruptive effect on wireless industrial communication systems in a paper plant”, Proc. IEEE EMC Symp. Austin-Texas, vol. 3, pp. 221-224, August 2009.

[2] J. Chilo, C. Karlsson, P. Ängskog and P. Stenumgaard, ”Impulsive noise measurement methodologies for APD determination in M2M environments”, Proc. IEEE EMC Symp. Austin-Texas, vol. 3, pp. 151-154, August 2009.

[3] Scheible, Dzung, Endresen, Frey ”Unplugged but connected”, *IEEE Industrial Electronics Magazine*, pp 25-34,Summer 2007.

Multipath Environment Simulator for evaluation of Terminals

Nima Jamaly, Jan Carlsson and Per-Simon Kildal
Antenna Group, Chalmers, University of Technology

Abstract

In the frame of our project we are working towards characterization of multi-element terminals within the different multipath environments. A Rayleigh fading circumstance is realized for different distributions of angle of arrival including uniform on azimuth and non-uniform on elevation plane (e.g. Gaussian, truncated Gaussian, Laplacian, double exponential, etc). These configurations can be equally well applied to double Rayleigh fading case too.

For this purpose, we have created a simulation tool called Multipath Environment Simulator for evaluation of Terminals (MEST) in Antenna Group at Chalmers. The work is a continuation of some previous work performed in the group [1]. The inputs to this simulator are embedded element patterns, reflection coefficients (or equivalently matching efficiencies) and maximum available power from the source by which the patterns were either measured or simulated. The number of realized scenarios as well as the number of incident waves form our further inputs. Then, MEST outputs different MIMO parameters like Apparent and Effective Diversity Gains, Mean Effective Gains, Capacity, Embedded Element Efficiencies and different correlation factors. Moreover, the multipath environment of unbalanced polarizations can be also emulated in MEST.

Therefore, by virtue of MEST, we are able to characterize a multi-element terminal in different multipath environments of Rayleigh and Double-Rayleigh fading characteristics. The software can be used for optimization purposes too. As an example of application of the software in our research, we shall refer to what has been revealed about the influence of the shape of patterns embodying the directivity upon performance of elements in isotropic scattering environment with less number of scatterers [2]. Besides, advantages of beamforming technique and its effects on diversity gain established another discipline that has been studied in our research. As an example for verification of MEST, results of measurements in Reverberation Chamber versus simulations are illustrated below. Results belong to four horizontal dipoles of 0.1λ distance between subsequent elements located horizontally over the ground.

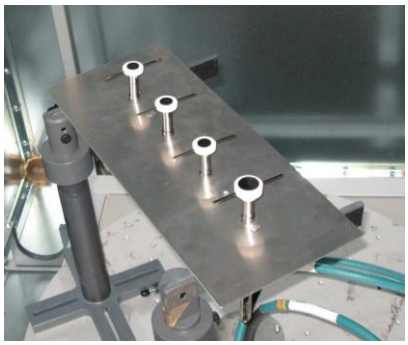

MEASUREMENT AND SIMULATION RESULTS

MIMO Parameters	*Simulated*	*Measured*
Effective Diversity Gain (dB)	9.6	9.7
Apparent Diversity Gain (dB)	11.9	12.5
Capacity at SNR= 15_{dB} (bps/Hz)	9.5	9.0
Embedded Element Eff. 1 (dB)	-2.3	-3.0
Embedded Element Eff. 2 (dB)	-5.0	-5.0
Embedded Element Eff. 3 (dB)	-5.0	-4.6
Embedded Element Eff. 4 (dB)	-3.0	-2.8
Amplitude Correlation btw 1 & 2	0.8	0.7
Amplitude Correlation btw 1 & 3	0.16	0.13
Amplitude Correlation btw 1 & 4	0.14	0.28
Amplitude Correlation btw 2 & 3	0.36	0.44

References:

[1] K. Rosengren and P.-S. Kildal, "Radiation efficiency, correlation, diversity gain and capacity of six monopole antenna array for a MIMO system: Theory, simulation and measurement in reverberation chamber," Proceedings IEE, Microwaves Antennas and Propagation, vol. 152, no. 1, pp. 7–16, 2005, see also Erratum published in August 2006.

[2] N. Jamaly, H. Zhu, P.-S. Kildal and J. Carlsson, "Performance of directive multi-element antennas versus multi-beam Arrays in MIMO communication systems", submitted to Eucap 2010, Barcelona, Spain.

Low-profile directive antenna using metamaterial slab for RFID tags

Xin Hu[#1, 2], Anders Rydberg[*2]

[1]*Centre for Optical & Electromagnetic Research, Zhejiang University, Hangzhou 310058, China*

[2]*Signals and Systems Group, Department of Engineering Sciences, Uppsala University, SE-751 21 Uppsala, Sweden*

[#]xin.hu@angstrom.uu.se, [*]anders.rydberg@angstrom.uu.se

With the rapid development of radio frequency identification (RFID) systems and the operating frequency rises into microwave region, the antenna design for the tags becomes more and more substantial [1]. In many applications, RFID tags need to be attached to metallic objects' surface. However, there are some difficulties for RFID tag especially label-type tags with dipole-like antennas (e.g., the loaded meander tag antenna [2]) to function properly on the surface of metallic objects. In this paper, the design of a low-profile directive dipole antenna over metallic surface is given. The antenna structure, which consists of a metamaterial [3] slab as the superstrate and a printed dipole antenna over the metallic surface, is shown in Fig.1.

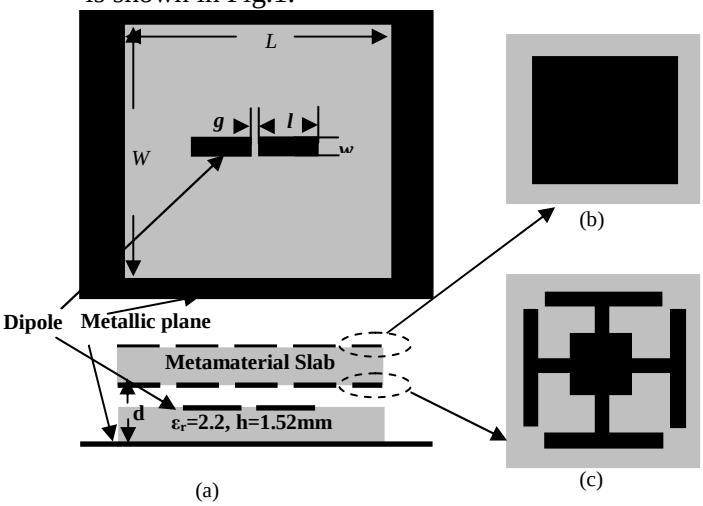

Fig. 1(a) the geometry of printed dipole antenna; (b) the unit cell of metamaterial slab (upper plane); (c) the unit cell of metamaterial slab (lower plane) (Black: metallization; Gray: substrate)

The metallic surface and the metamaterial superstrate form an ultra-thin resonance cavity compared to the wavelength of the working frequency *f*, where *f* satisfies [4]:

$$-4\pi fd / c + \Delta\phi_1 + \Delta\phi_2 = 2\pi n \qquad (1)$$

where d is the thickness of the cavity, c is the speed of light, and $\Delta\phi_{1(2)}$ is the reflection phase of the metallic surface (the metamaterial superstrate). The printed dipole antenna over metallic surface shows very good radiation efficiency regardless of the opposite image current induced by the metallic surface. The unit cell of the metamaterial slab, which is similar to [5], is given in Figs. 1(b) and 1(c). Different from [5], the upper plane in Fig. 1(b) is a square patch smaller than the unit cell. This allows the superstrate to be partially transmissive at the working frequency.

Fig.2 shows the simulated return loss and radiation pattern of the proposed antenna for the case of *d*=1.98mm, where the space between the superstrate and the printed dipole antenna is 0.46mm (~λ_0/125 at working frequency of 5.2GHz). We can see that the printed dipole antenna works at 5.2 GHz. Additional dip appears at 5.98GHz, but it does not correspond to directive emission. The dipole antenna shows a high average gain of 8dBi from 5.1 to 5.3 GHz. Consequently, this antenna provides a very good alternative for the RFID tags over metallic surface.

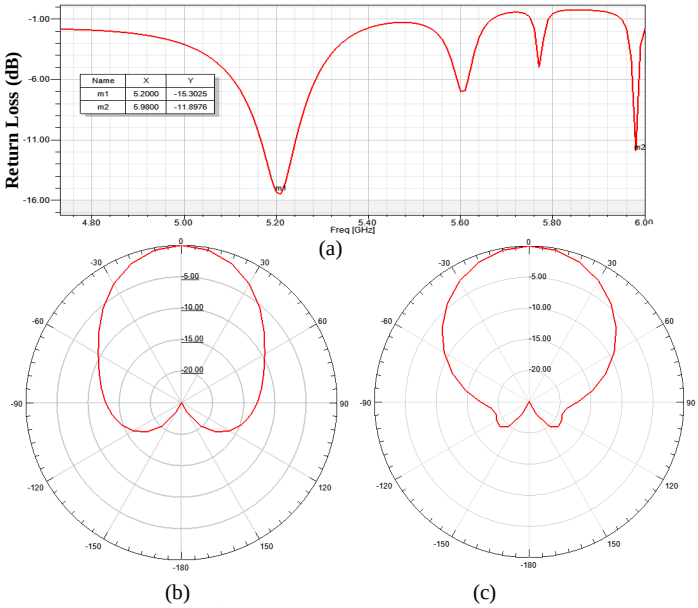

Fig. 2 (a) Return loss for the proposed antenna. Radiation pattern on H plane (b) and E plane (c) at 5.2GHz

REFERENCES

[1] K. Finkenzeller, "RFID handbook", JohnWiley & Sons, UK, 2003

[2] Rao, K.V.S., Nikitin, P.V., and Lam, S.F, "Antenna design for UHF RFID tags: a review and a practical application", IEEE Trans. Antennas Propag., 53, (12), pp. 3870–3876, 2005

[3] V.G. Veselago, "The electrodynamics of substances with simultaneously negative values of ε and μ ", Soviet Physics Uspekhi, vol. 10, no. 4, pp. 509-514, 1968

[4] L.Zhou, H.Q.Li, Y.Q.Qin, Z.Y.Wei, and C.T.Chan, "Directive emissions from subwavelength metamaterial-based cavities," Appl. Phys. Lett. 86, 101101 ,2005.

[5] Mustafa Al-Nuaimi, Anders Rydberg, Paul Hallbjorner, "Low Profile Dipole Antenna Backed by Novel Artificial Magnetic Conductor", European Microwave Week Conference Proceedings, Roma, Italy, September 2009

Characterization of Active Beamforming Phased-Array Feeds for the Next Generation Radio Telescopes: Numerical Modeling and Experimental Verification.

Marianna Ivashina

Netherlands Institute for Radio Astronomy (ASTRON)
P.O. Box 2, 7990 AA Dwingeloo, The Netherlands (ivashina@astron.nl).

An important limitation of conventional single-beam radio telescopes is that they can observe only a small region of the sky for each beam pointing. This problem can be surmounted by Phased Array Feeds (PAFs) of many electrically small antenna elements that are capable to perform instantaneous multibeaming with each reflector antenna. This technology opens up new directions in radio astronomy as the size of the instantaneous Field Of View (FOV) is expected to increase up to two orders of magnitude, so that the solutions to astronomical science cases, particularly to those requiring large-field surveys on short timescales, are yet within reach.

The new generation PAFs of reflector antennas are advantageous over conventional single-beam feeds and clusters of horns since they can provide many closely overlapping beams in one snapshot and, hence, greatly improve the size and continuity of the Field Of View (FOV). However, to meet the required field-sampling limit with a cost-effective number of PAF beams, their shapes should be optimized and the maximum achievable sensitivity should be traded against the maximum tolerable sensitivity ripple over the FOV. Future PAF-equipped telescopes are potentially accurate polarimeters thanks to the flexibility that digital beamforming offers. However, although the orthogonality of the beam pair in the direction of observation may be improved electronically, it is important that the intrinsic polarization characteristics of the beams are sufficiently high to minimize such corrections as they may compromise the receiving sensitivity.

In this paper we describe and model the performance of the PAF system named APERTIF ("APERture Tile In Focus"), which is currently being developed to operate on the Westerbork Synthesis Radio Telescope (WSRT). The aim of APERTIF is to increase the instantaneous FOV of the WSRT by a factor of 37 so as to enable deep all northern sky imaging surveys for a continuous frequency spectrum between 1.0 and 1.7 GHz, as well as at spectral line frequencies. This paper presents an extensive analysis, which is partly based on numerical models and measurements performed at the WSRT, of the PAF prototype comprising 144 TSA elements.

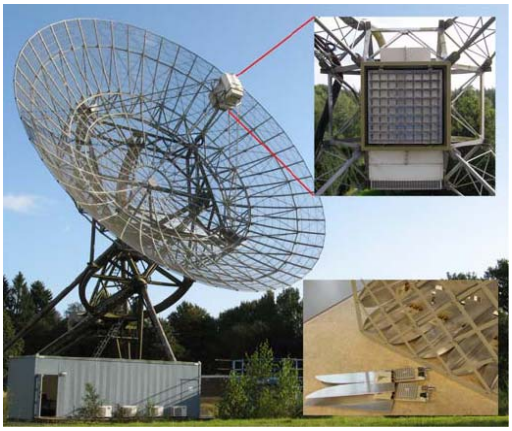

First, we propose an optimal beamforming strategy for performing large-field surveys with phased-array-fed reflector antennas using signal-processing algorithms that maximize the beam sensitivity and the continuity of multiple closely overlapping beams over a wide FOV. Then, we will present a newly developed numerical toolbox for the CAESAR software which interfaces this enhanced MoM solver with GRASP to be able to perform the PAF system analysis and optimization in its entirety. Afterwards, the numerical results are discussed: the resulting beam shapes, sensitivity, and polarization diversity characteristics are examined over a large FOV and frequency bandwidth. We consider weighting schemes to achieve a conjugate-field matched situation (max. power transfer), as well as the maximum SNR, and a reduced SNR scenario with constraints on the sensitivity ripple over the FOV. The numerical results demonstrate a very good agreement with the measurements performed at one of the telescope's dishes. The ability to perform an adequate polarization diversity is discussed as well.

Session 10

10.10-12.10 Wednesday 10 March 2010

340 GHz GaAs monolithic membrane supported Schottky diode circuits

Huan Zhao[1], Aik-Yean Tang[1], Peter Sobis[1,2], Vladimir Drakinskiy[3], Tomas Bryllert[3], Jan Stake[1,3]

[1]*GigaHertz center, Department of Microtechnology and Nanoscience, Chalmers University of Technology, SE-41296, Sweden*
[2]*Omnisys Instruments AB, V.Frölunda,Sweden*
[3]*Physical Electronics Laboratory, Department of Microtechnology and Nanoscience, Chalmers University of Technology*
Email: zhaoh@chalmers.se

Abstract—

There is a demand for compact heterodyne receivers operating in the sub-millimeter wave band above 300 GHz for earth observation instruments and space science missions. At such high frequencies, monolithic integrated diode circuits would be favorable over a traditional discrete design which is restricted by the alignment tolerance of the diode chips to the surrounding circuit. However, due to the mode effect, the high frequency circuits are often limited by the thickness of the support substrates. Recently, membrane technique has been proposed to overcome this drawback [1]. In this paper, frame less monolithic membrane supported Schottky diode circuits designed for 340 GHz have been developed. A schematic picture of a completed circuit is shown in Fig.1. The Schottky diode, filter structures, and gold beam-leads are supported by an ultra-thin (3 μm) GaAs membrane. The beam leads provide electrical connections, thermal contact, as well as physical support for the circuit. This technique could also be extensively used for monolithic integration of other active and passive components for higher frequency operation.

For electrical characterization of the membrane circuits, as shown in Fig.2, a TRL calibration kit has been developed for the WR-03 waveguide band (225 GHz – 320 GHz) using E-plane type split blocks in which the membrane structures are mounted. This will enable full S-parameter characterization of passive circuitry as well as extraction of the Schottky diode model parameters.

REFERENCE

[1] P. H. Siegel, R. P. Smith, M. C. Gaidis, and S. C. Martin, "2.5-THz GaAs Monolithic membrane-Diode Mixer", *IEEE Trans. Microwave Theory Tech.*, Vol.47, pp.596-604 (1999)

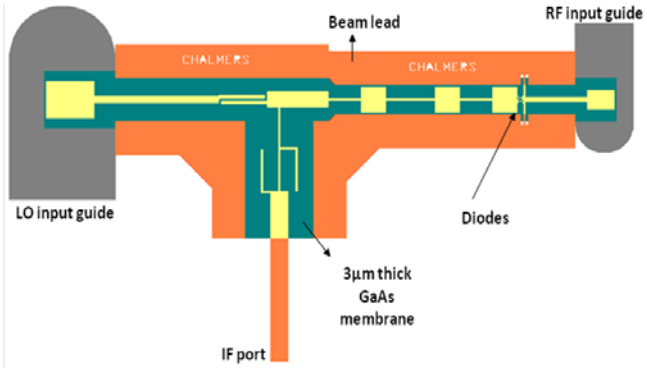

Figure 1: A schematic picture of a completed membrane supported circuit

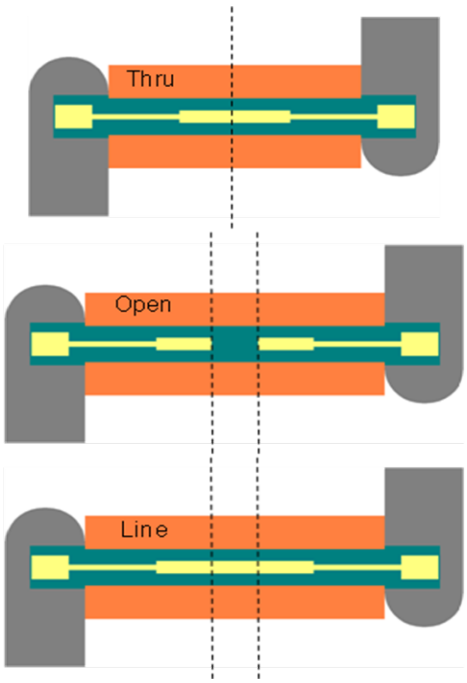

Figure 2: A TRL calibration kit designed for electrical characterization of the membrane circuits

Investigation of harmonic generation in suspended graphene

Omid Habibpour[(1)*], Sergey Cherednichenko[(1)] , Josip Vukusic[(1)] , Jan Stake[(1)]

[(1)] Physical Electronics Laboratory, Department of Microtechnology and Nanoscience, Chalmers University of Technology, SE-412 96 Göteborg, Sweden

[*]omid.habibpour@chalmers.se

Abstract- In this paper we investigate harmonic generation in suspended graphene illuminated with a 100 GHz pumping signal.

Keywords: Graphene, frequency multipliers, terahertz sources

INTRODUCTION

The region of the electromagnetic spectrum from 0.1THz to10THz (the so called terahertz band) is a current area for research in different sciences. One important issue is the lack of compact sources operating at room temperature which partly due to the limitation of the electron speed. Researchers are searching to find new materials having very high electron mobility to realize efficient terahertz sources. One such material is Graphene which was produced in 2005 for the first time [1]. Graphene is a single atomic layer of carbon atoms with a honeycomb crystal lattice. Its high intrinsic electron and hole mobility as well as unique band-structure introduces the possibility of making novel devices in the THz band.

New high-frequency devices based on Graphene may bridge the terahertz gap. There are some theoretical papers showing potential harmonic generation in Graphene at terahertz band [2-3] which brings the possibility of making frequency multiplier based on graphene. We have started investigating this effect experimentally at the lower end of the terahertz frequency band.

DEVICE FABRICATION AND MEASUREMENT

We produce graphene flakes by the exfoliation method and make them suspended in order to remove the substrate effect (Fig 1). A spiral antenna is fabricated for absorption of the illuminated signal and emission of the generated harmonics. The device is pumped at 100 GHz by a HBV multiplier source and the resulting spectrum is measured by the Fourier transform spectroscopy method. We measured the resulting spectrum at room temperature and compared it with the source spectrum, since the source has strong harmonics as well. We saw that the ratio between the 3rd harmonic and the pumping signal increased while Graphene was present. In order to completely remove the 3rd harmonic from the source a filter is included in the new setup which will also improve the pumping of the Graphene multiplier.

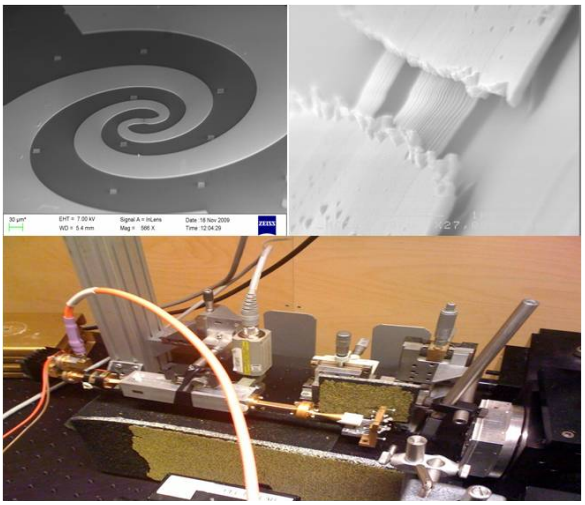

Fig. 1. Suspended graphene (top right), suspended graphene with a 90-450 GHz spiral antenna (top left), measurement setup (bottom)

ACKNOWLEDGMENT

The authors thank Swedish Foundation of Strategic Research for founding this project.

REFERENCES

[1] K. S. Novoselov, A. K. Geim, S. V. Morozov, D. Jiang, M. I. Katsnelson, I. V. Grigorieva, S. V. Dubonos, and A. A. Firsov, "Two-dimensional gas of massless Dirac fermions in graphene," *Nature*,vol. 438, pp. 197–200, Nov. 2005.

[2] S. A. Mikhailov and K. Ziegler, "Nonlinear electromagnetic response of graphene: frequency multiplication and the self-consistent-field effects," *Condensed-matter*, vol. 20, 384204, 2008.

[3] A. R. Wright, X. G. Xu, J. C. Cao, C. Zhang, "Strong nonlinear optical response of the graphene in the terahertz regime," *Applied Physics Letters*, vol. 95, 072101. 2009.

RF sensor for face recognition behind masking

J. Svedin[(1)], J. Kjellgren[(1)], M. Karlsson[(1)], H. Merkel[(2)], and, J. Dong[(3)]
[(1)] Swedish Defence Research Agency (FOI), [(2)] Chalmers Industriteknik, [(3)] Acquris IT

Introduction

The use of camera based surveillance systems has become more widespread during the last decades. A remaining problem is the fact that perpetrators often conceal their faces behind masks. Usual frequencies such as the visual band and the IR-bands are located in the higher end of the optical frequency region where a mask conceals a face efficiently. In contrast many masking materials are transparent for electro-magnetic waves in the microwave region and the lower end of the optical region. Around the border between the microwaves and the optical region at 300 GHz are the millimeter and sub-millimeter regions where many security applications are operated.

Purpose

The main purpose of the project is to study the potential of radar and radiometry methods at millimeter and sub-millimeter wavelengths for the recognition of a face behind a mask or concealing material. The goal is to determine the application possibilities and if applicable propose a suitable RF-system design including support system.

Measurements

The measurement system is a bistatic radar scatterometer transmitting a continuous-wave signal with adjustable frequency in the range 350-500 GHz. The transmitter antenna floodlights the target without any resolution. The image formation is done by mechanical scanning the receiving antenna system. It is a quasi-optical system based on a parabolic mirror and two plane mirrors where the latter two can be rotated for scanning the narrow receiving lobe in azimuth and elevation. Measurements of a model head (see Fig. 1) painted with silver have been carried out, see Fig. 2. The measurements include both the head in clear sight and concealed by cloth.

Fig. 1. Target used for measurements.

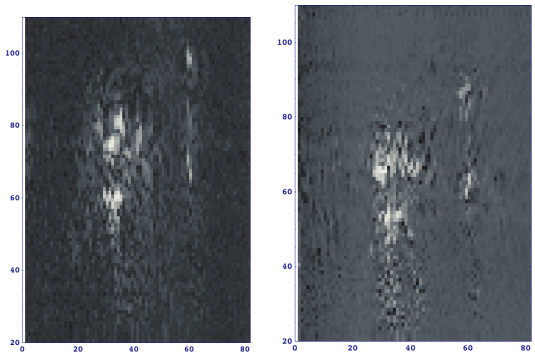

Fig. 2. Measured images w and w/o cloth (right).

Simulations

The measurements and experiments are supported by simulations. Through simulations it is possible to widen the overall view and e.g. study radar system and measurement cases not possible or reasonable to realize within the project. Radar measurements approximating data from a real system, have been simulated and an example is presented in Fig. 3

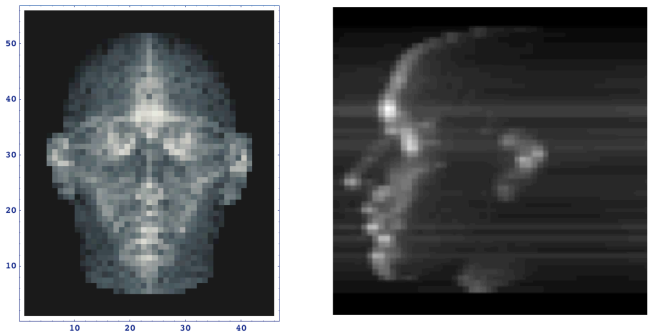

Fig. 3. Simulated 3D radar response.

Support systems

The system for alignment must be able to detect and follow humans of very different appearances and further to detect their faces and determine if a face is concealed. Softwares are being tested and developed that can detect and track faces in video data, see Fig. 4.

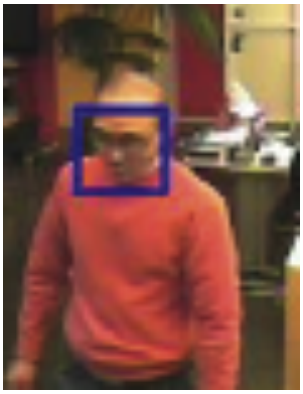

Fig. 4. Test of software for detection of faces.

A 210 GHz radar system for 3D stand-off detection

J. Svedin[(1)], S. Rudner[(1)], G. Thordarsson[(2)], N. Wadefalk[(3)], S. Gunnarsson[(3)], M. Abbasi[(3)], H. Zirath[(3)], J. Stake[(3)], T. Bryllert[(3)], J. Vukusic[(3)], and, S. Cherednichenko[(3)]
[(1)] Swedish Defence Research Agency (FOI), Linköping [(2)] SAAB Microwave Systems, Järfälla
[(3)] Chalmers University of Technology, Göteborg

Introduction

Mm-wave/THz radiation can 'see through' obscurants such as clothing fabrics and many other materials and detect concealed weapons, contraband and explosives. The research presented in this paper concerns novel or improved components that can help to open up the this frequency region for defence and security applications. A 210 GHz FMCW radar system for 3D stand-off detection research has been built using the developed components.

Radar system

The radar system is based on the FMCW principle and has a 210 GHz center frequency with a 12.8 GHz sweep bandwidth (1.2 cm range resolution). A block diagram of the system is given in Fig. 1.

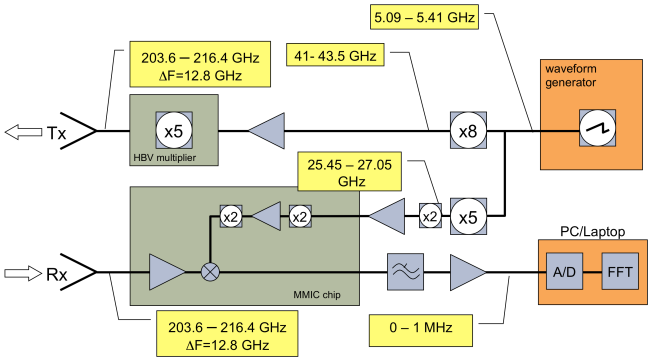

Fig. 1. Block diagram of FMCW radar system.

Receiver module

The RX module is based on a highly integrated MMIC [1] which contains a novel slot antenna, a three-stage LNA, a sub-harmonic mixer, and a multiplier chain for the LO, see Fig. 2. The measured NF is about 7 dB. The MMIC is mounted at the backside of a 5 mm AR-coated HR-Si substrate lens, which is mounted on a plate as shown in Fig. 3.

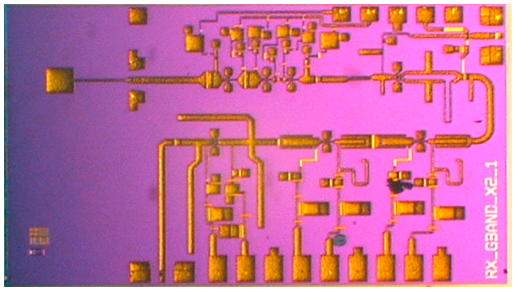

Fig. 2. Microphotograph of RX MMIC.

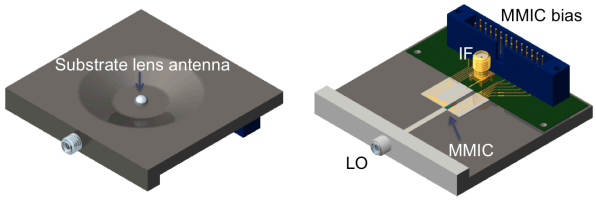

Fig. 3. Schematic view of RX module base plate.

Transmitter module

The transmitter is based on an ultra-compact HBV multiplier (X5) module, see Fig. 4. The measured output power and efficiency at 202 GHz was > 20 mW and 3 %, respectively [2].

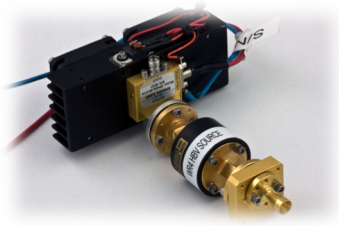

Fig. 4. Photo of HBV X5 transmitter module.

Person scanner

The 3D person scanner uses a mechanical scanner for imaging and SAR processing to achieve a cross-range resolution of roughly 1 cm, see Fig. 5.

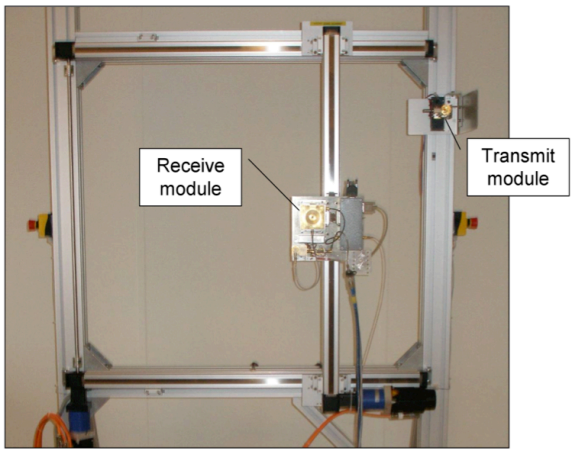

Fig. 5. Person scanner system.

References

[1] IEEE Microwave and Wireless Components Letter, vol. 18, no. 4, pp 284-286, 2008.

[2] Proc. of SPIE. vol. 6739 pp. 67390U, 2007.

Assessment of Various Epitaxial Lift-off Methods for Heterostructure Barrier Varactor

M. Hadi Tavakoli Dastjerdi *, Anke Sanz-Velasco, Josip Vukusic, and Jan Stake
Department of Microtechnology and Nanoscience, Chalmers University of Technology, SE-412 96 Göteborg, Sweden

**hadi.tavakoli@chalmers.se*

INTRODUCTION

Heterostructure Barrier Varactor (HBV) serves as one of the few potential power sources in the THz frequency range (100 GHz - 2 THz) [1]. A commonly used substrate for HBV materials is InP (indium phosphide). The epitaxially grown combinations of the InGaAs modulation and InAlAs barrier layers are lattice matched to InP. However, there are integration and thermal difficulties with this material system. It is highly desirable to be able to apply the common MEMS integration technologies to the device. Also, InP-based HBV material system suffers from the poor thermal conductivity of InP, especially for high power applications. This increases the temperature inside the device, causing high leakage current and potential self-heating problems in HBVs [2]. Silicon is a suitable candidate for a new host substrate for the HBV, providing the possibility of taking advantage of the mature SOI technology for integration schemes. Moreover, it has higher thermal conductivity compared to InP.

The main goal of this work is to transfer the up-side-down grown InP-based HBV material to silicon. There have been reports of III-V to silicon wafer bonding using an adhesive interlayer [3]. We have started applying different wafer bonding methods to attach the InGaAs surface to the target silicon substrate. Also some fabrication steps were modified to prevent the potential risks to the bond during device processing.

EXPERIMENTAL PROCEDURE

Plasma activated hydrophilic direct wafer bonding is a common bonding technique usually used for silicon-silicon systems. We have utilized a similar method for applying to InGaAs - Silicon bonding with very few voids [Fig.1 left]. A major problem of this material system is the difference between the thermal expansion coefficients of the two materials. Therefore, further processing steps might potentially risk the bonding. For this reason we have optimized and measured non-alloyed ohmic contacts with very low specific contact resistance. Successful material transfers were also done by adhesive bonding utilising SU-8 photoresist. Further fabrication and measurement of the device confirms perfect matching to the reference InP-based-device characteristics [Fig.1 right]

We are also involved with applying the eutectic bonding method for Si-Au system. This is expected to enhance the performance of the HBV diode by reducing the series resistance of the device.

We will be comparing different bonding techniques in terms of bonding quality, stability in further device fabrication steps, and also the DC characteristics of fabricated devices on different bonded samples.

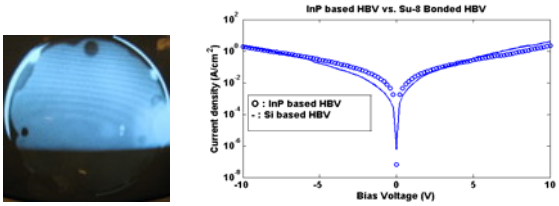

Fig. 1. InGaAs-Silicon direct Bonding (left), measured I-V curves of the adhesive bonded HBV and the InP-based reference HBV (right)

REFERENCES

[1] E. Kollberg and A. Rydberg, "Quantum Barrier-Varactor Diodes for High Efficiency Millimeter-Wave Multipliers", Electronics Letters, Vol. 25, pp. 1696-1697, December 1990.

[2] J. Stake, L. Dillner, S. Jones, C. Mann, J. Thornton, J. Jones, W. Bishop and E. Kollberg, " Effects of Self-heating on planar heterostructure barrier varactor diodes", IEEE Transactions on Electron Devices, vol. 45, issue 11 , pp.2298-2303, 1998.

[3] Arscott, S.; Mounaix, P.; Lippens, D. “Substrate transfer process for InP-based heterostructure barrier varactor devices”, Journal of Vacuum Science & Technology B: Microelectronics and Nanometer Structures, Volume 18, Issue 1, January 2000, pp.150-155

Development of a 0.6 THz HBV frequency tripler

Johanna Liljedahl, Tomas Bryllert, Josip Vukusic and Jan Stake

Physical Electronics Laboratory, MC2
Chalmers University of Technology
SE-412 96 Göteborg
Sweden
E-mail: johanna.liljedahl@chalmers.se

Abstract —

The Heterostructure Barrier Varactor (HBV) diode is promising for frequency multiplication up to THz frequencies for room temperature applications. Since the invention in 1989 the technology has grown more mature and today HBV diodes are used as high power multipliers for frequencies up till and above 200 GHz [1-2]. The HBV has the advantage of not requiring DC-biasing or idler matching when used as a tripler, enabling a simple and compact circuit design. Nevertheless, to date the highest output frequency published for HBV diode based multipliers is 450 GHz [3]. Our aim is to push this limit further into the sub-mm region.

We present the current status on the development of a HBV tripler for an output frequency of 600 GHz. There is a window in the water vapour absorption spectrum in this region, making it interesting for e.g. remote personnel scanning security applications or remote sensing for environmental purposes.

The HBV is based on a wide band gap semiconductor barrier between two narrow band gap, equally doped, semiconductor modulation layers. The characteristic C-V curve is symmetric, while the I-V curve is anti-symmetric. These properties cause the HBV to only generate odd harmonics. Thereby, when used as a frequency tripler, there is only need for circuit matching at the in and out ports, and no idler matching circuit is needed.

The designed HBV is based on the InGaAs/InAlAs/AlAs epitaxially grown on InP material system. Doping and layer structure has been optimised for maximum dynamic cut-off frequency at a pumping frequency of 200 GHz. Both current saturation and impact ionization has been taken into account for optimizing the multiplier characteristics, see Figure 1.

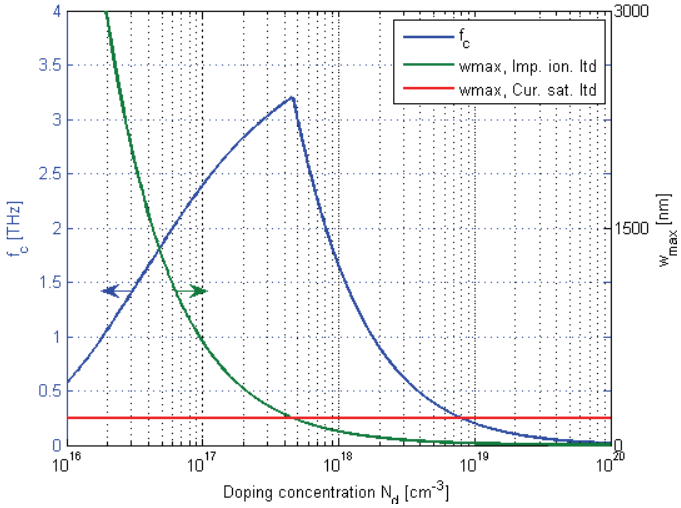

Figure 1: *Doping dependence of the cutoff frequency and the maximum depletion layer width for HBV with 2 barriers and 2 mesas in series.*

In order to increase the frequency the circuit dimensions must decrease, therefore sophisticated MMIC design and fabrication is used for the multiplier circuit. We present simulation results of the optimised circuit, the design as well as the fabrication progress.

References —

[1] E. Kollberg and A. Rydberg. Quantum-Barrier-Varactor Diodes for High-Efficiency Millimetre-Wave Multipliers. Electron. Lett. (1989) vol. 25 (25) pp. 1696-1698

[2] J. A. M Svedin et. al. Development of a 210 GHz near-field measurement radar system based on an antenna-integrated MMIC receiver front-end and an ultra-compact HBV transmitter source module. Proc. SPIE (2008) vol. 7117 (71170H) DOI:10.1117/12.800247

[3] M. Saglam, et. al. 450 GHz millimetre-wave signal from frequency tripler with heterostructure barrier varactors on gold substrate. Electron. Lett. (2002) vol. 38 (13) pp. 657-658

A Compact 340 GHz Heterodyne Imaging System

Robin Dahlbäck[1], Biddut Banik[1], Peter Sobis[3], Andreas Fhager[2], Mikael Persson[2] and Jan Stake[1]

[1]Physical electronic Laboratory, Department of Microtechnology and Nanoscience,
[2]Biomedical Engineering Division, Department of Signals and Systems,
Chalmers University of Technology, SE-412 96 Göteborg, Sweden.
[3]Omnisys Instruments AB
Email: dahlback@chalmers.se

I. Introduction and Background

Terahertz (THz, 10^{12} Hertz) imaging has attracted a lot of attention recently in various applications ranging from production process control to breast cancer imaging [1]. However, those practical applications require compact sources and systems offering room temperature operation. Contrary to time domain systems, continuous wave (CW) imaging systems are usually compact, simple, fast, and of relatively low-cost. High spectral resolution is another advantage. A common approach for realizing CW THz systems is up-conversion from microwave frequencies using frequency multipliers for signal generation and sub-harmonic mixers for detection [2].

We present a RT CW imaging setup operating around 340 GHz that consists of a multiplier chain and a receiver chain, shown in Fig. 1. The system provides heterodyne detection with an IF BW of 0-20 GHz with the possibility of extracting the phase information. Furthermore, the system utilizes the ultra-compact catadioptric lens for short range imaging applications.

The previous setup, described in [3], operated in direct detection mode at around 100 GHz. A catadioptric lens-horn combination was used as a focusing element producing a marked improvement in image resolution. However, the setup was based on direct detection technique and the phase information was missing. Therefore the setup was not able to resolve dielectric contrast. Moreover, the slow response time of the detector also limited the imaging speed.

The 340 GHz imaging setup, described here, is a heterodyne system and aims at collecting vector measurement data in order to improve image detail. For instance in biomedical applications this provides an advantage over scalar measurements. The system uses a sub-harmonic RT Schottky mixer as receiver [4]. Two separate multiplier chains are used to generate the LO drive and illumination signal.

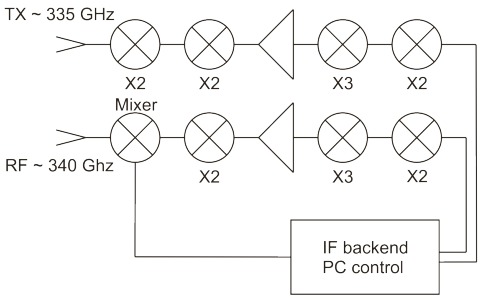

Fig. 1 Block diagram of the 340 GHz heterodyne imaging system.

II. Results

The system, shown in Fig. 2, is completely automated with 3-axis positioning stage and data acquisition. Being heterodyne in nature, the setup provides fast data acquisition and imaging speed. We will present detailed characterization results regarding beam diameter, spatial resolution and dynamic range. Furthermore, the setup will be employed for various applications including biomedical and object investigation and results will be presented.

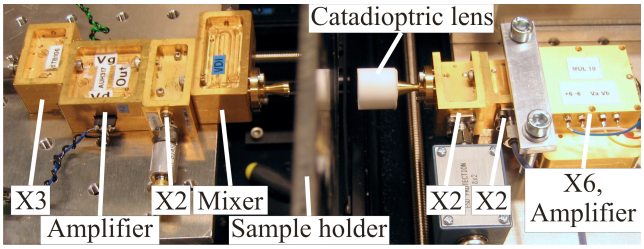

Fig. 2 The constructed 340 GHz heterodyne imaging setup in transmission-mode.

References

[1] Chan W.L., Deibel J., Mittleman D.M., "Imaging with terahertz radiation", *Rep. Prog. Phys*, vol.70, pp.1325-1379, 2007.

[2] Dengler, R.J.; Maiwald, F.; Siegel, P.H., "A Compact 600 GHz Electronically Tunable Vector Measurement System for Submillimeter Wave Imaging," *Microwave Symposium Digest, 2006. IEEE MTT-S International* , pp.1923-1926, 11-16 June 2006

[3] Banik, B.; Vukusic, J.; Stake, J., "Millimeter Wave Characterization of a Catadioptric Lens for Imaging Applications," *IEEE Microwave and Wireless Components Letters,* vol.19, no.11, pp.680-682, Nov. 2009.

[4] Sobis P., Bryllert T., Olsen A.Ø., Vukusic J., Drakinskiy V., Cherednichenko S., Emrich A., Stake J., "Compact 340 GHz Receiver Front-Ends", *ISSTT*, 2009

Investigation of passivation methods for HBV diodes

Aleksandra Malko[*], *Johanna Liljedahl, Jan Stake, Josip Vukusic and Tomas Bryllert*

Physical Electronics Laboratory, Department of Microtechnology and Nanoscience, Chalmers University of Technology, SE-412 96, Sweden.

E-mail: malko@chalmers.se

ABSTRACT

There is a need for high power sources in the sub-terahertz frequency range for several ground-based applications, especially, related to safety and security [1]. High output power is crucial for both radar transmitters but also for LO distribution in multi pixel receivers (imaging arrays). The Heterostructure Barrier Varactor (HBV) diode multiplier [2] is a promising device for these applications and offers also a compact and low weight solution.

So far, HBV devices have been successfully demonstrated in various circuits and applications [3]. A lot of emphasis has been on LO generation for radiometers and space applications, where efficiency and reliability are key parameters. However, for emerging ground-based applications, devices must also withstand high humidity and temperature variations without any degradation. The high humidity and unstable air conditions will influence the devices parameters, and can decrease the life time of semiconductor applications. In this paper, we will present shortly Heterostructure Barrier Varactors, and passivation possibilities for this device.

The HBVs consist of high bandgap semiconductor material (which prevents electron transport through the structure), surrounded by semiconductor with low bandgap energy. This layer structure produces a symmetric voltage dependent capacitance C(V) and anti-symmetric voltage dependent current density I(V).

In figure 1, the I(V) and C(V) characteristics of a test diode of a new unpassivated HBV material is demonstrated. The test diodes show high breakdown voltage V_{bd}=19V and maximum capacitance of C_{max}=0.88fF/μm^2.

Commonly used passivating materials, for high-frequency semiconductor devices, are silicon nitride (SiN_x) and silicon oxynitride (SiO_xN_y). Due to the lower dielectric constant compared to the SiN_x and SiO_xN_y the benzocyclobutene (BCB) [4] is also an attractive future passivating material, or as a buffer between device surface and a proper passivating layer. A passivating surface provides protection from surrounding environment and reduces effects caused by the surface states or trapping centers, thereby the performance of semiconductor devices is improved.

We will present experimental results for different HBV diodes with passivated surfaces and compare them to the unpassivated HBV test diodes. The investigated parameters will be: differential capacitance at zero bias voltage (C_{max}), maximum voltage (J_{max}), differential conductance at zero bias voltage (G_{min}) and breakdown voltage (V_{bd}).

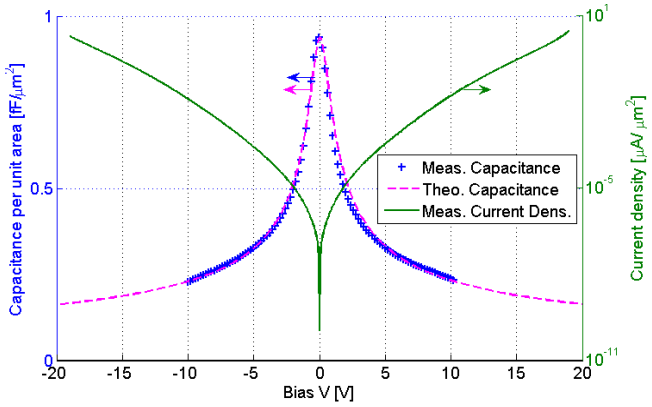

Fig. 1 C-V and I-V characteristics of a tested HBV diode

REFERENCES

[1] Appleby and Anderton. "Millimeter-Wave and Submillimeter-Wave Imaging for Security and Surveillance", Proc. IEEE (2007) vol. 95 (8) pp. 1683-1690.

[2]E. Kollberg, A. Rydberg "Quantum-Barrier-Varactor Diodes for High-Efficiency Millimetre-Wave Multipliers", 1989.

[3] Vukusic et al. "A 0.2-W Heterostructure Barrier Varactor Frequency Tripler at 113 GHz", IEEE Electron Device Lett. (2007) vol. 28 (5) pp. 340-342.

[4] C. L. Tan, h. Wang, K. Radhakrishnan, "Hot-Electron-Induced Degradation in BCB- and SiN Passivation $Al_{0.25}Ga_{0,75}As/In_{0,2}Ga_{0,8}As$ PHEMTs", 2007.

Multipixel terahertz receivers

S.Cherednichenko[1], V.Drakinskiy, W.Wei,

Physical Electronics Laboratory, Dep. Microtechnology and Nanoscience, Chalmers University of Technology, Göteborg, Sweden

[1] serguei@chalmers.se

ABSTRACT We develop multipixel receivers for terahertz frequencies. Here we discuss a solution for a high sensitivity superconducting receiver on thin SiN membranes.

Keywords: terahertz, multipixel, HEB, receiver.

Single pixel (one detector) terahertz receivers have been reported both for low noise superconducting detectors [1], and room temperature semiconducting (MMIC based) detectors [2]. Those find applications in space and ground based radioastronomy, atmosphere molecular spectroscopy, terahertz imaging, secure communication, etc. Here, most of the effort concentrated on the detector technology, and on-chip integration of the detector components (amplifiers, local oscillator). First terahertz multipixel detector arrays were developed for Cosmic Microwave Background experiments and other radioastronomical projects, where either superconducting Transition Edge Sensor or a semiconducting photoconductor/bolometer sensors were employed. This approach is good when the ultimate detector sensitivity is required, which is provided at the expense of the detector's response time. Fast terahertz detectors, also used for heterodyne receivers, are of micrometer dimensions and require integration with receiving antennas.

We investigate technology for large arrays of terahertz detectors based on "mini telescope" approach. Planar antennas, integrated with detectors, are lithographically made on thin SiN membranes. The antenna back-short makes the beam pattern to be unidirectional, hence increasing the antenna efficiency. The antenna is placed in the focus of 3mm parabolic mirror, which collimated the beam and sends to the receiver's primary optics. Our approach is to fabricate all elements in a "horizontal" integration: detector (antenna) array, back-short array, mirror array, mounted on top of each other.

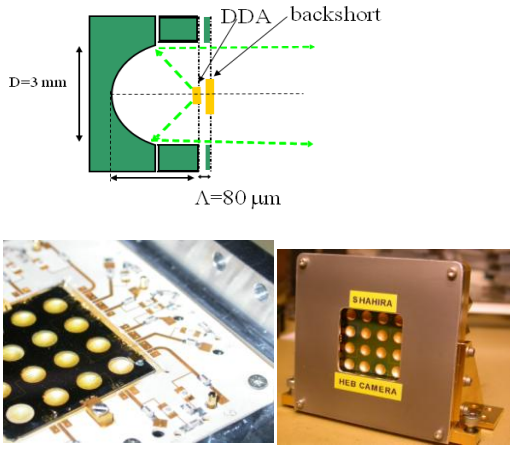

Fig.1. top, Optical layout of a pixel of the array. right, 16 pixel detector array in a prototype receiver. left, Prototype THz camera.

The project is supported by the Swedish National Space Board and Swedish Research Council (VR).

[1] S.Cherednichenko, V.Drakinskiy, T. Berg, P. Khosropanah, and E. Kollberg "Hot-electron bolometer terahertz mixers for the Herschel Space Observatory", Rev. Sci. Instrum. **79**, 034501 (2008)

[2] S.E. Gunnarsson, N. Wadefalk, J. Svedin, S. Cherednichenko, I. Angelov, and H. Zirath, "A 220 GHz Single-Chip Receiver MMIC with Integrated Antenna", IEEE MICROWAVE AND WIRELESS COMPONENTS LETTERS, VOL. 18, NO. 4, APRIL 2008, p. 284-286

Near Field Terahertz Imaging for Biological Tissue Measurements

Johannes Hjerdt[1], Mathias Grudén[1], Anders Rydberg[1], Titti Ekegren[2] and Jonas Bergqvist[2]
[1]Uppsala University, Signals And Systems, Box 534, 751 21 Uppsala, Sweden,(anders.rydberg@angstrom.uu.se)
[2]Department of Physical and Analytical Chemistry, Analytical Chemistry, Box 599, 751 24 Uppsala

Abstract -- Different types of biological tissues will absorb emitted radio waves differently. By transmitting radio waves in THz-range into a tissue it is possible to detect varying types of tissues. This is mainly due to amount of absorbed water. More water will cause changed ε_r and more reflections.

There are two types of measurements which are possible, monostatic experimental setup where the transmitter also works as a receiver, and the bistatic setup where the radio waves is transmitted through the test sample and received on the other side. The spots in the test sample where there is higher water content will be more reflective, less signal will pass through. In both cases two lenses made of polyethylene are used. The first lens is refracting the radio waves into parallel rays, and the second is concentrating the rays into a single focal point. The lenses are designed with a flat and a hyperbolic surface[1]. Other materials was considered such as silicon but lenses of polyethylene is very cheap and simple to manufacture.

In this paper two frequency ranges are used to investigate which of the frequencies that are most suitable for creating an image of the tissue. The ranges are 75-110 GHz and 220-325 GHz. The tissues which is used is freeze dried mouse brain which is sliced into 200 µm thin slices.

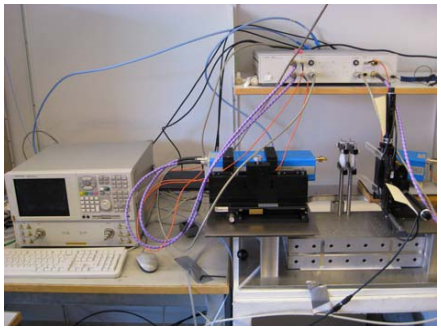

Fig 1. The bistatic experimental setup.

The best results were produced using the monostatic setup at the frequency range of 220-325 GHz. When using the lower frequency range it is possible to see the outline of the tissue but not the internal structure. Thigher frequency range makes it possible to increase the resolution for the measurements down to 250 µm. To be able to achieve the higher resolution image signal processing based on eq. 1 was used:

$$I(i,j) = \sum_{k=1}^{n} \left| M(i,j,k) \right|, \qquad (1)$$

where all points in the measurement is summed and displayed, n is number of measured positions, i and j is the position and I is the reconstructed image. The data M is the complex electric field according to

$$M(i,j) = Ae^{-j\varphi}. \qquad (2)$$

A result of the higher frequency range measurements along with signal processing is seen in Fig 2. For even higher frequencies the plastic parts that held the sample started to interact with the radio waves.

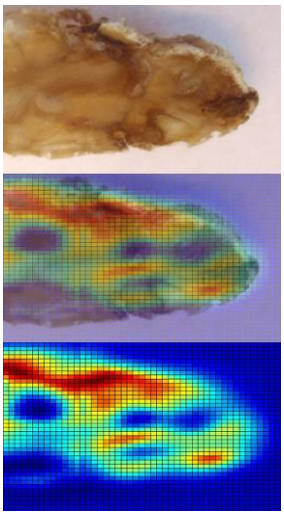

Fig 2. Sample of measurement at the higher frecuency range. The resolution is less than 0.25 µm

[1] J.Hjerdt, "Near field measurement of biological tissues using millimeter wave and terahertz frequencies", M.Sc Thesis, Uppsala University, Sweden, 2009.

[2] E. Pickwella et al, "Simulation of terahertz pulse propagation in biological systems", Applied Physics Letters 84, (2004).

Session 11

10.10-12.10 Wednesday 10 March 2010

Microwave Filters Suitable for Pick-and-Place Mounting

Simon Kristiansson
simon.kristiansson@saabgroup.com

Hans-Olof Vickes
hans-olof.vickes@saabgroup.com

Saab Microwave Systems, SE-412 89 Göteborg, Sweden

1 Introduction

A concept concerning surface mounting of microwave filters is presented[1]. Several filters, from S- to X-band, have been designed and tested, all with good results. In this paper, the results of a C-band filter is shown as an example.

All filters have been designed in a stripline configuration as separate units which are then surface mounted on a main circuit board by standard pick-and-place equipment, see the illustration in Fig. 1.

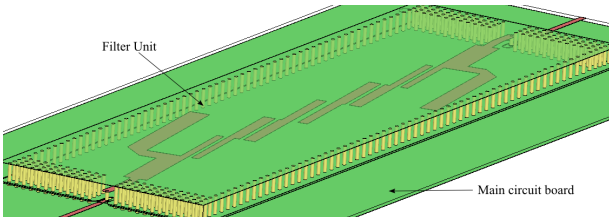

Figure 1 Illustration of the surface mounted filter concept, showing a schematic layout of a C-band filter.

Advantages of this approach comprises e.g. that filter characteristics do not govern the choice of material of the main circuit board, and that each filter can be designed and tested separately before mounting.

With the design of the filter follows also an integrated, vertical signal transition at each rf-port of the filter down to the main circuit board. The microwave transition have been designed and optimized using an electromagnetic simulator. Measured results of the transition show that the transmission loss is less than 0.3 dB, and the return loss is better than 20 dB, for frequencies up to 20 GHz.

All filters were designed in the high frequency material RO4350B® from Rogers Corporation. This laminate was chosen for its good microwave performance and low-cost. Furthermore, it is available from several suppliers with short delivery times, and with a robust manufacturing process. A photograph of a pick-and-place mounted filter is shown in Fig. 2.

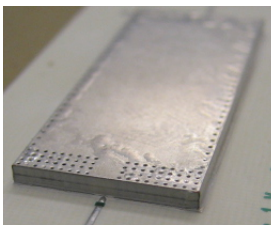

Figure 2 Picture of a surface mounted filter.

The full 3D electromagnetic simulator HFSS from Ansoft were used in all designs.

[1]This work have been carried out in the M-AESA project financed by the Swedish Defence Material Administration (FMV).

2 Measurements

This section show results from a bandpass filter with five pairs of coupled-strips. The lines are a quarter wavelength long at the passband center frequency, see Fig. 1. Open stubs and transformers have been added in order to suppress unwanted signal transmission at twice the passband frequency. The size of the filter unit is 65×20 mm.

The measured and simulated narrowband results of the filter are compared in Fig. 3a, and the corresponding broadband results are shown in Fig. 3b. The measured insertion and return losses are 2.5 dB and 20 dB, respectively. For the frequency band 6.5–14.0 GHz the measured suppression is better than 60 dB.

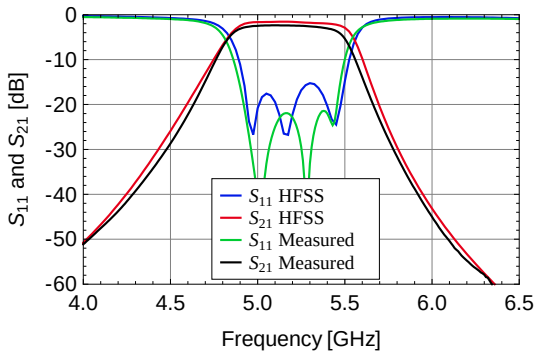

(a) Narrowband results.

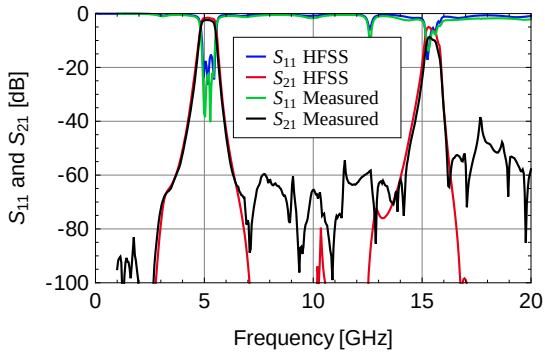

(b) Broadband results.

Figure 3 Comparison of measured and simulated results of the C-band filter; (a) narrowband, (b) broadband.

3 Conclusions

A surface mounted filter concept have been described and illustrated by a C-band filter. Measurements show very good results and match simulated results accurately for the frequency selectivity. The suppression of out-of-band signals was roughly 60 dB. The filters are manufactured in a low-cost material and have been pick-and-place mounted.

PACKAGING OF MICROSTRIP CIRCUITS USING GAP WAVEGUIDE APPROACH

E. Rajo-Iglesias[1,2], Ashraf Uz Zaman[1], Per-Simon Kildal[1] and Ahmed Kishk[3]
[1]Department of Signals and Systems, Chalmers University of Technology, Sweden
[2]Universidad Carlos III de Madrid, Spain
[3]Department of Electrical Engineering, University of Mississippi, USA.
eva@tsc.uc3m.es, zaman@chalmers.se, per-simon.kildal@chalmers.se, ahmed@olemiss.edu

Introduction: The suppression of parallel plate and cavity modes in shielded microstrip circuits is a critical problem in many applications. The use of artificial surfaces provides new options in designing efficient packaging. When dealing with microstrip circuits, the use of a metal lid can excite parallel plate cavity modes (depending on frequencies and dimensions) that are typically removed by using absorbers. However, recently a new type of waveguide has been introduced, named *gap waveguide* [1] which is based on the use of a surface texture in one of the plates of a conventional parallel plate waveguide, designed to stop propagation of modes in any direction within a given frequency range, except for a local quasi-TEM wave along a desired path. The textured surface can in principle have any periodic structure that provides the needed high surface impedance to generate cutoff of normal parallel plate waves [2]. We present in this work some results on using the same concept to remove cavity modes in microstrip circuit packages.

Results: The proposed concept is described in Fig.1 using a lid of nails above the circuit at a small distance, the *gap*. This distance is critical to determine the bandwidth of the solution.

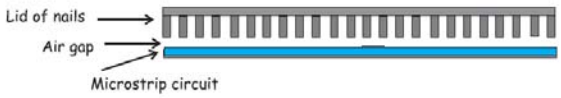

Figure 1: Description of the proposed concept for a lid of nails.

To verify the goodness of the solution a double bent microstrip line has been used as test circuit. This line will excite cavity modes if packaged with a smooth metal lid as shown in the upper graph in Fig. 2, illustrating the E field distribution in the gap at different frequencies. In the lower graph in the same figure there is shown the effect of when the ordinary smooth metal lid is replaced by a lid of nails designed to stop cavity modes in the required frequency range (10 to 20 GHz in this case). The improvement is very clear and was also experimentally verified with the prototype in Fig. 3. The proposed solution even outperforms the behavior of the unpackaged line when it is not located inside a shielded box. Therefore, the lid of nails is a very efficient way of preventing radiation from the line bends. Some of these results are included in [3] but new types of periodic structures are currently under study to be used in the same application. These will also be presented.

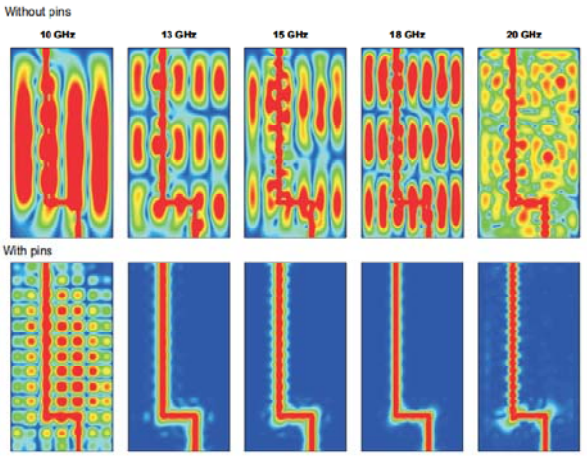

Figure 2: 2D plots for E-field showing how the cavity modes are effectively removed.

Figure 3: Manufactured prototype

Acknowledgment: This work has been supported by the Swedish Foundation for Strategic Research (SSF) within the Strategic Research Center Charmant.

REFERENCES

[1] P.-S. Kildal, E. Alfonso, A. Valero-Nogueira, E. Rajo-Iglesias, "Local metamaterial-based waveguides in gaps between parallel metal plates", *IEEE Antennas and Wireless Propagation letters (AWPL)*, Volume 8, pp. 84-87, 2009.

[2] Eva Rajo-Iglesias, Per-Simon Kildal, "Numerical studies of bandwidth of parallel plate cut-off realized by bed of nails, corrugations and mushroom-type EBG for use in gap waveguides", submitted to *IET Microwaves, Antennas & Propagation*, May 2009.

[3] E. Rajo-Iglesias, A. Uz Zaman, P.-S. Kildal, "Parallel plate cavity mode suppression in microstrip circuit packages using a lid of nails", accepted for publication in *IEEE Microwave and Wireless Components Letters*, Aug. 2009.

Single and Dual Fundamental Wideband Surface Mount VCO's covering 2-25 GHz

Ronny Christoffersen[1], Sten E. Gunnarsson[1,2], Anette Brandt[1], Christer Stoij[1], Dan Kuylenstierna[2]

[1]Sivers IMA AB, Torshamnsgatan 9, 16429 Kista, Sweden,
[2]Chalmers University of Technology, Microwave Electronics Laboratory, MC2, Göteborg, Sweden.
Email: ronny.christoffersen@siversima.com

Combining broad bandwidth and low phase noise in voltage controlled oscillators (VCO's) is a well-known challenge among microwave designers. Wideband low phase noise signal sources can dramatically reduce the system complexity, giving reduced overall cost and improved performance. In order to reduce the number of microwave components and layout space, it is also preferred to integrate more functions into the microwave components itself. It is also desirable to use surface mounted (SMD) packages, making it possible to pick-and-place (P-P) assemble the devices together with other SMD components on the same PCB.

Sivers IMA AB has designed a family of thin film VCO's covering 2-25 GHz which takes the step from custom coaxial devices to custom SMD components, intended for low and medium production volumes. Two versions of the VCO's exist, single and dual where the former contains one VCO and the latter two in the same package. The VCO's are hermetically packaged as well as reflow solderable which makes the design of the package extra challenging. The alumina (Al_2O_3) bottomplate is manufactured with filled vias and the plating is resistant to metal migration which may occur during the PCB assembly process. The lid is made of Kovar, matching the temperature expansion (Te) of the alumina bottomplate. The entire 2-25 GHz VCO series employs a generic footprint for the RF-ports.

As the VCO's are designed on alumina substrate, high Q tanks are obtained, resulting in low phase noise over a wide tuning frequency range. The VCO's consists of fundamental single ended oscillators, followed by an amplifier, low pass filter and a 10 dB directional coupler. Biased with 8V, and tuned with 0-20V, the VCO's output power is typically 10dBm. The single VCO's (VO5180-series) are divided in bands (2-3, 3-5, 5-8.4, 8.4-13.5, 13.5-20, and 20-25 GHz). All VCOs are equipped with a secondary RF output port intended for feeding an external PLL (if applicable).

The dual VCO's (VO5280-series) are two single VCO's merged together on one alumina substrate, where the band combination is custom specified. 3-5/5-8.4 GHz and 8.4-13.5/13.5-20 GHz are standard versions but any other combination can be manufactured on demand, Fig 1.

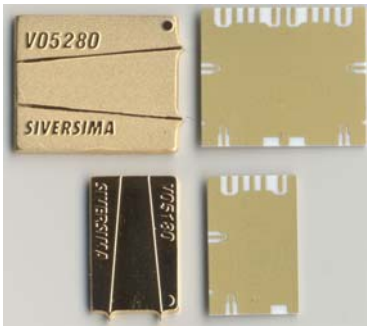

Fig. 1. Single SMD VCO (VO5180) and dual SMD VCO (VO5280).

A new generation of VCO's is under development using a generic MMIC VCO core. The same MMIC VCO core may be connected to different tanks, thus cover several different frequency bands with the same MMIC. This will lower the cost and increase flexibility further of the next generation of single and dual fundamental wideband SMD VCO's.

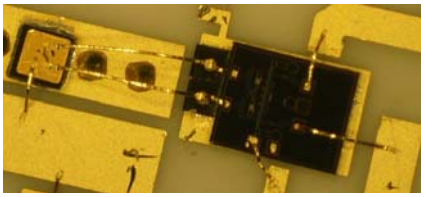

Fig. 2. Generic MMIC VCO core for next generation of VCO's.

If accepted to GHz2010, the presentation that is connected with this abstract will give a detailed presentation of the design, manufacturing, and performance of the single and dual fundamental wideband SMD VCO's, Fig. 1, as well as the generic MMIC VCO core, Fig 2.

ACKNOWLEDGMENT

The work on the generic MMIC VCO core has been carried out in the GigaHertz Centre in a joint research project financed by Swedish Governmental Agency of Innovation Systems (VINNOVA), Chalmers University of Technology, Sivers IMA AB, and Ericsson AB.

Embedded Circulators and Isolators with LTCC Compatible Ferrite Tapes

Thomas Jensen, tje@elektro.dtu.dk, Viktor Krozer, vk@elektro.dtu.dk

Abstract:
LTCC compatible ferrite tapes have been around for some time now and their use has mainly been limited to embedded inductors in LTCC substrates.
Circulators and isolators are important anisotropic components, e.g. for antenna sharing in T/R systems, protecting sensitive components from harmful load reflections, and improving power amplifier efficiency by ensuring a constant load impedance.
They have so far defied the trend towards increasing integration and miniaturization, whereas most active components can be integrated on one or a few chips in a given system, the junction circulator remains a detached component, typically in a SMD package, and the size is restricted by a frequency dependent fixed radius.
The magnetic properties of the ferrite tapes are important parameters in circulator design, they determine to a large degree the operating range of the device. And even though the developed ferrite tapes are branded as LTCC compatible, they are only compatible in a very limited sense and this places a range of restrictions on the practical design of junction circulators.
A magnetic bias field is required for proper circulator operation, It is provided by a permanent magnet that is not cofireable with LTCC modules and the location and attachment of this magnet has to be carefully considered.
This paper investigates the design of junction circulators based on these ferrite materials, points out the limitations imposed by the LTCC compatible materials in comparison with traditional junction circulator materials and suggests methods to overcome these limitations. Simulations showing the expected performance for a stripline circulator and a microstrip circulator based on commercially available ferrite tapes are given.
An overview of how the integration of the junction circulator can be realized within a LTCC multilayer substrate with regards to important aspects such as the placement of the ferrite tapes, the bias magnets, and ground plane metallization is also presented.

60GHz Si integrated cavity oscillator

D. Dancila[1, 2*], **X. Rottenberg** [1], **H.A.C. Tilmans**[1], **W. De Raedt** [1] **and I. Huynen**[2]
[1] IMEC/SSET, B-3001 Leuven, Belgium; [2] UCL/EMIC, B-1348 Louvain-la-Neuve, Belgium
[*]corresponding author: e-mail: dragos.dancila@imec.be

Abstract- This paper presents the realization of a hybrid multi-technology oscillator at 60GHz. The active circuit is realized in a BiCMOS, Silicon Germanium technology. The resonator is realized in a 100µm thick MCM-D substrate and is shaped by a double row of trough silicon vias (TSV). The vias define a substrate integrated waveguide (SIW), circular resonator with a diameter of λ/2. The MMIC active circuit is flip chipped on top of the MCM-D substrate and uses the cavity resonator as reference for the oscillator.

Consumer applications in the millimeter-wave range, for example RADAR-based adaptive cruise control (ACC) systems require high spectrum purity of the RF sources. In order to obtain high spectrum purity, a high loaded Q-factor, Q_l has to be employed since the phase noise is related to Q_l^2. Waveguide cavities are known for their high intrinsic quality factor Q_0 and represent therefore a very good option to be integrated in an oscillator scheme. The resonant frequency of a rectangular metallic cavity filled with a material of permittivity ε_r and permeability μ_r, is given by [1] and is adapted here to a circular cavity preserving the TE_{101} mode of resonance: $f_{101} = \frac{c}{\sqrt{2}\sqrt{\mu_r \varepsilon_r}} \frac{1}{D}$, where D is the diameter of the circular resonator, seen in Figure 1. A diameter D=1025µm corresponds to a frequency of resonance of 60GHz and is used as starting point for FEM simulations, performed with HFSS. The feeding of the resonator is realized through a metallic patch, which diameter d determines the value of the coupling and the impedance at resonance. It differs from [2] where the coupling was realized by shorting the ML line through a TSV, to allow our architecture more freedom for a co-design with the MMIC. The oscillation condition $Re(Z_R+Z_A)<0$ and $Im(Z_R+Z_A)=0$ is fulfilled by trading off Q_l. While Q_0 is in average 130, the loaded quality factor is Q_l=20. This reduction is a consequence of increasing the coupling by increasing the diameter of the feeding patch d=175µm, required by the oscillation conditions. The final measurements of the oscillator show an output power of 5.73dBm at a frequency of 54.12GHz, with a phase noise of -100dBc/Hz, measured at 1MHz offset from the carrier.

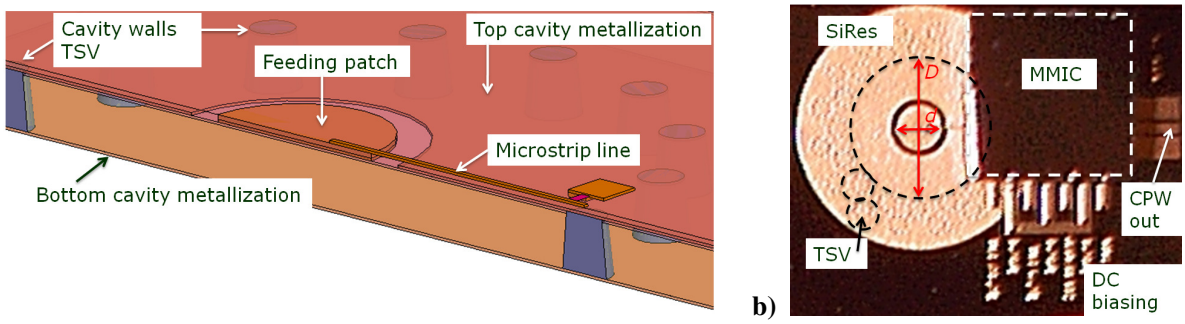

Figure 1: a) Circular cavity resonator defined by TSVs. The diameter of the feeding patch allows adapting the output impedance to fulfill the oscillator condition. b) Assembled MMIC on top of the 100µm thick MCM-D.

REFERENCES

1. D. M. Pozar, *Microwave Engineering,* Addison-Wesley, 1990.
2. G. P. Quijano "Horizontal Integration of Cavity Filters on Thin-Film System in a Package Technology", T-MTT, 2008.

Ultra low-noise HEMT amplifiers at cryogenic temperatures

J. Grahn, P-Å Nilsson G. Moschetti, M. Malmkvist, J. Halonen,
N. Wadefalk, P. Starski, G. Alestig, B. Nilsson, H. Zirath
jan.grahn@chalmers.se

Department of Microtechnology and Nanoscience – MC2
Chalmers University of Technology, SE-412 96 Göteborg, Sweden

Introduction

The development of the microwave HEMT for extremely low-noise amplification at 5-15 K depends on high mobility heterostructures with high indium (In) channel content. Today the device technology is based on the InGaAs/InAlAs (InP) heterostructure. Progress in low-noise performance for InP HEMT has been very slow the last ten years.[1] There is a need to better understand the design and engineering of very low-noise devices and LNAs and also to investigate higher mobility alternatives to the InP HEMT, e.g. the InAs/AlSb heterostructure using 100% In in the channel. We here present cryo LNA results on InP HEMTs benchmarked against state-of-the art. Also we show promising device results of the more spectacular InAs/AlSb HEMT technology.

Experiment

InP HEMTs have been fabricated in a standard III-V process involving epitaxial growth, mesa definition, ohmic contact formation, gate definition, passivation and contacts. Promising InP HEMT wafers have been subject to back-end processing and dicing, and mounted in hybrid IF LNA designs. InAs/AlSb HEMTs have been prepared in a modified InP HEMT process.

Results

100 nm gate-length InP HEMTs were tested in a 4-8 GHz three-stage LNA cooled to 10 K. In Fig. 1, gain and noise data for LNAs with different HEMTs are shown based on either 53% or 65% In in the active channel. The InP HEMT results are compared with the so-called Cryo 3 HEMT, a state-of-the-art benchmark in the ultra low-noise community [2]. Under optimum bias conditions, the 65% InP HEMT LNA is fully comparable in gain and noise with Cryo 3. The 130 nm InP HEMT device with 65% In was compared with 225 nm InAs/AlSb HEMT. In Fig. 2, it is shown that despite almost twice as large gate length, the InAs/AlSb HEMT exhibits 60% higher dc transconductance than the InP HEMT. This is a most essential advantage for low-noise and low-power LNAs. The gate current is however 1,000 times larger. This must be reduced by novel device design.

Conclusion

Noise measurements of cryogenic low-noise amplifiers at 4-8 GHz demonstrated that the InP HEMTs are in parity with the best published results. Furthermore, it has been found that InAs/AlSb HEMTs exhibit device properties which make them interested for low-noise applications where low-power dissipation is important.

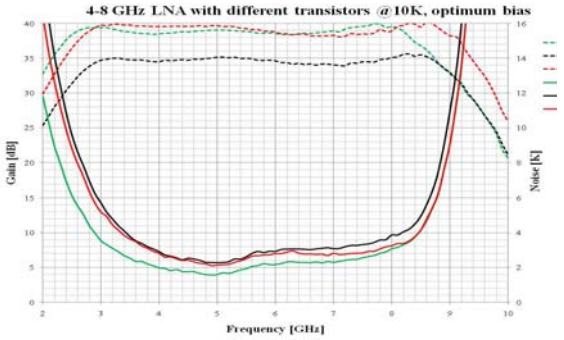

Figure 1. Gain and noise temperature for three InP HEMT cryo LNAs at 10 K. Red (65% In), black (53% In).and green (Cryo 3- benchmark) measured under optimum bias.

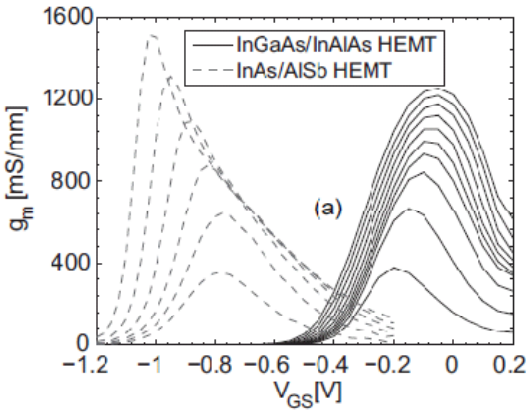

Figure 2: Transconductance for 130 nm InP HEMT (max Vds=1.0 V) and 225 nm InAs/AlSb HEMT (max Vds=0.6).

References

[1] M.W. Pospieszalski, IEEE Microwave Magazine, 6(3), 62-75 (2005).
[2] N. Wadefalk et al, IEEE Microwave Theory Techn. 51, 1705-1711 (2003).

Cryogenic 2-14GHz low noise receiver for radio astronomy based on Eleven feed

Miroslav Pantaleev[1] ,Jian Yang[2], , Per-Simon Kildal[2], Yogesh Karadikar[4], Leif Helldner[1], Benjamin Klein[3], Niklas Wadefalk[4], Rüdiger Haas[1], Ashraf Zaman[2], Mojtaba Zamani[2]
[1]Onsala Space Observatory, Chalmers University of Technology, Sweden
[2]Dept. of Signals and Systems, Chalmers University of Technology, Sweden
[3]School of Electrical and Information Engineering University of the Witwatersrand, and Hartebeesthoek Radio Astronomy Observatory (HartRAO) , South Africa
[4]Dept. of Microtechnology and Nanoscience, Chalmers University of Technology, Sweden

The new generation radio astronomical systems are aiming wider bandwidths in the GHz frequency range. Such an example is the upgrade of the radio telescopes used for Very Long Base Interferometry experiments with systems covering the 2-14GHz range. Key component of the receiver system is the wideband feed. Here we present the recent development of the integration of the cryogenic 2-14 GHz Eleven feed for reflector radio telescope antennas with Low Noise Amplifiers in cryogenic receiver to achieve the lowest possible system noise temperature (Figure 1). The Eleven feed is designed for dual linear polarization and is built up by 4 pieces of log-periodic folded dipole array on microstrip substrate. Each pair of array is fed by a differential two-wire transmission line connected either to balun or differential LNA. The requirement for lowest possible system noise temperature requires cooling of the feed which sets challenges on the mechanical design. We did extensive study of possible microwave substrate materials and different mechanical constructions including thermal and mechanical analysis with computer-aided simulation software in order to create design suitable for multiple temperature recycling. In the paper we present also the design of cryogenic receiver for the Eleven feed (Figure 2) and the measurement results obtained from the tests of several prototype feeds in order to investigate the mechanical and cryogenic performance and evaluate the reliability of the manufacturing and assembly. By the time of the Syposium we hope that we will be able to present measurement of the feed electrical parameters in cryogenic conditions and evaluation of the receiver noise temperature.

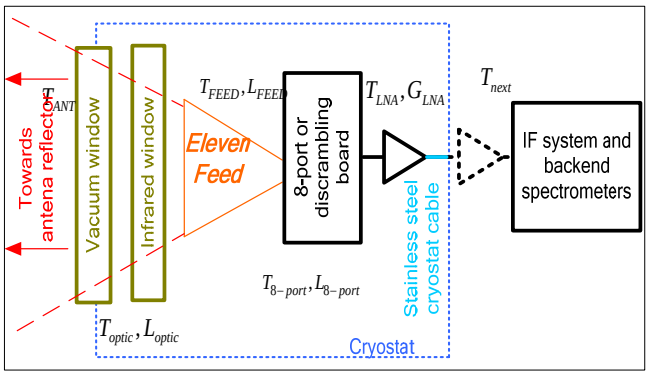

Figure 1: Block diagram of the cryogenic receiver

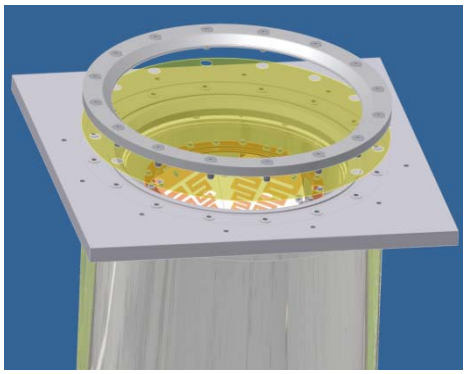

Figure 2: CAD drawing of the receiver cryostat with exploded view of the vacuum window

Extensive design study was done to evaluate Aeff/Tsys and the expected noise performance of cryogenic receiver based on Eleven feed and also to estimate the advantages of different feeding structures. We will present also preliminary design of matching optics to use the 2-14GHz receiver on the 20m antenna at Onsala Space Observatory.

A 24 GHz SOP VCO with 20 % tuning range

Markus Törmänen, Henrik Sjöland
Electrical and Information Technology, Lund University
Box 118, SE-221 00 Lund, Sweden
{markus.tormanen,henrik.sjoland}@eit.lth.se

***Abstract*— A 24 GHz System-on-Package (SOP) VCO is demonstrated. The core operates at 6 GHz and employs a high-Q on-carrier inductor. Using two cascaded on-chip frequency doublers the centre frequency is 24.6 GHz with a 20 % tuning range. The phase noise is below -107dBc/Hz at 1MHz offset over the tuning range, with a FOM between 188 and 192dB at a power consumption of 6.9mW.**

System-on-Package VCO

The System-on-Package, SOP, concept can be used to improve the performance of VCOs by moving critical passive components from chip to a low loss carrier. Here we demonstrate a 24 GHz VCO with 20% tuning range in 130-nm CMOS using the SOP concept. The schematic of the oscillator is shown in Fig. 1. The LC-oscillator core operates at 6 GHz, using an inductor on the glass carrier with a Q value above 80 at 6 GHz. The frequency of the signal is then multiplied by four using two cascaded frequency doublers.

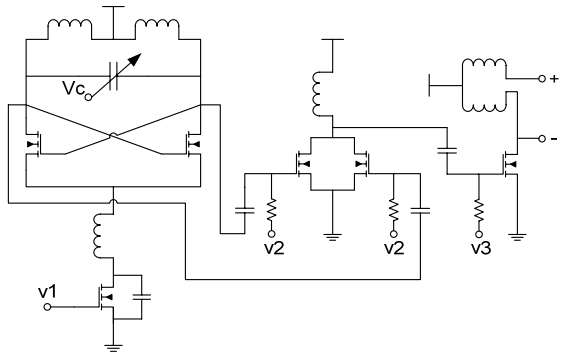

Fig. 1. Schematic of VCO including frequency doublers

Measurement results

The die photograph and photograph of the chip mounted on carrier are shown in Fig. 2.

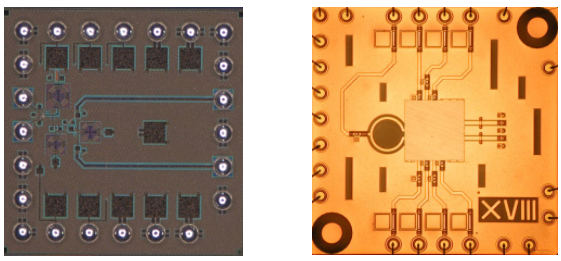

(a) (b)

Fig. 2. (a) Die photograph, 0.97mm^2. (b) Photograph of chip mounted on carrier, 5x5 mm^2.

Two VCO versions have designed, one using regular Vt and one using low Vt transistors. Two samples of each VCO version have been measured. A supply of 1.3V was used for the VCO core and 1V for the frequency doublers. The regular Vt VCO consumed 7.3mW, with a core current consumption of 4.1mA and 2mA used in the doublers. The low Vt VCO consumed slightly less, 6.9mW, with 3.9mA in the core and 1.8mA in the doublers. The frequency tuning characteristic is shown in Fig. 3. As can be seen the tuning range is 20%.

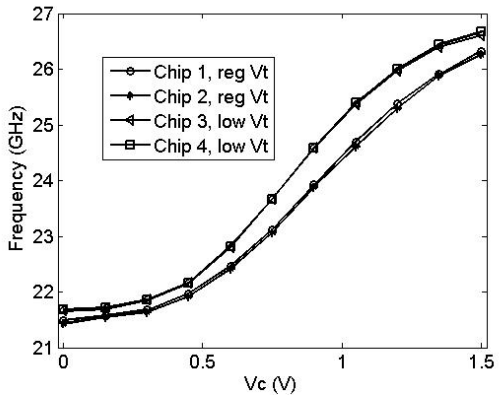

Fig. 3. Frequency tuning characteristic of the VCO

The measured phase noise is shown in Fig. 4. The low Vt version has slightly better performance and achieves a FOM of 191dB and FOM$_T$ of 197dB when measured at the centre frequency, 24.6 GHz.

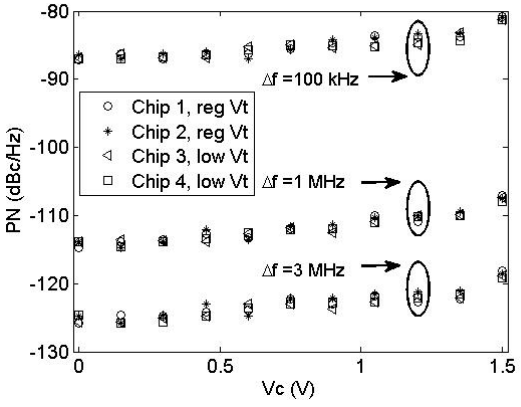

Fig. 4. Phase noise vs. varactor control voltage

References

Markus Törmänen and Henrik Sjöland "A 24 GHz VCO with 20% tuning range in 130-nm CMOS using SOP Technology" *Proc. IEEE Radio Frequency Integrated Circuits Symposium, RFIC 2009*, Boston, Massachusetts, USA, pp. 473-476, Jun. 2009.

Six-Port Multi-Gigabit Receiver

Joakim Östh[1], Adriana Serban[1], Owais[1], Magnus Karlsson[1] and Shaofang Gong[1]
Jaap Haartsen[2] and Peter Karlsson[2]
[1]Linköping University, Department of Science and Technology ITN, Sweden
[2]Sony Ericsson Mobile Communications AB, Lund, Sweden
email: joaos@itn.liu.se

THERE is an increasing demand for high speed wireless data transmission. One promising receiver solution utilizing the ultra-wideband between 6 and 9 GHz to achieve multi-gigabit data rates at short distances has been studied. Measurement results from a prototype receiver are presented.

The receiver is built around a passive device called six-port correlator; which can be integrated into a Printer Circuit Board (PCB). It is a linear passive device and hence has good wideband performance. It also allows to build a receiver and transmitter with a low number of components. Figure 1 shows a schematic of the basic receiver based on the six-port correlator. The six-port correlator is shown inside the dashed lines. The six-port correlator is built of three 90° branch-line couplers and one power divider. The input RF and LO signals are assumed to be correlated and are added with different phase shifts between them. The outputs from the six-port correlator is then connected to non-linear power detector diodes. The non-linear operation will among other frequencies, generate the demodulated baseband signal. Amplifying and taking difference between specified ports result in the I and Q data in two different paths.

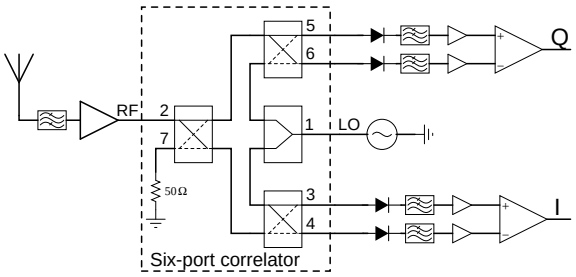

Figure 1. Schematic of the receiver based on the six-port correlator

Simulated and measured performance of the six-port correlator is shown in Figure 2 and indicating good performance in the 6 to 9 GHz band.

Performance measurements on the receiver were conducted with different modulation orders, i.e., QPSK and 16-QAM and with different symbol rates. A typical

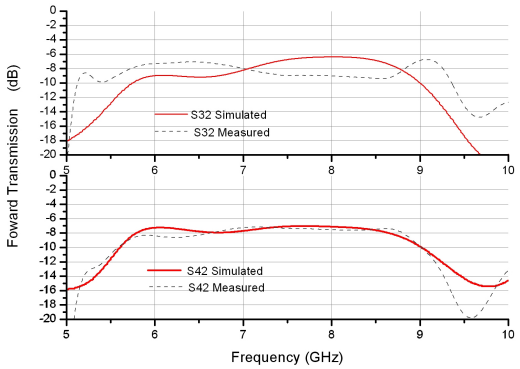

Figure 2. Simulated and measured performance of the six-port correlator designed for the 6 to 9 GHz band

result is shown in Figure 3 for a 16-QAM signal at 250 Msymbols/s for a data rate of 1 Gbit/s. Present limitation of symbol rate is due to the used amplifiers with a bandwidth of about 600 MHz. Important parameters for receiver to be able to process high data rates are a) high bandwidth of components in the receiver chain, b) good gain and phase match between ports in the six-port correlator, c) LO and RF frequency and phase must be correlated.

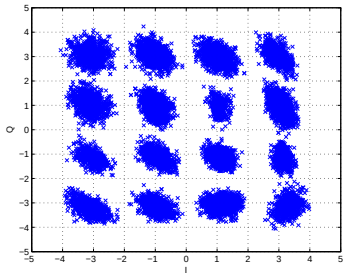

Figure 3. Measured constellation for a 16-QAM signal with a symbol rate of 250 Msymbols/s, i.e., a data rate of 1 Gbit/s

In conclusion, the prototype receiver based on the six-port correlator shows that high data rates of 1 Gbit/s or more can be processed by the receiver. Therefore a receiver built around the six-port correlator is one option to achieve multi-gigabit data rates in the future.

Six-Port Direct Carrier Modulator at 7.5 GHz

Adriana Serban[1] , Joakim Östh[1], Owais[1], Magnus Karlsson[1], Shaofang Gong[1], Jaap Haartsen[2] and Peter Karlsson[2]
[1]Linköping University, Department of Science and Technology, SE-60174 Norrköping, Sweden
[2]Sony Ericsson Mobile Communications AB, Lund, Sweden
e-mail: Adriana.Serban@liu.se

Among different solutions, the six-port receiver architecture for broadband communications has recently gained high interest. Usually implemented with a direct conversion scheme, it has the main advantages of low power consumption, good linearity and low noise figure. However, on the transmitter side there are very few studies demonstrating efficient modulation techniques using the six-port correlator.

In this paper, a 7.5 GHz six-port direct-carrier modulator is presented. Six-port modulators for quadrature phase shift keying (QPSK) schemes were previously reported. In these studies passive impedance termination values corresponding to SHORT and OPEN conditions at the six-port ports 3-6 (see Fig. 1) were used. However, for higher data rates M-level quadrature amplitude modulation (M-QAM, M = 16, 64, etc.) technologies are necessary. Therefore, more impedance termination levels must be generated and controlled.

Fig. 1 shows the simplified schematic of the proposed six-port modulator. It includes a 7-8 GHz wideband six-port correlator, i.e., a 3-dB power divider and three quadrature (90°) branch-line couplers, and four controllable impedance terminations implemented with cold field-effect transistors, (cold-FET). Cold-FET stands for FET operated at zero drain-source voltage. The proposed encoding schemes is based on equal impedance values at I and Q ports, such that $\Gamma_3 = \Gamma_4$ and $\Gamma_5 = \Gamma_6$ for every symbol in the constellation diagram. The cold-FET topology includes a source resistor for symmetrical spreading of the reflection coefficients around the origin. The modulator has been tailored around an existing wideband 7-8 GHz six-port correlator.

In order to validate the 7.5 GHz six-port modulator with cold-FET impedance terminations, a six-port modulator prototype has been realized on a ROGERS4350B substrate of 0.254-mm thickness. The voltage-controlled FET impedance terminations are generated using NEC3512S02.

Figs. 2a and 2b show the six-port modulator spectral response for symbol rates of 10 Msymbols/s with QPSK (= 20 Mbit/s) and 250 Msymbols/s with 16-QAM (= 1 Gbit/s), respectively. For a realistic evaluation, the six-port modulator was also tested with a six-port demodulator (receiver). Figs. 2c and 2d show the input baseband data and the demodulated signal from one channel (I) for QPSK and 16-QAM modulations, respectively.

The LO signal leakage seen in Figs. 2a and 2b is explained by amplitude and phase errors in the ideal reflection coefficient map. For future implementations, following conclusions are drawn: (1) pair of FETs in the same package must be used. For a given transistor (2) the baseband signal levels must be optimized for symmetrical spreading of the reflection coefficients around the origin, and (3) methods for compensation of the parasitic components of the transistor can be identified and evaluated. In this way multi-level modulation, hence Gb/s data rates, can be achieved.

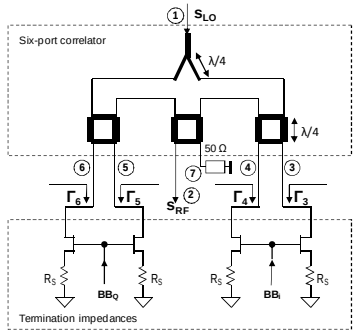

(a) (b)

Fig. 1 Six-port modulator simplified schematic.

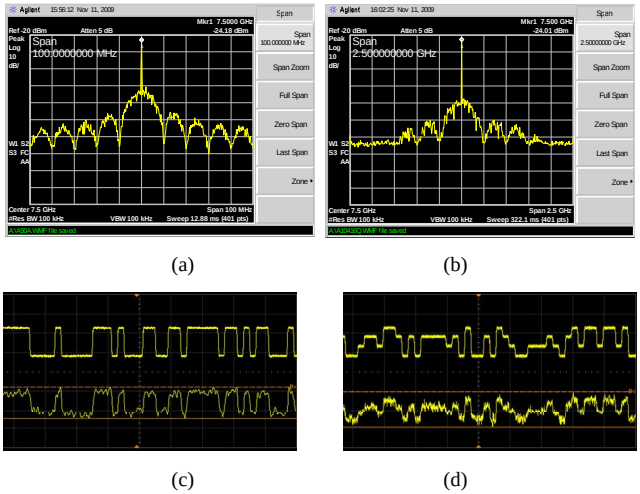

(a) (b)

(c) (d)

Fig. 2. Measured spectrum (a) QPSK 10 Msymbols/s and (b) 16-QAM 250 Msymbols/s. Mod/demod test (c) QPSK 10 Msymbols/s and (d) 16-QAM 1 Msymbols/s. The input baseband signal (up) and demodulated signal (down).

Session 12

13.20-15.05 Wednesday 10 March 2010

Indium Antimonide based High-speed Transistors for Low Power Dissipation Applications

T. Ashley[1], M.T. Emeny, M. Fearn, D.G. Hayes, K.P. Hilton, R. Jefferies, J.O. Maclean, S.J. Smith, W.H.A. Tang, D.J. Wallis, P.J. Webber and G.M. Williams

QinetiQ, Malvern Technology Centre, St Andrew's Road, Malvern, WR14 3PS, UK

[1]tashley@qinetiq.com

III-V compound semiconductor quantum-well field effect transistors (QWFETs) are well established in the analogue field, for example in mobile communications, and are also one of the most promising device candidates for future high speed, low-power digital logic applications due to their high electron mobility [1]. Indium antimonide has the highest electron (and hole) mobility and highest electron saturation velocity of all semiconductors, so offers the potential for the highest speed to power consumption ratio. High-performance InSb n-channel QWFETs have been demonstrated for digital functionality [2], [3] and, more recently, InSb p-channel QWFETs have also been demonstrated [4]. Initial results on n-channel InSb QWFETs for analogue applications were presented in [5]. In this paper we summarise the developments of both digital and analogue InSb based devices in order to assess their potential for high frequency, low power dissipation circuits.

The transistors are fabricated from compressively strained InSb quantum well material grown onto semi insulating GaAs (100) using solid source MBE. The InSb quantum well structure employs a metamorphic $Al_xIn_{1-x}Sb$ buffer to accommodate lattice mismatch and barrier layers of higher bandgap $Al_yIn_{1-y}Sb$ to minimise device leakage. The electron mobility in the n-channel material is in excess of 20,000 cm^2/Vs, whilst the hole mobility in material for p-channel devices is up to 1200 cm^2/Vs. The biaxial compressive strain that is applied to the QW as a consequence of the confining structures has been shown to lead to the hole mobility being significantly greater than in bulk InSb.

For the digital devices, the gate structure is formed using a single resist process, and gate lengths of 85 nm for the n-channel and as low as 30 nm for the p-channel devices have been employed. These structures have resulted in values for current gain cut-off frequency, f_T, with only 0.5 V applied between source and drain, of up to 340 GHz for the n-QWFETs and 140 GHz for the p-QWFETs. We have demonstrated that ratios between maximum on-current and minimum off-current, I_{on}/I_{off}, of more than 10^3, within the constraint of $\Delta V_G \leq V_{DS}$, can be achieved for both types of QWFET. In both cases a 10x reduction in power consumption is seen compared with Si devices of comparable speed. The I_{on}/I_{off} is, in general, presently limited by the behaviour of the Schottky gate, indicating that development of a dielectric gate is a high priority. Thermal generation in the InSb QW is not expected to be a limiting factor, as the narrow band-gap material forms only a very small proportion of the overall device and is also highly quantised.

A key difference between a transistor designed for digital circuits and one for analogue circuits is that the latter tends to be considerably wider, in order to present the required impedance, hence minimization of the resistance along the width of the gate is crucial in order to prevent power loss and phase differences. Consequently a T-shaped gate profile is conventionally adopted. For our InSb QWFETs, a dual-resist, single exposure process was used to form the T-shaped gate metal structure using Ti/Au metallization.

The DC performance was determined by mapping at room temperature across each quarter wafer. The median maximum G_m for 2 x 10 μm devices is typically ~ 800 mS/mm, at V_{DS} = 0.5 V. The r.f. behaviour was determined by measuring S-parameters to 110 GHz, then fitting an equivalent circuit and extrapolating the circuit model to higher frequencies. Values for f_T are in excess of 250 GHz and f_{max} is approximately 500 GHz. The noise has been assessed by measurement up to 26 GHz, then extrapolation of a fitted noise model. This indicates values for NF_{min} of ~ 0.5 dB at low frequencies, rising to only 4 dB at 200 GHz. Outline circuit designs indicate that a 3-stage amplifier with gain of 12 dB, at a centre frequency of 200 GHz and bandwidth of 40 GHz, with 7 dB noise figure and power dissipation of only a few mW is practical.

[1] R. Chau, S. Datta, M. Doczy, B. Doyle, B. Jin, J. Kavalieros, A. Majumdar, M. Metz and M. Radosavljevic, "Benchmarking Nanotechnology for High-Performance and Low-Power Logic Transistor Applications", *IEEE Trans. Nanotechnology*, vol. 4, pp. 153-158, 2005.

[2] T. Ashley, A.R. Barnes, L. Buckle, S. Datta, A.B. Dean, M.T. Emeny, M. Fearn, D.G. Hayes, K.P. Hilton, R. Jefferies, T. Martin, K.J. Nash, T.J. Phillips, W-H.A. Tang, P.J. Wilding and R. Chau, "Novel InSb-based Quantum Well Transistors for Ultra-High Speed, Low Power Logic Applications", *Proc. ICSICT 3*, 2004, pp. 2253-2256.

[3] S. Datta, T. Ashley, J. Brask, L. Buckle, M. Doczy, M. Emeny, D. Hayes, K. Hilton, R. Jefferies, T. Martin, T.J. Phillips, D. Wallis, P. Wilding and R. Chau, "85nm Gate Length Enhancement and Depletion mode InSb Quantum Well Transistors for Ultra High Speed and Very Low Power Digital Logic Applications", *IEDM Tech. Dig.*, pp. 763-766, 2005.

[4] M. Radosavljevic, T. Ashley, A. Andreev, S.D. Coomber, G. Dewey, M.T. Emeny, M. Fearn, D.G. Hayes, K.P. Hilton, M.K. Hudait, R. Jefferies, T. Martin, R. Pillarisetty, W. Rachmady, T. Rakshit, S.J. Smith, M.J. Uren, D.J. Wallis, P.J. Wilding and R. Chau, "High Performance 40nm Gate Length InSb P-Channel Compressively Strained Quantum Well Field Effect Transistors for Low-Power (VCC=0.5V) Logic Applications", *IEDM Tech Dig.*, pp. 727-730 , 2008.

[5] T. Ashley, M. T. Emeny, D. G. Hayes, K. P. Hilton, R. Jefferies, J. O. Maclean, S. J. Smith, A. W-H. Tang, D. J. Wallis and P. J. Webber, "High-Performance InSb Based Quantum Well Field Effect Transistors for Low-Power Dissipation Applications", *IEDM Tech. Dig*. pp. 849-852, 2009

Vertical InAs Nanowire Wrap Gate Transistors for Integration on a Si Platform

Lund, Sweden
E-mail: Anil.Dey@eit.lth.se

A. W. Dey[1], M. Egard[2], S. Johansson[2], A-C Johansson[2], K-M Persson[1], M. Borg[2], C. Thelander[2], P. Nilsson[1], H. Sjöland[1], E. Lind[2], L-E Wernersson[1,2]

In this paper we present DC and RF measurements on vertically standing InAs III/V nanowire MOSFETs with gate all around. The wires are epitaxially grown on a semi-insulating InP substrate, and electrode definition is made by UV-lithography. The pads follow 50 Ω waveguide standards, allowing high frequency S-parameter measurements. Measurements are presented for an array with 70 wires and with a gate length of about 100 nm. A unity current gain frequency, f_t, of 7.4 GHz and a maximum frequency of oscillation, f_{max}, higher than 20 GHz, is shown.

It has been well established that the electrostatic control of the channel in field effect devices is severely diminished when shrinking the gate length. This has lead to the development of novel device geometries such as the FinFET and Tri-gate[1]. We have recently reported vertical InAs III/V nanowire transistors with a gate all around design[2] grown epitaxially on a semi-insulating substrate. Since optical lithography is used to form all subsequent layers after the epitaxial growth, the method is suitable for up-scaling to large scale fabrication. More complex circuits are thus viable for production with this method. Another advantage with a vertical geometry is that the gate length is not set by a lithography step and that III/V channel materials can be integrated on a Si substrate.

The S-parameter measurements were performed using ground-signal-ground (GSG) microprobes.

The measurements were performed from 60 MHz to 20 GHz with an Agilent E8351A vector network analyzer. DC biasing was applied to the transistor gate and drain through bias tees.

A low frequency current gain of more than 30 dB was obtained. The average unity current gain frequency, f_t, was 5.6 GHz and the maximum oscillation frequency, f_{max}, of 20 GHz was achieved. The maximum f_t measured on nominally identical devices on the same chip was 7.4 GHz.

1) Department of Electrical- and Information Technology, Lund University, Box 118, 221 00, Lund, Sweden.
2) Department of Solid State Physics, Lund University, Box 118, 221 00, Lund, Sweden.

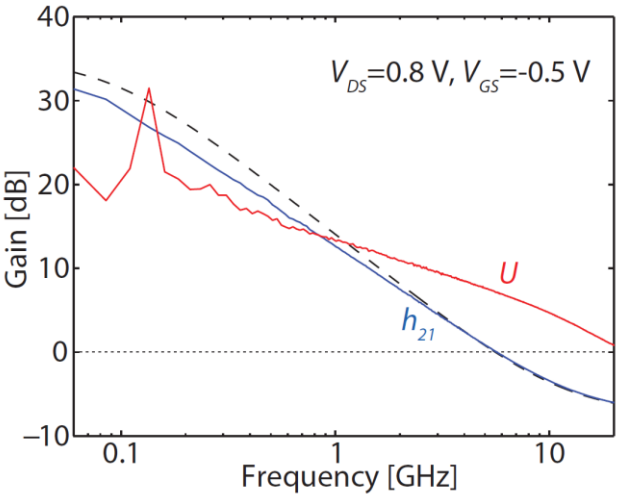

Figure 1. Current gain h_{21} and unilateral power gain.

From the RF-data, we conclude that the f_t of 7.4 GHz and f_{max} of above 20 GHz is strongly limited by the extrinsic parasitic source, drain and gate capacitances, and we are currently implementing devices with considerably reduced pad sizes.

Besides the RF-devices, samples with InAs nanowires on a Si substrate have been grown. We have also designed and fabricated several different circuit layouts such as mixers and ring oscillators.

To conclude, a processing scheme for vertical InAs NW MOSFET fabrication has been developed. Substrates include both semi-insulating InP and Si. Several circuits, both analog and digital have been designed and are currently being implemented.

References

[1] Doyle, B.; Datta, S.; Doczy, M.; Hareland, S.; Jin, B.; Kavalieros, J.; Linton, T.; Murthy, A.; Rios, R.; Chau, R. "High Performance Fully-Depleted Tri-Gate CMOS Transistors", *Electron Device Letters, IEEE* **2003**, *24*, 263–265.

[2] Thelander, C.; Fröberg, L.; Rehnstedt, C.; Samuelson, L.; Wernersson, L.-E. "Vertical Enhancement-Mode InAs Nanowire Field-Effect Transistor with 50-nm Wrap Gate", *Electron Device Letters, IEEE* **2008**, *29*, 206–208.

60, 70, and 80 GHz front-end modules for multi-Gbps wireless communication

Sten E. Gunnarsson[1,2], Christer Stoij[1], Staffan Bruce[1], Rolf Persson[1], Anette Brandt[1], Olle Westblom[1]

[1]Sivers IMA AB, Torshamnsgatan 9, 16429 Kista, Sweden.
[2]Chalmers University of Technology, Microwave Electronics Laboratory, MC2, Göteborg, Sweden.
Email: sten.gunnarsson@siversima.com

The need for multi-Gbps wireless data-transfer is increasing rapidly. One of the largest areas where this need is urgent is mobile backhaul networks, i.e. the fixed wireline and/or wireless interconnections of mobile service base stations to the core telecommunication network. With the upcoming transformation from existing 2G and 3G mobile systems to 4G, these backhaul networks is the bottleneck which limits the datarates in the overall system, and thus, also limits the datarates offered to the end-user, [1]. This bottleneck can be solved with many different technologies which all possesses different pros and cons. The two main technologies are fiber and multi-Gbps mm-wave radio links.

Optic fiber offers the highest data transfer rate (up to 100 Gbps) over virtually unlimited distances but is very expensive to install. Multi-Gbps mm-wave links may offer up to 10 Gbps over 1-3 km and is installed in a few hours for a fraction of the cost of burying a fiber, [2]. Optic fiber and multi-Gbps mm-wave links are thus complementary rather than competing technologies.

Multi-Gbps wireless links can be utilized in many different ways at different frequency bands. It is possible to reach roughly 1 Gbps using several channels in parallel at today's higher radio-link frequency bands (i.e. 24, 38, and 40 GHz). Purchasing the necessary licensees to use several channels in parallel as well as obtaining the mm-wave performance necessary (using e.g. 256QAM or 1024QAM) to achieve 1 Gbps at those frequencies is however both costly and technically very challenging.

Generally speaking, spectrum is a precious resource. Frequencies in vicinity of 60 GHz are one rare exemption. Around 60 GHz, several GHz of unlicensed bandwidth is available, [3]. The main application for 60 GHz is wireless high-speed communication over very short distances, such as WLAN and WPAN due to the high absorption in air, close to 20 dB/km at 60 GHz. Point-to-point links at 60 GHz with a performance of 1.25 Gbps are however common in some places in the USA. A 60 GHz link is a very good choice for a campus or corporate installation where the user does not want to bother with spectrum regulations. Fig 1 a) shows such a 60 GHz front-end (up- and down-converter) module designed and manufactured by Sivers IMA AB. This module contains single-chip 60 GHz transmit and receive MMICs designed at Chalmers University.

In October 2003, FCC in USA issued a ruling that the previously closed frequency bands at 71-76 and 81-86 GHz (commonly referred to as "E-band") would be opened for commercial usage. This initiated a strong activity in the field. Today, less than a handful of US companies offer mm-wave links and front-end modules for this purpose. At the time of writing, Sivers IMA AB is the only European company that offers an E-band front-end module, Fig 1 b). The E-band front-end module from Sivers IMA AB includes features such as integrated X6 LO-chain, high-speed ON/OFF control, single +5/-5 V bias input, and high-Q waveguide filters.

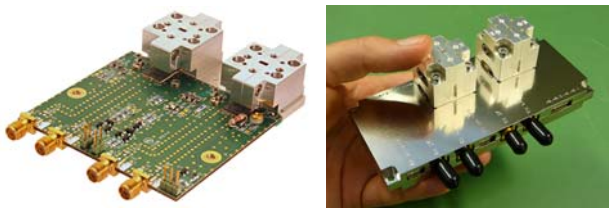

a) b)

Fig. 1. a) 60 GHz up- and down-converter module from Sivers IMA AB. b) E-band (71-86 GHz) up- and down-converter module from Sivers IMA AB.

If accepted to GHz2010, the presentation that is connected with this abstract will give insights into the systems operating at 60, 70, and 80 GHz. It will also give a detailed presentation of the design, manufacturing, and performance of the 60, 70, and 80 GHz front-end modules by Sivers IMA AB, Fig. 1.

REFERENCES

[1] S. Chia, M. Gasparroni, and P. Brick, "The next challenge for cellular networks - backhaul", *IEEE Microwave Magazine*, August 2009.
[2] J. Wells, "Multigigabit wireless technology at 70 GHz, 80 GHz and 90 GHz", *Microwave Journal*, July 2005.
[3] J. Wells, "Faster than Fiber: The Future of Multi-Gbps Wireless", *IEEE Microwave Magazine*, May 2009.

Integrated receivers for 220 GHz SAR-applications

Herbert Zirath, Vessen Vassilev, Sten E. Gunnarsson, Niklas Wadefalk, Rumen Kuzhuharov, Sergey Cherednichenko, Iltcho Angelov, Morteza Abbasi, Bertil Hansson Chalmers University, Göteborg, Sweden

Jan Svedin, Staffan Rudner, FOI, Linköping Sweden.
Ingmar Kallfass, and Arnulf Leuther, Frauhofer Institute IAF, Freiburg, German

SUMMARY Integrated receivers for remote sensing applications have been developed within the NanoComp and Vinnova IKT-program. An integrated superheterodyne receiver was demonstrated with state-of-the-art performance. The MMIC-design consist of an antenna, 3-stage Low noise amplifier, subharmonically pumped mixer, and a x2 frequency multiplier.

I. Introduction

Millimeterwave systems operating in the millimeter wave and sub-mmwave range have gained increased interest due to the recent availability of industrial semiconductor processes capable of amplifying and processing signals up to several hundred GHz. GaAs and InP MMIC technologies based on HEMTs or HBTs have now advanced to a level where it is feasible to design multifunction MMICs for applications such as remote sensing and wireless communication up to and above 300 GHz. A complete receiver MMIC including LNA, mixer, LO-frequency generation and IF LNA is therefore feasible to design. Although it is possible to build a complete receiver or transmitter by mounting single chips into one module, integration of all circuits into one chip would open many new possibilities to design very compact, low cost, low weight millimeterwave systems. Applications include e.g. very high-speed (>10 Gbps) wireless communication, high-resolution passive and active millimeter-wave (mm-wave) imaging sensors, and systems for detection of concealed weapons, plastic explosives etc.

II. RECEIVER DESIGN AND RESULTS

The design is shown in Fig 1. This receiver consist of an antenna, a three stage LNA, a sub-harmonically pumped HEMT-mixer, and an x2 frequency multiplier. The design measures 3.0·2.0 mm. including pads and the empty space surrounding the antenna. The active area is significantly smaller. The novel slot-square substrate lens feed antenna is derived from a coplanar waveguide (CPW) fed slot-square antenna by moving the ground-plane to the backside of the chip and using a microstrip feed line instead of CPW. The simulated impedance bandwidth and radiation efficiency, using the semi-infinite substrate approximation and excluding the losses related to the lens, are roughly 40 GHz and 80%, respectively. The LNA is a three-stage design where the input, interstage, and output matching are all optimized for maximum and flat gain. The sub-harmonically pumped resistive mixer, is based on two paralleled 2·10 um mHEMTs with drains and sources connected. Only half of the LO frequency (110 GHz) is required compared to a fundamentally pumped mixer. The lower LO frequency is the main advantage of the sub-harmonically pumped resistive mixer since it simplifies the design of the LO multiplication chain significantly. The x2 frequency doubler increase the usefulness of the receiver chip considerably since the required LO-frequency input is 55 GHz instead of 110 GHz.

The receiver was manufactured in a 100nm gate length GaAs metamorphic high electron mobility transistor (mHEMT) MMIC process available at the Fraunhofer Institute for Applied Solid-State Physics (IAF) in Germany. A 2·20 um mHEMT microstrip device on the standard 50 um thick GaAs substrate from this process has a ft and fmax of 170 and 300 GHz, respectively.

The DSB-noise figure and gain was measured, a DSB noise figure of 7-8 dB was obtained which to our best knowledge is the lowest noise figure measured for an integrated receiver made in a 100nm HEMT technology.

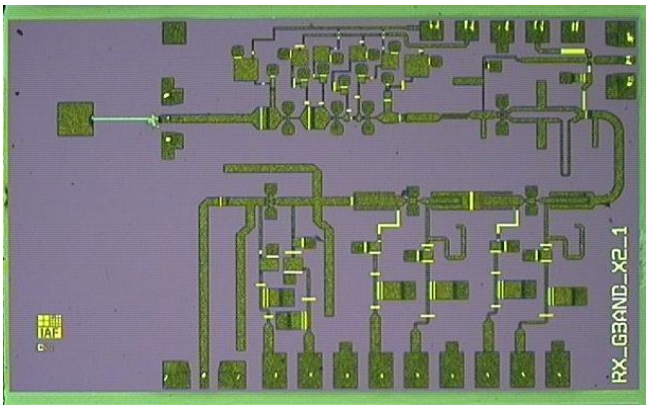

Fig. 1 Chip photo of the developed 195-225 GHz receiver MMIC

IV. CONCLUSION AND DISCUSSION

Newly developed mHEMT MMIC receivers demonstrate competitive results compared to Schottky receivers up to approximately 200 GHz. With available HEMT technologies it is feasible to design receiver MMICs up to 300 GHz. In the future, more functions like image rejection, IF-amplifiers, local oscillator can be integrated. Silicon based technologies have been demonstrated up to and above 100 GHz but have significantly higher noise figure.

Acknowledgment

The authors would like to thank the manufacturing staff, Fraunhofer Institute for Applied Solid-State Physics (IAF), Germany, for the manufacturing of the MMIC. This work was funded by the Swedish Defense Material Administration, FMV, within the NanoComp-project, the Swedish Foundation for Strategic Research, SSF, within the CHARMANT-project, and the Swedish Innovation System, VINNOVA's, THz-platform program. Agilent is acknowledged for ADS-licences.